AN ANALYTICAL AND EXPERIMENTAL STUDY OF THE

TWO-PHASE FLOW OF A HIGH VELOCITY

VAPOR CONDENSING IN A TUBE

By

WINTHROP EDWARD HILDING

Bachelor of Science
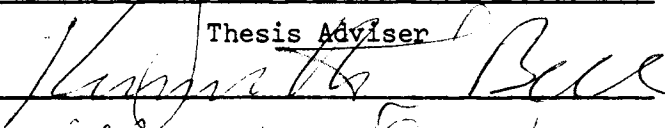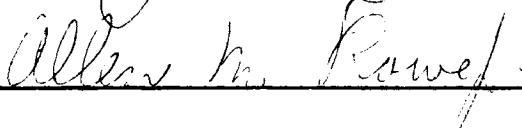University of Connecticut
Storrs, Connecticut
1938
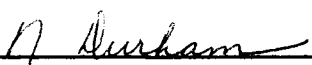
Master of Science
The Pennsylvania State University
University Park, Pennsylvania
1944

Submitted to the faculty of the Graduate College
of the Oklahoma State University
in partial fulfillment of the requirements
for the degree of
DOCTOR OF PHILOSOPHY
May 1968

AN ANALYTICAL AND EXPERIMENTAL STUDY OF THE

TWO-PHASE FLOW OF A HIGH VELOCITY

VAPOR CONDENSING IN A TUBE

Thesis Approved:

_____
Thesis Adviser

_____

_____

_____
Dean of the Graduate College

ii

PREFACE

Condensation of high velocity vapors inside long small diameter tubes occurs in distillation apparatus, certain cryogenic devices, and in vapor driven power systems designed for use in long range space missions. Although considerable experimental data have been reported on the overall pressure losses encountered with two-phase, two-component flow in small tubes (e.g., air and water), much less information, either analytical or experimental, is available on the pressure losses and heat transfer rates occurring with the condensation of a high velocity vapor in a tube.

It was the objective of this investigation to develop an effective analytical treatment of the complete process of condensation of a high velocity pure vapor in a long, small diameter tube. In order to better understand the mechanics of the condensation process and to test the analytical methods developed, it was necessary to conduct a series of experiments with the condensation of high velocity steam in three different sized condenser tubes. The results of both the analytical and experimental work undertaken is reported in this thesis.

I wish to acknowledge gratefully the assistance of the following persons in the completion of this dissertation: Dr. Jerald D. Parker, Oklahoma State University, whose patience, guidance, and long-range assistance is sincerely appreciated; Dr. Kenneth J. Bell and Professor Faye C. McQuiston, Oklahoma State University, for their review of and suggestions for the thesis; Professor Charles H. Coogan, Jr., University

TABLE OF CONTENTS

    IN THE LIQUID AND VAPOR FLOW REGIMES 85

F. INITIAL LIQUID BOUNDARY LAYER EQUATION 99

G. CALCULATION OF INITIAL CONDITIONS NECESSARY FOR DIGITAL
    COMPUTER SOLUTION OF THE DIFFERENTIAL EQUATIONS OF CHANGE. . 105

H. ANALYSIS OF EXPERIMENTAL DATA FOR HIGH VELOCITY STEAM
    CONDENSATION IN SMALL TUBES. 110

        Recorded and Computed Data. 112
        Method of Computation 113

I. DETERMINATION OF THE LOCAL INTERFACIAL AND WALL SHEAR
    STRESS 135

        Two-Phase Friction Factors. 139
        Local Wall Shear Stress Determination by Velocity
            Distribution Analysis 148
        A Universal Correlation for Local Wall Shear Stress . . 158
        Turbulence Intensity in the Liquid Layer. 163

J. CORRELATION OF LOCAL HEAT TRANSFER SURFACE COEFFICIENTS IN
    HIGH VELOCITY CONDENSING TWO-PHASE FLOW. 167

K. NUMERICAL TECHNIQUE FOR THE COMPUTER SOLUTION OF THE
    SIMULTANEOUS NON-LINEAR FIRST ORDER DIFFERENTIAL EQUATIONS
    OF CHANGE FOR HIGH SPEED, TWO-PHASE FLOW WITH CONDENSATION
    IN SMALL STRAIGHT TUBES. 175

        Summary of Method of Solution 175
        An Explanation of the Computer Program Used on the
            IBM-7040 Computer 177
        Program for Solution of Two-Phase Flow Equations. . . . 180

LIST OF TABLES

LIST OF FIGURES

NOMENCLATURE

Dimensional Quantities

A = cross sectional area of tube

A_L = cross sectional area of liquid in tube

A_v = cross sectional area of vapor in tube

C = sonic velocity in saturated vapor

C_L = specific heat of liquid

D = D_i = inside diameter condenser tube

D_o = outside diameter condenser tube

D_v = local diameter of vapor core

E = total energy of the two-phase stream

g = gravitational acceleration at sea level (32.174 ft/sec^2)

h_L = specific enthalpy of saturated liquid

h_v = specific enthalpy of saturated vapor

$(h_v - h_L) \equiv h_{fg}$ = latent heat enthalpy change

$\overset{*}{h}$ = surface convection coefficient

J $\equiv$ 778 ft. lb$_f$ per B.t.u. — conversion constant

k_L = thermal conductivity of liquid

k_v = thermal conductivity of vapor

L = local axial distance from start of condensation

P = absolute stream pressure (static)

P_e = absolute stream pressure at start of condensation

P_o = absolute stagnation pressure

xi

Q' = total energy removed per foot of tube

Q_L = total energy removed up to L feet

R = gas constant for saturated water vapor

T = temperature

u' = fluctuating component of u velocity in Schlichting notation

v' = fluctuating component of v velocity in Schlichting notation

w' = fluctuating component of w velocity in Schlichting notation

U_∞ = free main stream velocity in Schlichting analysis

V = axial velocity in condenser tube

$V_L(y)$ = local axial liquid velocity at wall distance, y

$V_L \equiv \bar{V}_L$ = local mean velocity of liquid in liquid annulus

V_{Li} = local liquid velocity at liquid-vapor interface

$V_v \equiv \bar{V}_v$ = local mean velocity of vapor in vapor core

V_{vi} = local vapor velocity at liquid-vapor interface

V_{ve} = mean velocity of vapor at start of condensation

$V_{Lw}^* \equiv \sqrt{\tau_w/\rho_L}$ = wall friction velocity of liquid

$V_{Li}^* \equiv \sqrt{\tau_v/\rho_L}$ = interfacial friction velocity of liquid

$W_T \equiv (W_L + W_v)$ = combined mass rate of flow of vapor plus liquid

W_L = mass rate of flow of liquid

$W_L' \equiv W_L/\pi D$ = mass rate of flow of liquid per unit of tube circumference

W_v = mass rate of flow of vapor

y = radial distance from inside tube wall

δ = thickness of annular liquid layer

μ_L = dynamic viscosity of saturated liquid

μ_v = dynamic viscosity of saturated vapor

ν_L = kinematic viscosity of liquid

ν_v = kinematic viscosity of vapor

ρ_L = mass density of liquid

ρ_v = mass density of saturated vapor

τ_w = unit shear stress between liquid and tube wall

τ_v = unit shear stress between vapor and liquid at liquid-vapor interface

Non-Dimensional Quantities

C_f = coefficient in friction factor function

$C_L \equiv V_{Li}/\overline{V}_L$

$C_v \equiv V_{vi}/\overline{V}_v$

d = differential operator

$f_w \equiv \dfrac{\tau_w}{\rho_v V_v^2/2}$ = superficial friction factor (called superficial because the unit wall shear stress τ_w is related to the vapor dynamic pressure instead of the liquid dynamic pressure)

$f_v \equiv \dfrac{\tau_v}{\rho_v V_v^2/2}$ = interfacial vapor friction factor in annular two-phase flow

$H \equiv \left[\dfrac{DQ'}{W_T V_{ve}^2}\right]$ = non-dimensional heat transfer rate

$I_T \equiv \sqrt{1/3(\overline{u'^2} + \overline{v'^2} + \overline{w'^2})}/U_\infty$ = intensity of turbulence

$K_p \equiv \left[\dfrac{\rho_v \overline{V}_v^2}{\rho_L \overline{V}_L^2}\right]^{1/2}$

$M \equiv V_v/C$ = local Mach number of the vapor

$N \equiv \left[\dfrac{4P_e}{\rho_{ve} V_{ve}^2}\right]$ = non-dimensional constant

Nu = Nusselt number

Pr = Prandtl number

Re = Reynolds number

$S \equiv \dfrac{k\left[1 + \frac{k-1}{2} M^2\right]^{1/k-1}}{\left[(1 + \frac{k-1}{2} M^2)^{k/k-1} - 1\right]}$ = dimensionless variable

$V_L^+ \equiv V_L^+(y) \equiv V_L(y)/V_{Lw}^*$ = non-dimensional liquid velocity

$\overline{V}_L^+ \equiv \overline{V}_L/V_{Lw}^*$ = non-dimensional mean liquid velocity

$y^+ \equiv yV_{Lw}^*/\nu_L$ = wall friction Reynolds number of liquid at $y = y$

$\delta^+ \equiv \delta V_{Lw}^*/\nu_L$ = wall friction Reynolds number of liquid at $y = \delta$

$\delta_i^+ \equiv (\delta/\nu_L)\sqrt{\tau_v/\rho_L}$ = interfacial friction Reynolds number of liquid

$\delta_m^+ \equiv (\delta/\nu_L)\sqrt{\tau_{wm}/\rho_L}$ = experimental wall friction Reynolds number of liquid

$\delta_u^+ \equiv \delta_u^+(W_L'/\mu_L)$ = analytical wall friction Reynolds number of liquid

Δ = incremental quantity prefix

$X \equiv L/D$ = non-dimensional axial distance from start of condensation

$\alpha \equiv V_L/V_{ve}$ = non-dimensional local liquid velocity

$\beta \equiv V_v/V_{ve}$ = non-dimensional local vapor velocity

$\theta \equiv W_v/W_T$ = non-dimensional local vapor flow rate

$1 - \theta \equiv W_L/W_T$ = non-dimensional local liquid flow rate

$\phi \equiv P/P_e$ = non-dimensional local stream pressure

$\varepsilon \equiv \dfrac{h_{ve}}{V_{ve}^2}$ = non-dimensional constant

$\eta \equiv \dfrac{h_{Le}}{V_{ve}^2}$ = non-dimensional constant

$\lambda_e \equiv \dfrac{h_{fge}}{V_{ve}^2}$ = non-dimensional latent heat at entrance

$\lambda \equiv \lambda_e/\phi^C$ = local non-dimensional latent heat

$\sigma \equiv \rho_{ve}/\rho_{Le}$ = non-dimensional constant

$\xi \equiv \tau_v/P_e$ = non-dimensional vapor shear stress parameter

$\psi \equiv \tau_w/P_e$ = non-dimensional shear stress at the tube wall

Exponents

a = exponent in pressure function for saturated liquid enthalpy

b = exponent in pressure function for saturated vapor enthalpy

c = exponent in pressure function for latent heat

j = exponent in pressure function for saturated vapor density

k = isentropic exponent for vapor

m = exponent in pressure function for saturated liquid viscosity

n = exponent in pressure function for saturated vapor viscosity

s = exponent of Reynolds number in empirical expression for friction factor

t = exponent in empirical expression for sonic velocity in saturated vapor

Subscripts

e   refers to state at start of condensation in tube

f   refers to friction factor

i   refers to liquid-vapor interface or inside surface

L   refers to saturated liquid

m   refers to momentum equation

o   refers to stagnation state of fluid or outside surface

t   refers to turbulent state

u   refers to universal velocity distribution function

v   refers to saturated vapor

w   refers to tube wall

x   refers to axial location in non-dimensional variable

α refers to shear stress induced by change of liquid momentum

β refers to shear stress induced by change of vapor momentum

θ refers to shear stress induced by decrease of momentum due to phase change

ϕ refers to shear stress induced by pressure changes

CHAPTER I

INTRODUCTION

For the effective design of high performance condensing tube type
heat exchangers for use in Rankine power cycle systems, in cryogenic
devices, or in distillation apparatus, a thorough knowledge of the me-
chanics of heat transfer and fluid flow of vapor and liquid during con-
densation in small tubes is desirable. During the past two decades, an
increasing volume of analytical and experimental research on the me-
chanics of two-phase flow systems has been reported in the technical
literature. Investigation of two-phase flow systems has taken several
different directions. The accompanying chart, Table I, is an attempt to
classify some of the areas in which research in two-phase flow mechanics
has been or might be done. Introduction of the chart is intended only to
show the relationship of the work presented in this paper to the whole
spectrum of two-phase flow research. No claim of completeness or orig-
inality of the chart is implied. It should also be noted that research
done in any one area may be closely related to research done in another
area listed on the chart.

Pioneering experimental work on two component, two-phase systems
was done by Lockhart and Martinelli (29)[1] in developing empirical

_____

[1]Numbers in parentheses designate references listed in the Biblio-
graphy.

1

Table I

A CLASSIFICATION OF AREAS OF TWO PHASE FLOW RESEARCH

TWO PHASE FLUID SYSTEMS

* SINGLE COMPONENT FLUID SYSTEMS

TWO OR MORE COMPONENT FLUID SYSTEMS

ADIABATIC SYSTEMS

* SYSTEMS WITH EXTERNAL ENERGY TRANSFER

ADIABATIC SYSTEMS

SYSTEMS WITH EXTERNAL ENERGY TRANS.

NO MASS INTER-CHANGE BETWEEN PHASES OR ADDITION OR REMOVAL FROM SYSTEM

* CONDENSATION OF PURE VAPORS

EVAPORATION OR BOILING SYSTEMS

SIMILAR TO SAME COLUMN UNDER SINGLE COMPONENT SYSTEM

EVAPORATION OR BOILING OF ONE OR MORE COMPONENTS

CONDENSATION OR ABSORPTION OF ONE OR MORE COMPONENTS

MECHANICAL MASS INJECTION OR REMOVAL FROM SYSTEM EITHER PHASE

* CONDENSATION IN TUBES OR CHANNELS

BOILING IN TUBES OR CHANNELS

BUBBLES OF NON CONDENSABLE GASES IN LIQUID SYSTEMS

DISTILLATION PROCESSES

MASS INTERCHANGE BETWEEN PHASES

SPRAY CONDENSATION I.E. ON LIQUID DROPLETS SPRAYED INTO VAPOR PHASE

FLASH BOILERS

LIQUID SLUG IN MULTI-COMPONENT VAPOR SYSTEMS

GAS REFRIGERATION

FIRE TUBE TUBE BOILERS

CHEMICAL PROCESSES

CONDENSATION OUTSIDE TUBES OR CHANNELS OR OTHER COOLED SURFACES

VARIOUS LIQUID VAPOR MIXTURES OF MULTI-COMPONENT SYSTEMS

CAVITATION IN LIQUID SYSTEMS E.G. VAPOR BUBBLES DUE TO LOCAL PRESSURE DROP

OTHER BOILING SYSTEMS E.G. VARIOUS NUCLEAR DEVICES

CLOUD FORMATION AND ASSOCIATED PHENOMENA

FILM CONDENSATION

CHEMICAL PROCESS SYSTEMS

LIQUID SLUGS IN VAPOR SYSTEMS E.G. IN STEAM PIPES, CONDENSATION DUE TO PRESSURE DROP

GAS REFRIGERATION SYSTEMS

CONDENSATION OF PURE VAPORS IN PRESENCE OF NON-CONDENSABLE GASES

DROPWISE CONDENSATION

BOILING IN PRESENCE OF DISSOLVED NON-COND. GASES

* CATEGORY OF PRESENT WORK

2

correlations for pressure losses in isothermal, two-phase, two-component flow in pipes. Additional experimental work has been done by a number of investigators working with steam-water, air-water, air-oil, nitrogen-mercury, and other gas-liquid mixtures. Extensive experimental data for two-phase, two-component flow in both horizontal and vertical tubes are given in the works of Bergelin and Gazley (1) and Bergelin, et al., (2). These investigators present a fictitious friction factor as a function of a superficial vapor Reynolds Number and also use the liquid mass flow rate per unit tube circumference as a function parameter. One of the more important results of this experimental work was the indication that the relatively high pressure losses encountered in two-phase flow are caused by the effect of a wavy annular liquid-vapor interface in generating a high degree of turbulence in the annular liquid layer. The experimental work of Robson and Hilding (31) was directed toward a more complete understanding of the mechanics of the interfacial wave activity encountered in annular two-phase flow. While the wave mechanics in annular condensing flow were carefully documented in this work, no techniques were suggested for reducing the intensity of wave activity.

The method of correlation of the superficial friction factor described above was evidently first used by Kegel (24) in his Bachelor's thesis at the University of Delaware, where the experimental work cited above, (1) and (2), was also conducted. Carpenter (6) in his doctoral dissertation dealt with vapors condensing in vertical tubes. He also used an empirical correlation of the friction factor based on Kegel's data. Carpenter calculated overall pressure losses in condensing flow and compared them to his experimental data with fair success - the calculated pressure losses averaged about 35 percent higher than the

experimental values. The vapor velocities in these tests were of the order of 100 feet per second or less, so that the vapor flow was essentially incompressible.

There have been a number of other investigators who have made experimental measurements of pressure loss in two-phase flow. One of the earliest papers reporting such data for two-component flow was by Boelter and Kepner (3) in 1939; a more recent paper was presented by Chien and Ibele (8) in 1964, and dealt with the combined flow of air and water in tubes.

The contributions to the analytical treatment of two-phase flow are less numerous than the experimental works. The analytical papers of Dukler and Bergelin (13), Calvert (5), and Levy (26) appeared at about the same time. Dukler and Bergelin used the universal velocity profile method of von Karman and also Prandtl's mixing length theory to determine the shear stress in annular liquid films for both laminar and turbulent flow. Calvert also used the theory of von Karman and Prandtl to find the velocity distribution in the annular liquid layer. Levy, too, dealt with the annular flow model for a non-condensing system. His theoretical results compared favorably with the essentially empirical work of Lockhart and Martinelli (29). The later analytical work of Levy (27), (28) did not use the strictly annular flow model. The last-mentioned paper by Levy (28) is an analytical treatment of the two-phase system as a continuous medium with the liquid component dispersed as small droplets or mist of varying concentration throughout the vapor component.

The experimental investigations of Fauske (16) included measurements of adiabatic critical mass flow rates of steam and water from small diameter tubes at various supply or header pressures and including total

vapor qualities from 1 to 96 percent. Fauske derived analytical

expressions for predicting the critical total mass flow based on the

annular flow model similar to Fig. 2, except that he assumed friction-

less pipe flow. In a graphical presentation, Fauske compared the ana-

lytically predicted values for critical total flow with experimental

measurements of his own and those of several other investigators. In

addition, he analytically calculated the critical total flow assuming a

homogeneous mist flow system. The agreement between the analytical

values and experimental data for the annular flow model was excellent

for all qualities from 1 to 96 percent. Contrariwise, critical mass

flow rates calculated, assuming the homogeneous model, predicted total

mass flow rates as low as one-quarter of the experimentally measured

rate at the same total quality of 1 percent.

After consideration of the comparative results of Fauske and also

the preliminary experimental work of the writer, as well as the high

speed photographic studies of several other investigators, the annular

flow model was chosen for the analytical study of condensing vapors pre-

sented in this work. However, it should be recognized that even with an

essentially annular flow system a portion of the liquid present may be

dispersed as fine droplets or mist in the vapor core as represented by

Fig. 1. In addition, it is known that the annular interface between vapor

and liquid is perturbed by traveling surface waves of varying amplitude--

except at quite low vapor and liquid velocities. The presence of the

surface waves has an effect similar to that of a corrugated pipe surface.

Only the increased wall shear stress due to wave induced equivalent

roughness has been considered in the current analysis. The analytical

solution of the difficult problem of the flow mechanics of the
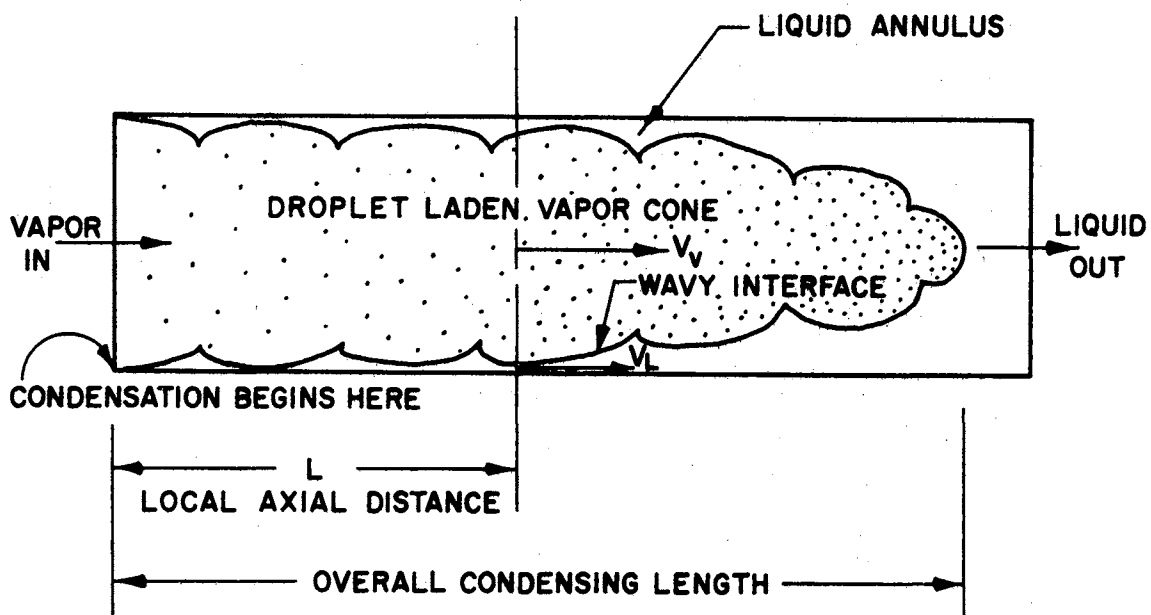
Figure 1. Annular-Mist Flow Condensing Model
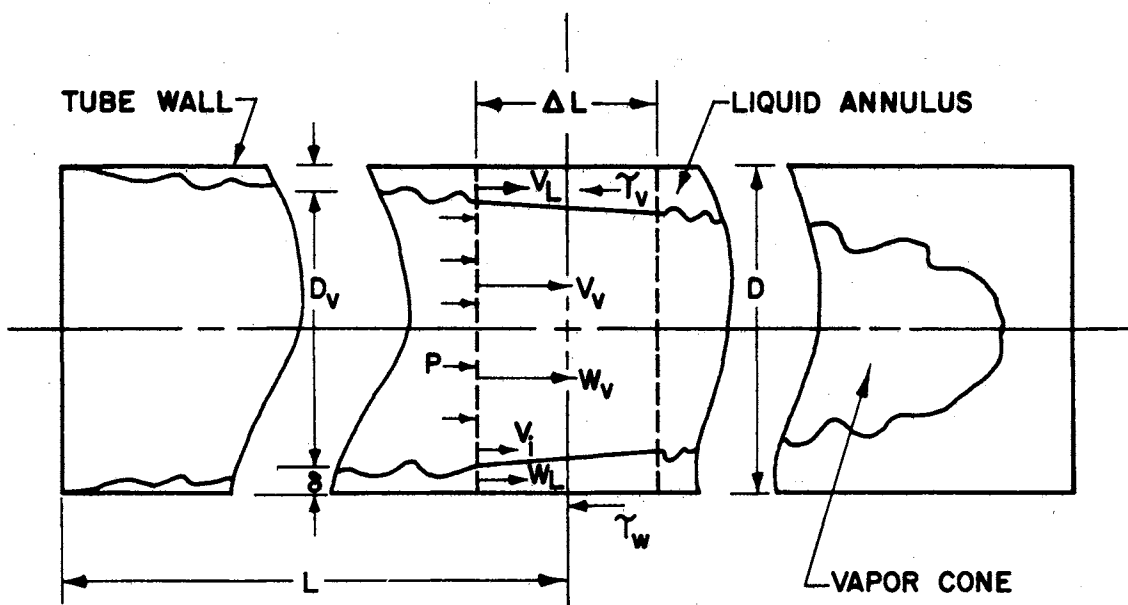
Figure 2. Annular Flow Condensing Model

annular-mist model, with traveling interfacial waves, is left to future
investigators.

In this investigation, the one-dimensional annular flow model of
Fig. 2 has been used to derive a system of simultaneous, non-linear,
ordinary differential equations of change which have been solved (inte-
grated) numerically in incremental steps over the full condensing length
for long, small diameter condenser tubes. These equations describe mathe-
matically the continuously changing local flow mechanics in the condenser
tube. From this analytical solution, the vapor and liquid velocities,
stream static pressure, and mass flow rates of vapor and liquid are
thereby determined at each axial location along the length of the con-
denser tube.

In order to test the validity of the proposed mathematical model and
the analytical results obtained by use of this model, several single tube
condenser test units were constructed. These test units were used to
measure experimentally the same quantities which were determined analyti-
cally by solution of the derived system of equations. Four test units,
including three different tube sizes, 0.190, 0.550, and 1.025 inches I.D.,
were constructed and tested. The test data reported include values of
the local mass flow rate of vapor and liquid, local mass average veloci-
ties of vapor and liquid, as well as local values of stagnation and stream
pressures. Secondary calculations were made from the experimental data to
determine local values of interfacial and wall shear stresses, as well as
local heat transfer coefficients.

For the same operating conditions as found in the experimental work,
analytical data were obtained for each of the local flow variables mention-
ed in the previous paragraph. Graphical comparison of the experimental

and analytical values of local pressures and fluid velocities are given, for each of the three tube sizes tested, for the full condensing length.

Secondary investigations have been made in an attempt to improve upon the available empirical correlations of local wall shear stress and local heat transfer coefficients for condensation with high velocity vapors. The results of this work, both experimental and analytical, are reported in Appendixes I and J.

The graphical comparison of the analytical and experimental results obtained, for three different condenser tube sizes and over a considerable range of vapor velocities and densities, shows good agreement with each of the flow variables over the full condensing length in most cases. The close agreement between the analytical and experimental data reported in this work indicates that the essentially one dimensional annular flow model, adopted for the analytical treatment presented, gives a reasonable approximation of the mechanics of high velocity vapor condensation.

It is believed that the analytical results and experimental data presented in the succeeding pages of this work can be used as a base to build a still more precise analytical treatment of the mechanics of high velocity condensing vapors.

CHAPTER II

ANALYTICAL DEVELOPMENT

Mathematical Model

As indicated in Chapter I, experimental evidence gathered by

Robson (31), as well as by several other investigators, both of a

qualitative and a quantitative nature, including visual observations,

shows that the major fraction of the liquid phase in condensing flow

accumulates as an annular ring of pure liquid flowing along the tube

wall. For condensation in horizontal tubes at low vapor velocities the

liquid may accumulate and flow in a more or less stratified layer along

the bottom of the tube. At quite low vapor velocities there may also

occur an oscillating type of liquid slug flow superposed upon the

stratified layer. This investigation, however, is concerned only with

those conditions of condensation in which condensed liquid flows in an

annular ring with essentially axial symmetry about the tube axis. The

evidence presented in (31) indicates that axial symmetry is approached

whenever the average vapor velocity exceeds the mass average velocity in

the annular liquid ring by the approximate velocity ratio of $V_v/V_L \geq 100$.

This will be true even for condensation in horizontal tubes, as well as

for downflow in vertical tubes, and for condenser tubes located in a

zero gravity field.

Depending on the local vapor velocity, as well as the total vapor

quality θ, a small fraction of the liquid may be dispersed as mist or droplets in the vapor core (see Fig. 1). Earlier measurements made by the author (19) indicate that the mass concentration of droplets in the vapor core remains at a figure of less than 10 percent of the local mass flow rate of vapor down to quite low vapor to liquid total mass flow ratios, e.g., $W_v/W_L \geq 0.20$.

In this analysis of the high velocity vapor-liquid system, the effect of the variable liquid droplet concentration has been neglected. In addition, several other simplifying assumptions have been made in the mathematical model which has been adopted for this work. Following is a summation of the major simplifications which have been used in the analytical treatment:

1. The presence of a liquid droplet mist in the vapor core is neglected. Experimental evidence (19) shows, however, that the vapor core may include 10 percent or more by weight flow rate of liquid droplets at low vapor qualities, e.g., $\theta \leq 0.20$. It remains for future investigators to consider the much more difficult analysis of the mathematical model representing the annular-mist flow regime.

2. Radial pressure gradients across the tube are considered to be insignificant relative to other forces acting on the system.

3. The annular interface between vapor core and outer liquid ring is assumed to be essentially conical and concentric to the tube axis. However, the actual physical interface is known to have annular surface waves, which penetrate more or less deeply into the annular liquid layer (see Figs. 3 and 4). Evidently, one important effect of the wave penetration of the liquid surface is that turbulence in the liquid layer is such that the radial distribution of the time average axial liquid velocity is essentially flat up to very close to the wall. The resulting sharp velocity gradient in the thin liquid laminar sublayer results in a high wall shear stress as is demonstrated by Fig. 46, page 154. See also Appendix I.

4. The mass average axial velocity of the liquid, as well as that of the vapor, is assumed to be steady and constant at any axial location, although some radial variation in axial velocities is known to exist. Time and mass average axial
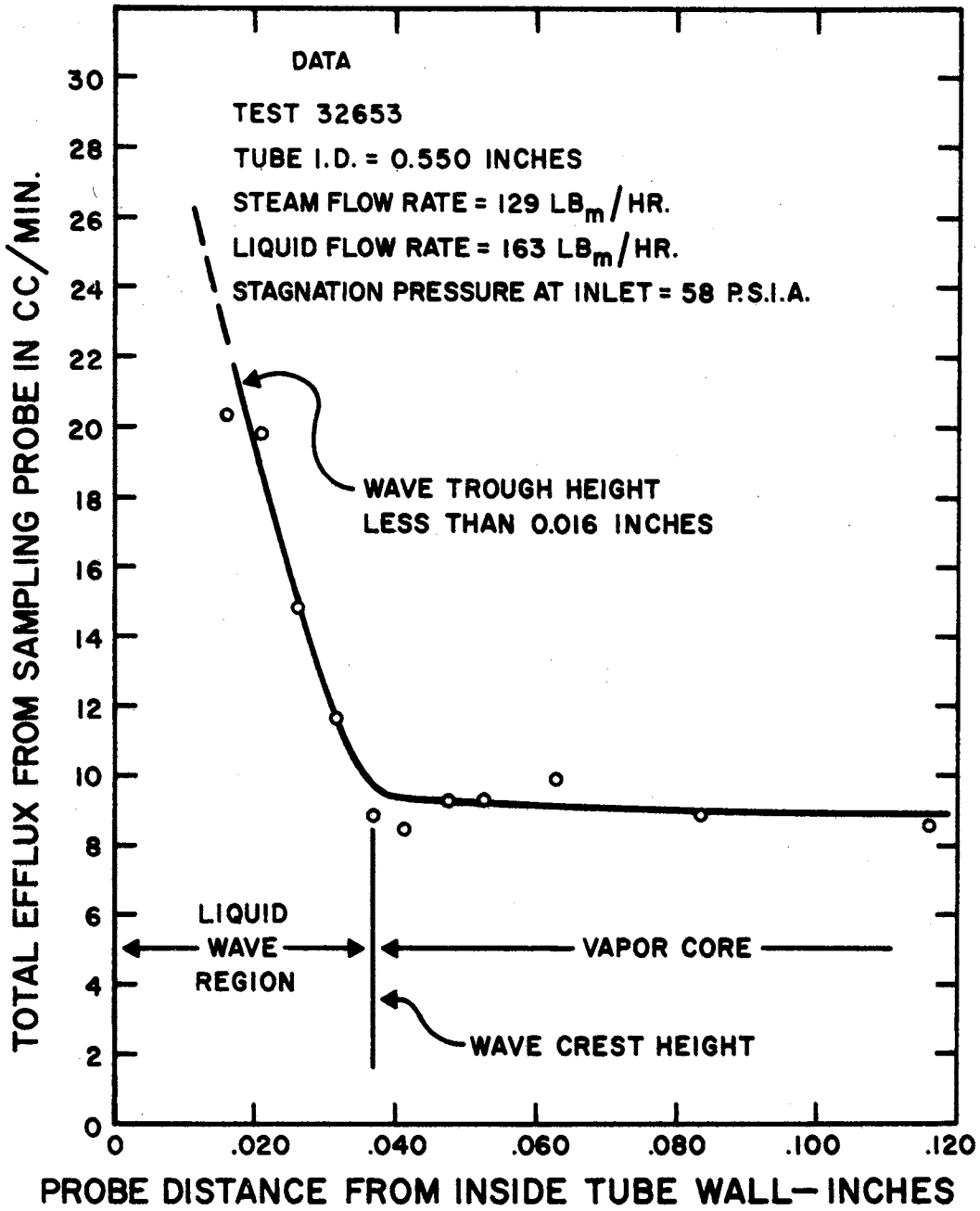
Figure 3. Liquid Layer Thickness as Determined by a Sampling
Probe
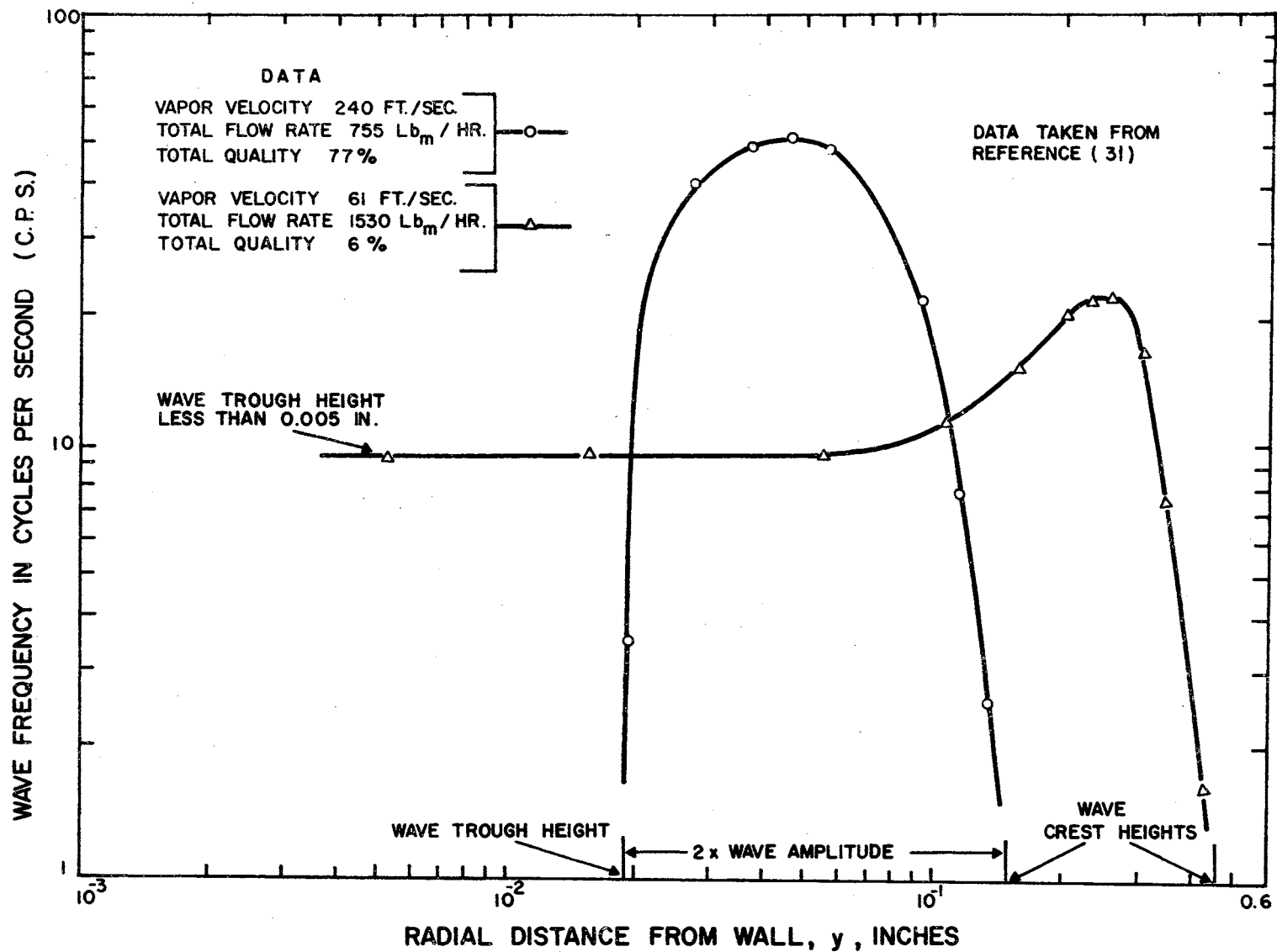
Figure 4. Liquid Layer Thickness as Determined by Electric Contact Probe

velocities for the liquid (V_L) in its annular ring and for the vapor (V_v) in the vapor core have been used throughout except at the interface. The relation of the interfacial velocity (V_i) to the vapor and liquid velocities is discussed in Appendix E.

5. The condenser tube is assumed to exist in a zero gravity field or to be in a horizontal position with sufficient vapor velocity ($V_v/V_L \geq 100$) to ensure axial symmetry of the annular liquid layer.

Fig. 2 is intended to describe graphically the system and the forces which are acting upon the two fluids flowing through it in the axial direction.

Derived Equations

In the analytical treatment presented herein, the annular flow model described by Fig. 2 has been used to develop a system of differential equations of change for the co-current annular, one-dimensional, steady flow of a pure condensing vapor and its liquid in a straight cylindrical tube with radial heat transfer through the tube wall.

Differential control volumes were drawn for the annular liquid layer and for the vapor core at a cross section of the condenser tube (see Figs. 35 and 36, page 78). Macroscopic mass, energy, and momentum balances were then made for a differential length of tube for both vapor and liquid control volumes (see Appendixes B, C, and D). Addition of the equations obtained for the two control volumes resulted in three simultaneous, independent, non-linear ordinary differential equations, which may be expressed in general functional form as follows:

Continuity:

$$\phi_1 \; (V_v, \; V_L, \; W_v, \; P, \; L, \; Prop) = 0 \qquad\qquad (1)$$

Momentum:

$$\phi_2 \; (V_v, \; V_L, \; W_v, \; P, \; L, \; Prop, \; \tau_W \; \text{or} \; \tau_v) = 0 \tag{2}$$

Energy:

$$\phi_3 \; (V_v, \; V_L, \; W_v, \; P, \; L, \; Prop, \; Q') = 0 \tag{3}$$

where 'Prop' represents the various thermo-physical properties of both

vapor and liquid. The other symbols are as given in the nomenclature.

In equations (1), (2) and (3) the fundamental variables involved in

each equation can be reduced to a total of five variables: four de-

pendent variables, V_v, V_L, W_v, P; and one independent variable which is

the axial position or distance L. The thermo-physical properties (Prop)

of vapor and liquid which are involved can be directly related to the

local vapor saturation pressure by simple empirical functions. This

operation is discussed in later paragraphs of this chapter, and the

empirical functions are developed in Appendix A. The local energy

transfer rate Q' is influenced by external heat transfer resistances and

temperatures, as well as the local inside surface coefficient of heat

transfer. Very often external factors dominate the determination of Q'

and are more or less independent of the internal flow mechanics of the

two-phase system. These external resistances, therefore, constitute a

separate problem which may be considered wholly apart from the work at

hand. Nevertheless, local values of Q' must be specified either arbi-

trarily or from experimental data in order to obtain an analytical

solution to the proposed system of equations.

Use of either the vapor momentum equation or the combined momentum

equation (see equation (2)) requires input data on the local value of

either the local interfacial shear stress τ_v or the local wall shear

stress τ_w. These quantities are entirely dependent on the internal flow

mechanics of the condensing system and, therefore, must be correlated in

terms of the internal flow data. This difficult correlation problem is

the subject of Appendix I and is discussed also in Chapter IV, page 53.

It is seen that the analytical determination of the local flow

mechanics of this system can be reduced to the determination of the

successive local values of the four dependent variables, V_v, V_L, W_v, and

P. Obviously, this involves the simultaneous solution of at least four

independent equations of which only three have been mentioned up to this

point.

At the entrance to a condenser tube the flow regime may begin with

either laminar or turbulent flow of the vapor accompanied by a develop-

ing annular laminar liquid layer. For the region of interest of this

investigation, the vapor flow either begins or changes to a fully tur-

bulent flow regime in a very short axial distance. If the analysis is

started with dry saturated vapor at the condenser tube entrance, the

development of an annular laminar liquid layer begins and continues un-

til the liquid thickness is such that the smooth cylindrical liquid

surface (liquid-vapor interface) becomes unstable and a wavy annular

interface between liquid and vapor begins to develop. The flow regime

downstream from this point consists of a turbulent vapor core surrounded

by a highly turbulent annular liquid layer. Normally the initial lam-

inar liquid layer will exist for only a very short distance (1 to 5

diameters or less) near the tube mouth. The non-dimensional boundary

layer thickness parameter $\delta^+ = (\delta/\nu)\sqrt{\tau_w/\rho_L}$ has been used to determine

the point of transition from laminar to turbulent flow in the liquid

layer. A value $\delta^+ = 1$ for the liquid layer apparently gives a good

indication of this transition point.

For the laminar liquid layer existing near the tube mouth, a differential boundary layer equation has been developed in Appendix F. The most general form of this equation is given by the expression

$$\frac{2}{V_L} \frac{dV_L}{dL} - \frac{2-s}{V_v} \frac{dV_v}{dL} - \frac{1}{W_L} \frac{dW_L}{dL} - \frac{j(1-s)}{P} \frac{dP}{dL} = -\frac{s}{L} \quad (4)$$

where s and j are empirical constants. This equation must be used, in conjunction with the differential forms of equations (1), (2), and (3) of this chapter, as the fourth equation which is necessary to begin the numerical integration over the condensing length. A detailed analysis of the developing laminar liquid layer is given in Appendix F.

At the point of transition to turbulent flow in the annular liquid layer, e.g., $\delta^+ \simeq 1$, the differential equation of equal velocity pressures replaces the boundary layer equation in the stepwise integration process. The relation of equal interfacial velocity pressures was deduced as the result of the experimental observation of the lack of any radial discontinuity in the value of the dynamic pressure, $(P_o - P)$, in the interfacial region or on either side of it (see Fig. 37, page 86). For an essentially incompressible vapor, the phenomenon of equal interfacial velocity pressures may be represented by the equation

$$\frac{\rho_L V_{Li}^2}{2} = \frac{\rho_v V_{vi}^2}{2} \quad (5)$$

where V_{Li} and V_{vi} are considered to be the time average velocities of liquid and vapor at the highly turbulent and intermittent wavy interface. Equation (5) indicates that the momentum flux of vapor and liquid on their respective sides of the interface is the same. Careful consideration of the mathematical model and the available experimental

data indicates that the radial position of the interface should be taken at the crest of the annular waves. If the variation in liquid density is neglected over the condensing length, logarithmic differentiation of equation (5) leads finally to the equation

$$\frac{1}{V_L}\frac{dV_L}{dL} - \frac{1}{V_v}\frac{dV_v}{dL} - \frac{j}{2P}\frac{dP}{dL} = 0 \tag{6}$$

where j is the same empirical constant that appeared in equation (4).

Equation (6), for essentially incompressible flow, or equation (28E), for compressible vapor flow, replaces equation (4) as the fourth equation required to complete the analytical solution of the condensation process for annular two-phase flow in a tube. A more extensive analysis of the interface problem for both incompressible and compressible vapor flow is given in Appendix E.

Physical Properties of Vapor and Liquid

In Appendix A simple empirical equations have been established which express each of the several physical properties of liquid and vapor as a particular function of the saturation pressure of the fluid. For example, the specific enthalpy of saturated vapor is given by the simple power function

$$h_v = C_2 P^b \tag{6A}$$

where C_2 and b are particular constants. This local value of vapor enthalpy can also be non-dimensionalized by comparing it to the vapor enthalpy at the tube entrance where the entering vapor pressure is known, thus

$$h_v = h_{ve}(P/P_e)^b = h_{ve}\phi^b \tag{8A}$$

Each of the necessary thermo-physical properties of vapor and liquid has been treated in the same fashion in Appendix A. Values of the power function exponents a, b, c, etc. have been plotted in Figs. 27 through 34 for both water and potassium. Note that the need for the constant coefficient (e.g., C_2) in each of the functions has been eliminated by normalizing the local property in terms of the value of the property for the saturated vapor at the known entering pressure as in equation (8A) above.

Examination of the Figs. 27 through 34, pages 62 through 69, shows some variation of the power exponents for each of the physical properties for water and potassium. However, in most cases the error encountered in the value of the particular property over a moderate range of pressures is less than one percent. For example, in the case of saturated steam expanding from a pressure of 50 psia to 15 psia, the value of the latent heat at 15 psia, determined from equation (13A) by using a mean value of the power function exponent c taken from Fig. 29, is $h'_{fg} = 972$ Btu/lb$_m$ as compared to the value $h_{fg} = 969.7$ Btu/lb$_m$ as given in the tables of the Thermodynamic Properties of Steam by Keenan and Keyes (23). In most cases the error in the calculated value of the property will be less than in the example cited. It should be obvious that other assumptions in the analytical treatment may cause greater errors in the predicted data than that caused by small errors in the property values as calculated by the method described above.

Integration of the System of Differential Equations

Given In Table II

The simultaneous mathematical solution (integration) of the

necessary set of four independent non-linear ordinary differential equations was evidently possible or practical only by numerical or ana-logical methods. For the purposes of numerical solution and computer programming it was advantageous to normalize the five fundamental variables and to express the variable coefficients in non-dimensional form (see Nomenclature and/or Table II). By introducing the particular flow conditions existing in the saturated vapor at the start of con-densation in the tube (not necessarily at the tube mouth) as a reference state, the four fundamental dependent variables were there-after expressed as a non-dimensional function of this saturated vapor state. Thus $\alpha \equiv V_L/V_{ve}$, $\beta \equiv V_v/V_{ve}$, $\theta \equiv W_v/W_T$, and $\phi \equiv P/P_e$. The axial tube position is represented in terms of tube diameters from the start of condensation, i.e., axial distance $X = L/D$ (diameters).

Starting with the particular initial values of the four normalized variables at $X = 0$, the appropriate set of four simultaneous differ-ential equations was solved algebraically to determine the local values of the four derivatives at that point $(X = 0)$. The derivatives so determined were then applied over a small increment of ΔX along the tube, to determine new values of the same four dependent variables. Usually the incremental value of X was taken at $0.01 \leq \Delta X \leq 1.0$. Proceeding forward in the positive X direction, the above process was continually repeated until the total quality θ had decreased from $\theta = 1$ to $\theta = 0$. It was necessary, as noted earlier, to change from the laminar liquid layer equation to the equal velocity pressure equation at $\delta^+ = 1$ during this numerical integration process.

Because of the tremendous number of calculations and the inherent possibilities of error accumulation, the stepwise integration process

TABLE II

A TABLE OF NON-DIMENSIONAL DIFFERENTIAL EQUATIONS OF HIGH SPEED TWO-PHASE FLOW WITH CONDENSATION IN LONG SMALL TUBES

The general differential equation is written in the following non-dimensional form

$$A\frac{d\alpha}{dX} + B\frac{d\beta}{dX} + C\frac{d\theta}{dX} + D\frac{d\phi}{dX} = K$$

The coefficients A, B, C, D and K for the different physical equations are given below:

Equation source	A	B	C	D	K
1. Combined equations of continuity	$\left[\dfrac{1-\theta}{\theta}\right]\dfrac{\sigma\beta\phi^j}{\alpha^2}$	$+\dfrac{1}{\beta}$	$+\dfrac{1}{\theta}\left[\dfrac{\sigma\beta\phi^j}{\alpha}-1\right]$	$+\dfrac{j}{\phi}$	$= 0$
2. Momentum equation of the vapor	0	$+\theta$	$+[\beta-2\alpha]$	$+\dfrac{\theta N}{\beta\phi^j}$	$=-2f_v\beta^{3/2}\sqrt{\theta\phi^j}$
3. Combined momentum equations of vapor and liquid	$[1-\theta]$	$+\theta$	$+[\beta-\alpha]$	$+N$	$=-2f_w\beta^2\phi^j$
4. Combined energy equation of vapor and liquid	$[1-\theta]\alpha$	$+\beta\theta$	$+\left[\dfrac{\lambda}{\phi^c}+\dfrac{1}{2}(\beta^2-\alpha^2)\right]$	$+\left[\dfrac{b\epsilon\theta}{\phi^{1-b}}+\dfrac{a\eta(1-\theta)}{\phi^{1-a}}\right]$	$= -H$
5. Velocity pressure at interface for incompressible flow	$\dfrac{1}{\alpha}$	$-\dfrac{1}{\beta}$	$+0$	$-\dfrac{j}{2\phi}$	$= 0$
6. Velocity pressure at interface for compressible flow	$\dfrac{2}{\alpha}$	$-\dfrac{SM^2}{\beta}$	$+0$	$+\left[\dfrac{SM^2 t-2t-j}{\phi}\right]$	$= 0$
7. Initial liquid boundary layer equation	$\dfrac{2}{\alpha}$	$+0$	$+\dfrac{1}{1-\theta}$	$-\dfrac{j}{2\phi}$	$=-\dfrac{1}{2X}$

The derivations of the equations summarized in this table are reported in appendixes B, C, D, E and F.

was programmed for machine computation, first on an I.B.M. 1620 digital computer and later on the I.B.M. 7040 digital computer. All analytical data presented have been compiled by this system of machine computation. The Fortran program for the computer solution to this system of equations is given at the end of Appendix K. Detailed information about preparing data for the machine integration process is also given in Appendix K.

CHAPTER III

EXPERIMENTAL METHOD AND APPARATUS

In order to confirm the validity of the mathematical model dis-
cussed in Chapter II and the accompanying analytical results presented
in the several Appendices it was necessary to construct experimental
apparatus which would make it possible to measure the same variables
which were to be predicted analytically.

Altogether four (4) different test units were constructed and
tested. The dimensional details of these units are summarized in
Table III. Figs. 6, 7, and 8 present detailed diagrams for the three
different size condenser tubes tested, i.e., 0.190, 0.550, and 1.025
inches I.D. respectively. Fig. 5 presents a general line and block
layout of the test system including instrumentation. In addition,
Figs. 9 and 10 give details of the construction and installation of the
thermocouple and pressure probes used for making experimental measure-
ments.

Each of the four test units consisted of a single copper condenser
tube enclosed in a larger copper tube which formed the outer annulus
for the flow of cooling water. Each test unit was constructed so as to
permit the flow of cooling water to be counter to or in parallel with
the flow of condensing vapor. Tests were conducted with both parallel
and counter flow of the cooling water. Each test unit was instrumented
so as to permit the measurement of local stagnation pressure P_o and

Table III

Major Dimensions of Experimental Condenser Heat Exchangers From Which the Experimental Data were Recorded

Test Unit	Condenser Tube I.D. Inches	Condenser Tube O.D. Inches	Outer Tube I.D. Inches	Overall Condenser Tube Length In Feet	Cooling Water Flows	Annulus Thermo-Couples	Detailed Diagram In **
Heat Exchanger No. 1	0.550	0.625	1.026	10.3	Counter Flow	Traveling Probe Only	
Heat Exchanger No. 2	0.550	0.625	1.026	10.3	Parallel Flow	Fixed in Annulus and Traveling*	Figure 6
Heat Exchanger No. 3	0.190	0.250	0.550	11.7	Parallel Flow	Fixed in Annulus and Traveling	Figure 7
Heat Exchanger No. 4	1.025	1.125	2.010	19.0	Parallel or Counter Flow	Fixed in Annulus Only*	Figure 8

*In Heat Exchanger No. 2 and in No. 4, thermocouples were also fastened to the outer wall of the inner condensing tube.

INSTALLATION DIAGRAM FOR HEAT EXCHANGER NO.- 4

STEAM SUPPLY LINE

⊗ — SHUT OFF VALVES

NOTE : Cooling water can be used in parallel
or counter flow to condensing steam.

AUTOMATIC / PRESSURE
REGULATING   VALVE

ELECTRIC
HEATER

Q

STEAM
CALORIMETER

I9 FT. TEST CONDENSER

PRESSURE PROBE
INSERTED AT TEE

STEAM ENTERS
CONDENSER

TO
DRAIN

TO
DRAIN

(See figure 8 for details)

ORIFICE TO
METER COOLING
WATER

MANOMETER

TO AFTER CONDENSER
AND WEIGH TANK

COOLING WATER SUPPLY LINE

Figure 5.   Line Diagram of Test Apparatus
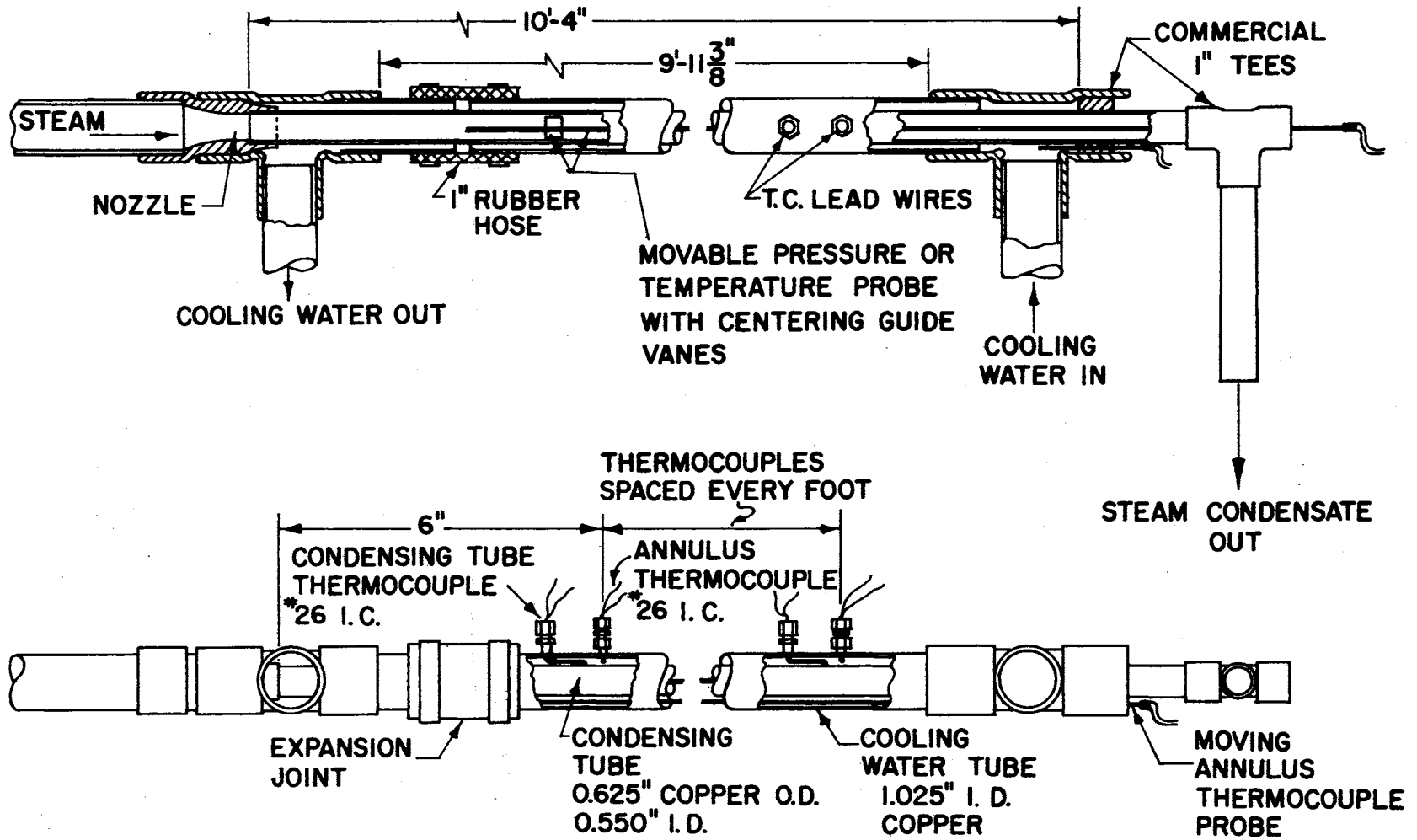
Figure 6. Detail Diagram of Condenser No. 2

EXCHANGER NO. 3

THERMOCOUPLE	SPACING
2,3	2" (2 is 2" from ref. line)
4 to 10 inc.	3"
11 to 16 inc.	6"
17 to 21 inc.	12"
22	17"
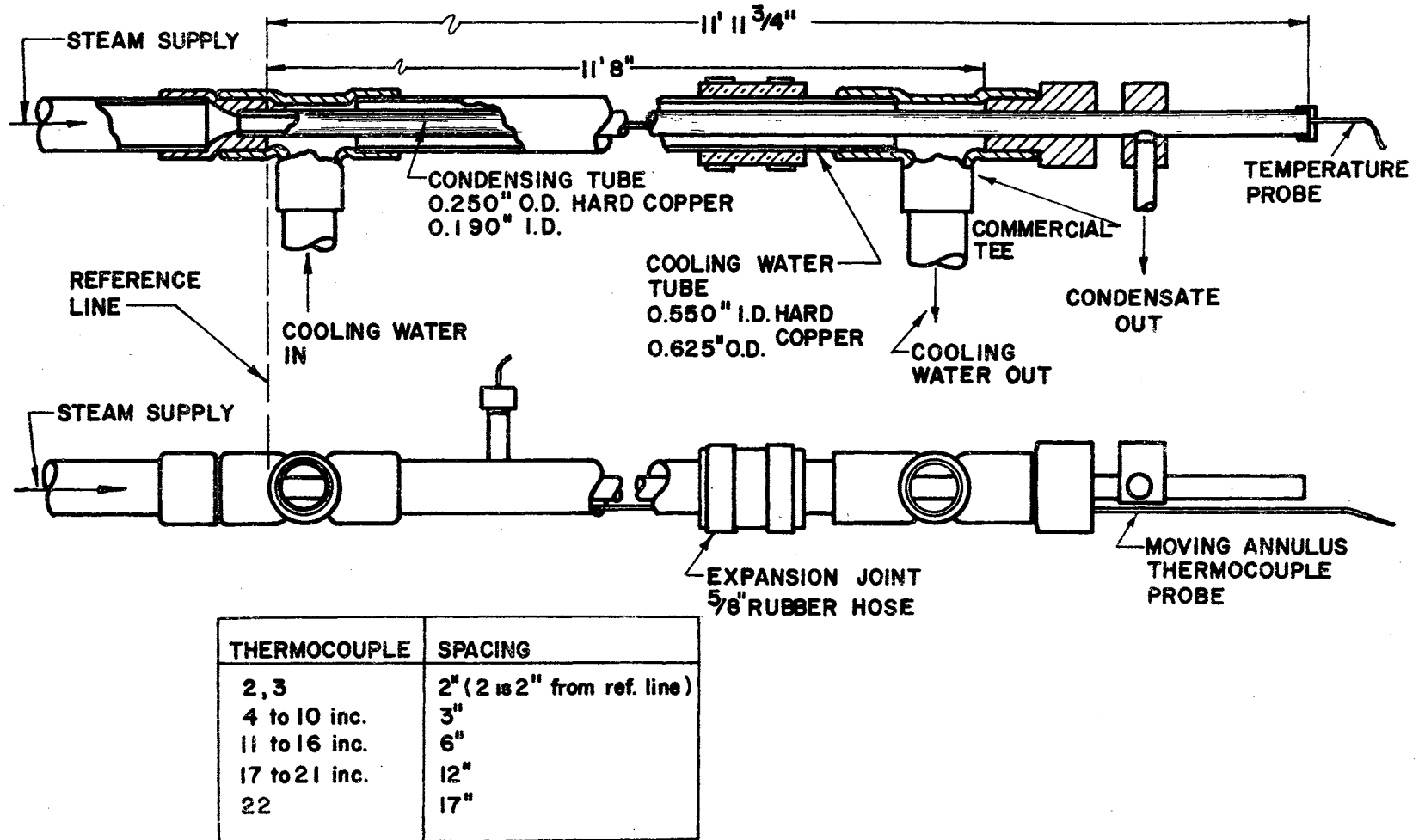
Figure 7. Detail Diagram of Condenser No. 3

HEAT EXCHANGER NO. 4
(not to scale)

THERMOCOUPLE FOR
COOLING WATER
TEMPERATURE

THERMOCOUPLE FOR
WALL TEMPERATURE
MEASUREMENT

TO RECORDING
POTENTIOMETER

2.010 IN. I.D.   1.025 IN. I.D.

FLOW DIRECTION →

0.250 IN. O.D.

TO MANOMETERS FOR WALL
STATIC PRESSURE MEASUREMENTS

MOVING PRESSURE PROBE
FOR LOCAL STAGNATION
PRESSURE MEASUREMENT
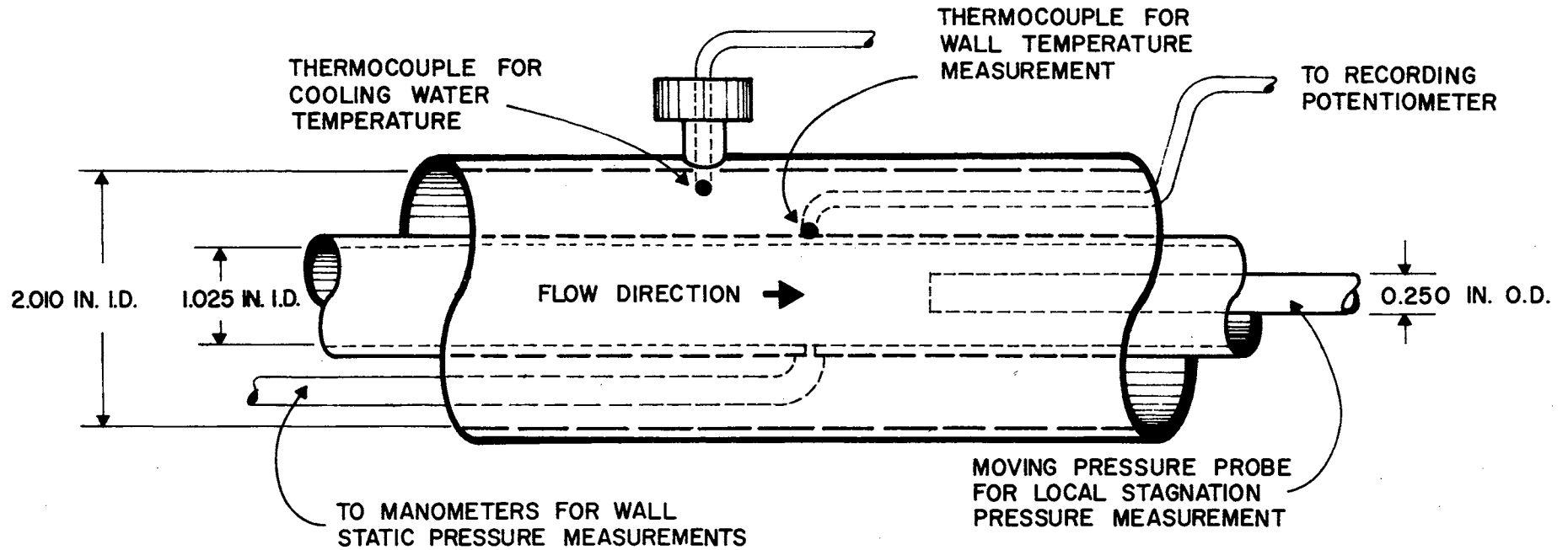
THE FIXED INSTRUMENTATION ABOVE IS REPEATED AT INTERVALS ALONG THE AXIAL TUBE LENGTH.

Figure 8.   Detail Diagram of Condenser No. 4
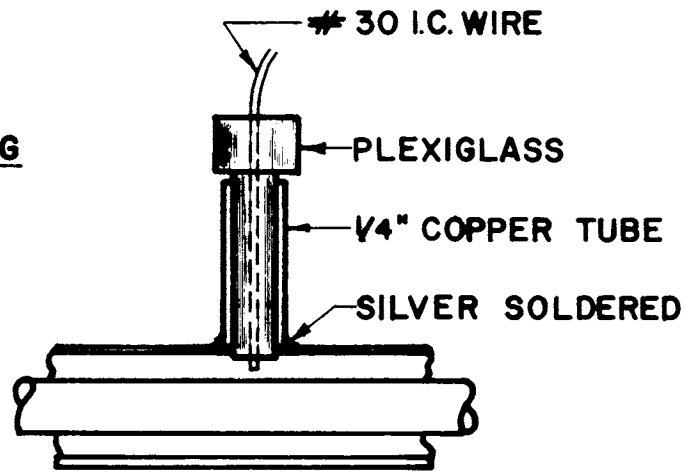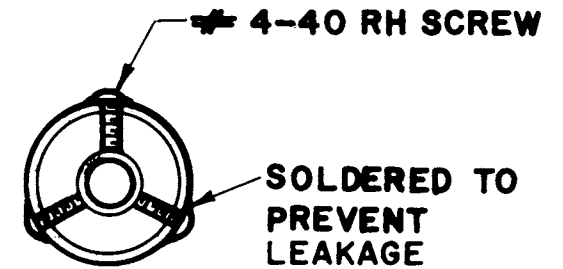
Figure 9. Detail Diagrams for Condenser Tube Installation

PROBES FOR HEAT EXCHANGER NO. 3

TEMPERATURE PROBE FOR ANNULUS

$11'\ 10\frac{3}{4}"$

0.130"

#30 I.C.WIRE — 0.065 STAINLESS TUBE — THERMOCOUPLE JUNCTION — ANNULUS

TEMPERATURE PROBE FOR CONDENSING TUBE

$12'\ 3\frac{1}{2}"$

$1\frac{1}{2}"$ $\frac{3}{4}"$

#30 I.C.WIRE — 0.065 STAINLESS TUBE — GUIDE VANES — CONDENSING TUBE

IMPACT PRESSURE TUBE FOR CONDENSING TUBE

$12'\ 6\frac{1}{2}"$

$1\frac{1}{2}"$ $\frac{7}{8}"$

0.042 STAINLESS TUBE — GUIDE VANES — END OPEN

STATIC PRESSURE TUBE FOR CONDENSING TUBE

$12'\ 8\frac{1}{2}"$

$1\frac{1}{2}"$ $\frac{7}{8}"$ $\frac{1}{2}"$

0.042" STAINLESS TUBE — GUIDE VANES — END CLOSED

3 HOLES EQUALLY SPACED 80 DRILL

Figure 10. Detail Diagrams of Temperature and Pressure Probes

static pressure P of the vapor, as well as the local vapor temperature

and local cooling water temperature. In addition, heat exchangers

numbers 2 and 4 were equipped with thermocouples fixed to the outer

wall of the condenser tube itself to facilitate the calculation of

local heat transfer coefficients. The method of analysis and inter-

pretation of the experimental data recorded is reviewed in detail in

Appendix H.

The experimental data recorded and the quantities calculated there-

from make possible the determination of the local values of the vapor

and liquid velocities, the local mass flow rate of vapor and liquid, as

well as the local heat transfer coefficients and both interfacial and

wall shear stresses. The experimental determination of the local inter-

facial and wall shear stresses requires in addition the evaluation of

the local gradients of the static pressure, vapor and liquid velocities,

and vapor mass flow rate--see equations (2C) and (11C). The determina-

tion of these gradients has been done by both graphical and curve

fitting techniques. Both methods seem to have given satisfactory

results. The curve fitting method is faster once a computer program has

been established to handle the data; however, the graphical method is

preferable for examining data which include some questionable or

obviously spurious points as well as otherwise valuable information.

The local temperature and the temperature gradient of the cooling

water is fundamental to the calculation of the local mass flow rate of

vapor and liquid as well as the local rate of condensation. Two methods

of temperature measurement were used in these tests. Heat exchanger num-

ber 1 was equipped only with a single moveable or traveling thermocouple

probe which was read repeatedly as the probe was moved over the

condensing length.   Heat exchangers numbers 2 and 3 were equipped with both

a traveling probe and with thermocouples fixed in the annulus at a

number of locations along the condensing length.   Heat exchanger number 4

was equipped only with a series of thermocouples fixed in the annulus

between the tubes.   Each method has some advantages and disadvantages.

The traveling probe gives greater flexibility in positioning, but does

not lend itself to the use of automatic and continuous temperature

recorders.   The use of multiple fixed installations permits the rapid

and simultaneous recording of temperatures over the tube length of both

cooling water and tube wall temperatures.

One important source of error encountered in these tests was

the position lag in the cooling water temperature measurement relative

to the actual point of heat transfer at the pipe surface.   The cooling

water annulus was designed so as to operate well into the turbulent

region, but some position lag at the annulus thermocouple position was

certain to occur.   In addition, there was some uncertainty as to the

radial position of each thermocouple in the annulus.   This resulted in

an unevenness in the error, described above, from one couple to the next.

It is almost impossible to give a quantitative estimate   of   the

magnitude of this error.   The effect of this error was most noticeable

in parallel flow cooling at the start of condensation.   In such a case

the uncertainty in the location of the cooling effect causes an indica-

tion of a local liquid condensate flow rate less than the true value and

a local vapor flow rate in excess of the true value.   Because of the

error in the determination of the vapor mass flow rate, the calculated

cross section area allotted to the vapor may have been excessive and

that   to   the   liquid too small.   Since the average local liquid

velocity must be calculated indirectly from the combined continuity equation, one would expect that the liquid velocity calculated from the experimental data for parallel flow cooling might be too high, particularly at the start of condensation where a small error in the calculated oversize vapor cross section would have a magnified effect in minimizing the liquid cross section, due to the wide density difference between the two fluids. It would be quite possible, for example, to calculate a negative liquid cross section if the response error described was great enough. It is gratifying therefore, to note that no such calculated negative values of liquid cross section were encountered in the analysis of this experimental data. It is probable however that the sharp peak in the experimental liquid velocity curve at the 1/4 foot length of Fig. 20, page 46, is a result of just such a position lag in the cooling water temperature measurement as has been described above.

Because of the large consumption of steam (up to 1,000 lb_m per hour) and cooling water (in excess of 20,000 lb_m per hour), it was necessary to use plant steam and water for these tests. Small fluctuations in line pressure for both steam and water were reduced by the use of automatic pressure and flow control devices. Some fluctuation in the temperature of the cooling water and of the quality of the steam was encountered during the test periods. However, these fluctuations were not great enough to have been a major source of error.

Probably the greatest experimental errors were caused by the unavoidable use of the temperature and pressure probes in the condenser tube itself. For each test unit the probes were made as small as possible--the probe cross section was less than 10 percent of the tube cross section for all units. During every test all temperature, pressure, and

flow measurements were repeated at each probe station as the probe was gradually withdrawn from the tube. Insofar as possible the temperature, pressure, and flow measurements were regulated and reconstructed so as to represent the flow conditions for the probeless tube, but for the experimental value of the local stagnation pressure P_o this was almost impossible to achieve. For the smallest condenser tube (0.190 inches I.D.) the presence of the pressure probe caused a reduction of steam rate of as much as 12 percent when the inlet pressure was held constant. For the larger test units the effect of the probe presence on the steam rate was a smaller percentage.

An error in the measurement of the stagnation pressure P_o of the vapor is also encountered because of the presence of entrained liquid droplets in the vapor core. The analysis of this problem was the subject of the doctoral dissertation of Dussourd (15). Dussourd developed a special impact probe that permits corrections to be made to the experimental measurement of the stagnation pressure P_o of a droplet-laden gas stream. Such a 'Dussourd Probe' was constructed and used for the experimental tests conducted on the 1.025 I.D. condenser tube. An analysis by the author (19) shows that the droplet concentration in the condensing vapor remains at a value of less than 10 percent in the vapor core until about 80 percent of the vapor has condensed, after which the droplet concentration apparently increases until the vapor disappears. For the test data gathered on the 1.025 inch I.D. condenser tube, corrections to the local measurements of P_o have been made in accordance with the method outlined in (15). In every condensing test conducted on the 1.025 inch I.D. condenser tube, the correction to impact pressure measurements, due to the presence of liquid droplets, increases

gradually from a zero correction at the start of condensation to a correction amounting to a reduction of about 25 percent in vapor velocity near the end of condensation--as compared to the value calculated from the uncorrected measurement. Over the major portion of the condensing length the correction to vapor velocity was usually a reduction of less than 10 percent.

CHAPTER IV

DISCUSSION OF RESULTS AND CONCLUSIONS

The chief aim of this work was to develop a method of analysis
which would make possible the analytical evaluation of the local flow
properties--including the heat transfer characteristics--of the two-
phase system of a high velocity vapor condensing in a long circular tube.
A one-dimensional mathematical model with annular flow of the condensed
liquid surrounding a high velocity vapor core was selected to describe
the condensing system (Fig. 2, page 6). A system of non-linear first-
order ordinary differential equations of change has been developed (see
Table II, page 20) which may be solved (integrated) simultaneously over
the length of the tube. As discussed in Chapter II the fundamental
dependent variables involved are the time average local vapor and liquid
velocities, V_v and V_L, the local mass flow rate of vapor W_v, and the
local static pressure P. The single independent variable is the tube
length or distance from the start of condensation. Mathematical solu-
tion of the system of equations has been accomplished by stepwise
numerical integration using a digital computer to carry out the multiple
calculations involved. The print out statement of the computer program
for this solution is included in Appendix K.

A series of analytical solutions to representative condensing flow
conditions has been made for single condenser tubes of three sizes--
0.190, 0.550, and 1.025 inches I.D. respectively. Analytical solutions

for the condensation of both water vapor and potassium vapor are in-
cluded. Figs. 11 through 24 give analytical solutions for the condensa-
tion of water vapor. Figs. 25 and 26 show typical analytical solutions
for the flow properties for the condensation of potassium vapor.

In order to test the validity of the mathematical model selected and
the analytical method of solution which was developed from it, it was
necessary to devise and build experimental apparatus capable of measur-
ing the several physical flow properties predicted by the analytical
solution described above. Four such test units were constructed and a
series of condensing tests were made with each unit. The recorded and
calculated data from these tests are reported in Tables IV through XVII
of Appendix H. The construction of the experimental apparatus and the
experimental measurements made with it are discussed in Chapter III.
The method of data reduction and calculation details are given in
Appendix H.

The comparison of the experimental and analytical results is
generally favorable even for the most rigorous test conditions encounter-
ed. For example, Figs. 17 and 18 compare experimentally and analytically
determined local values of static pressure and vapor and liquid veloci-
ties over the condensing length for the extremely high vapor velocities
of up to 1,800 feet per second. Figs. 20, 21, 23, and 24 give the same
comparison for vapor velocities under 1,000 feet per second. These data
cover the three tube sizes tested. While there is some discrepancy be-
tween the experimental and analytical data in each case, the general
agreement obtained for the wide range of vapor velocities and tube sizes
investigated certainly gives a considerable degree of confirmation as to
the soundness of the mathematical model chosen. As has been stated at
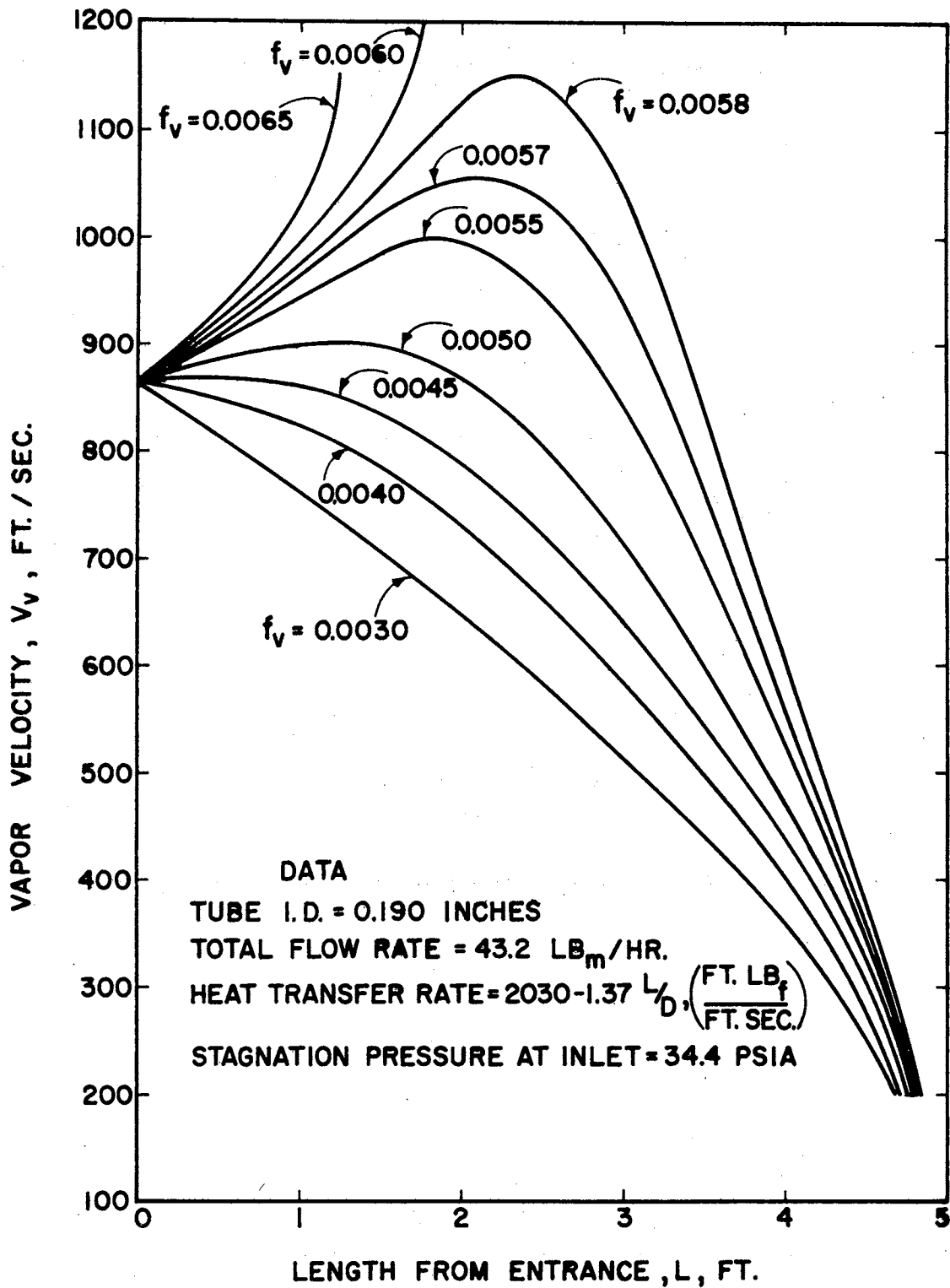
Figure 11. The Effect of Interfacial Friction Factor on Local Vapor Velocity; Analytical Solution
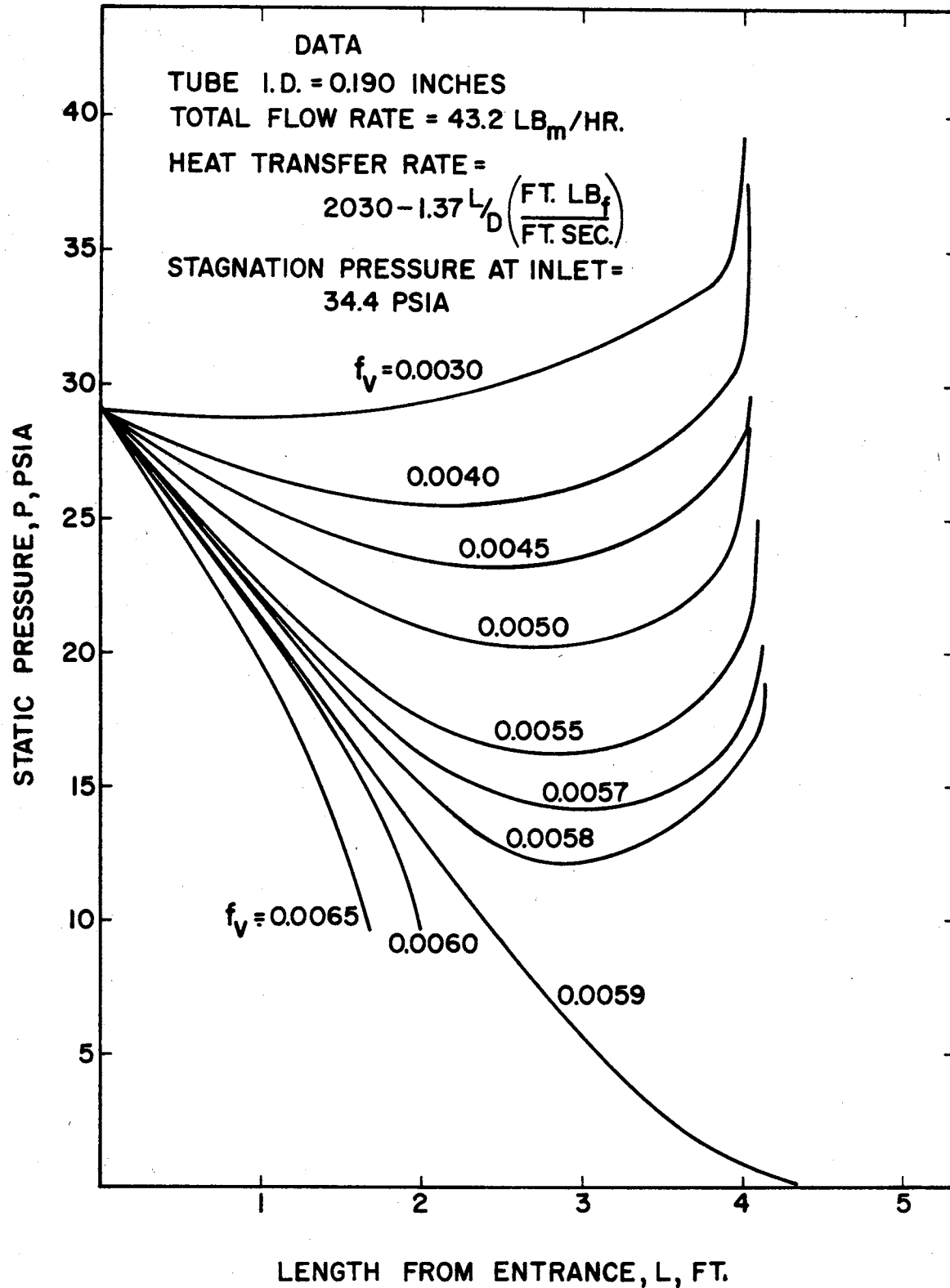
Figure 12. The Effect of Interfacial Friction Factor on Local Static Pressure; Analytical Solution
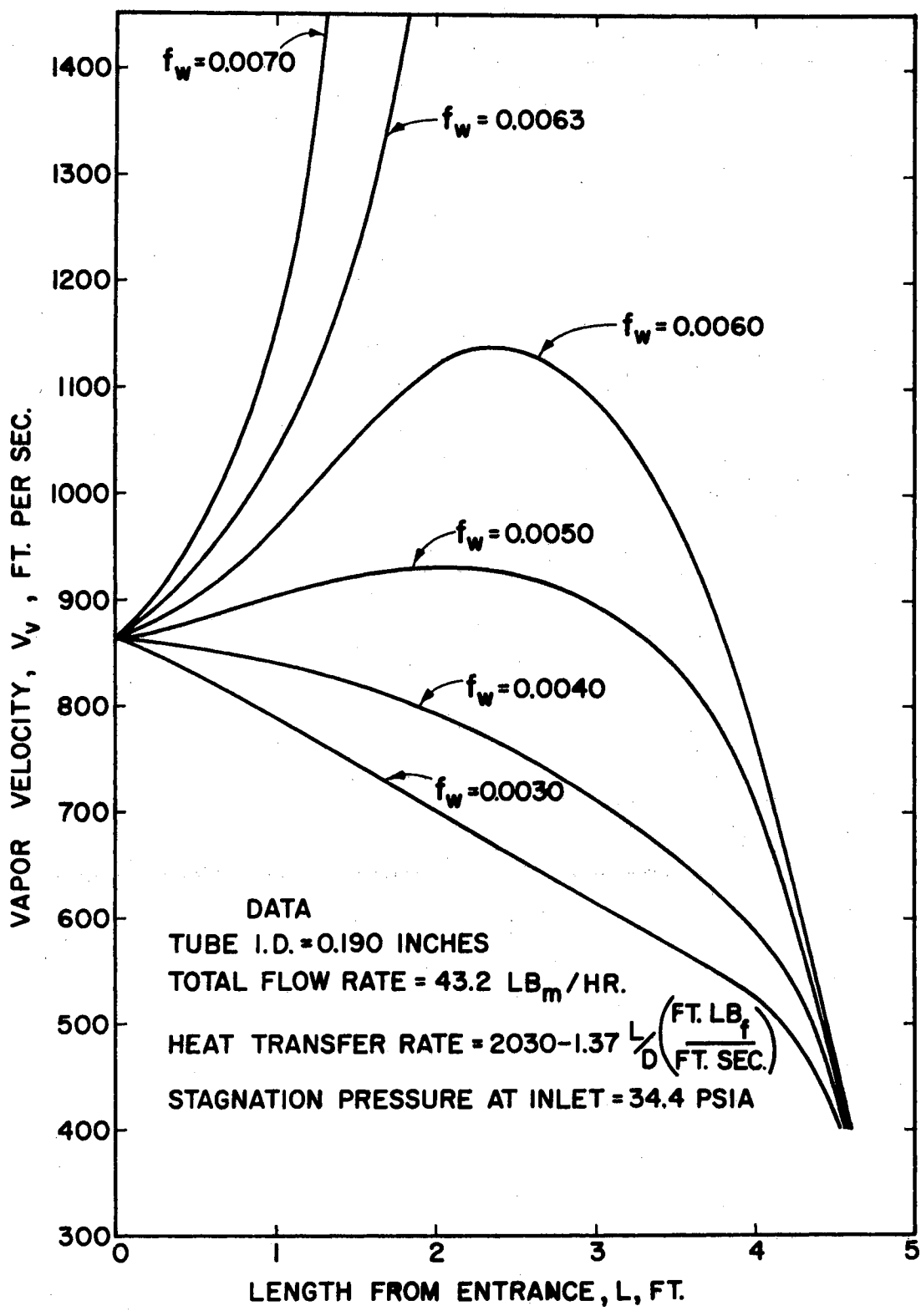
Figure 13. The Effect of Wall Friction Factor on Local Vapor
Velocity; Analytical Solution
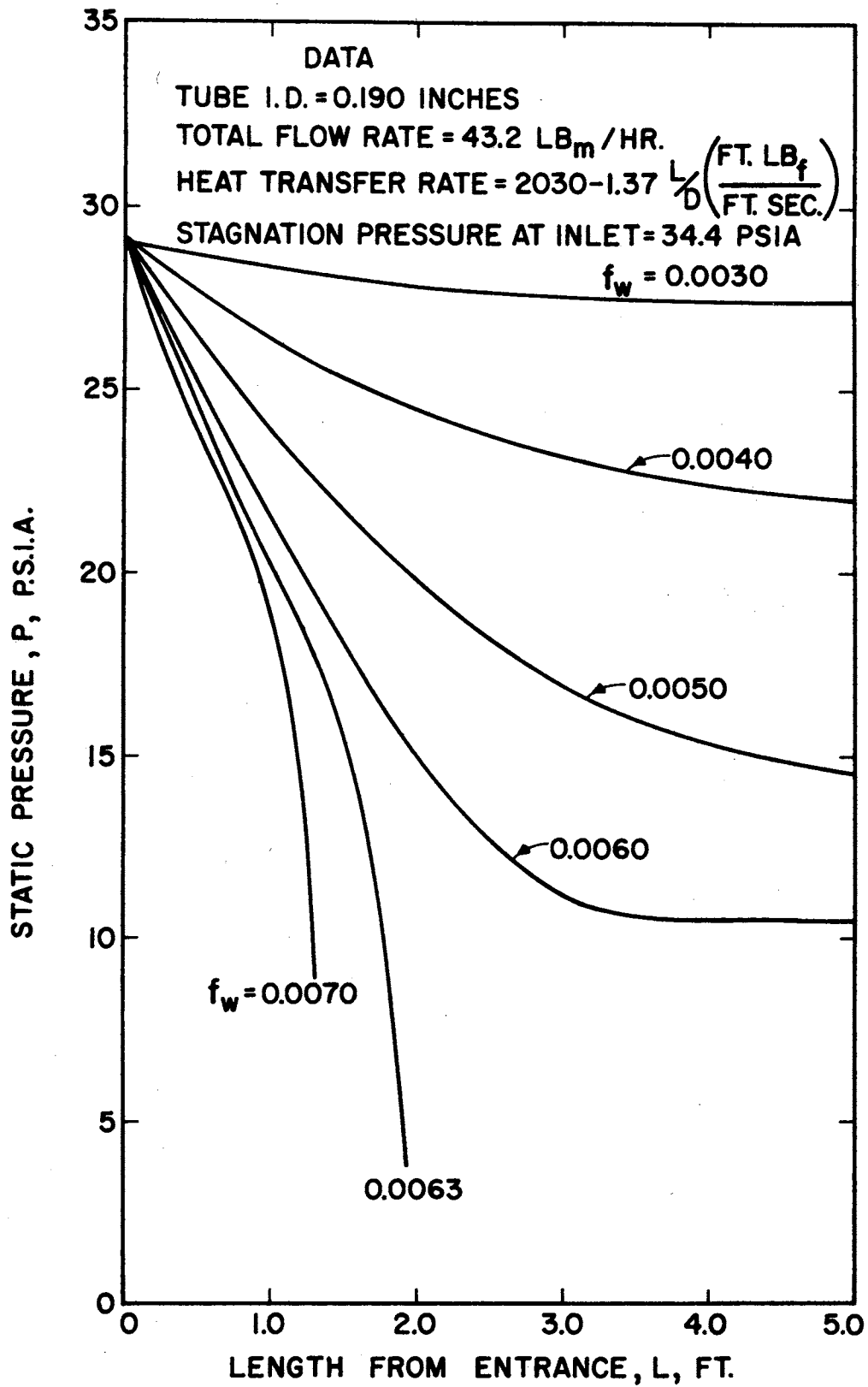
Figure 14. The Effect of Wall Friction Factor on Local
Static Pressure; Analytical Solution
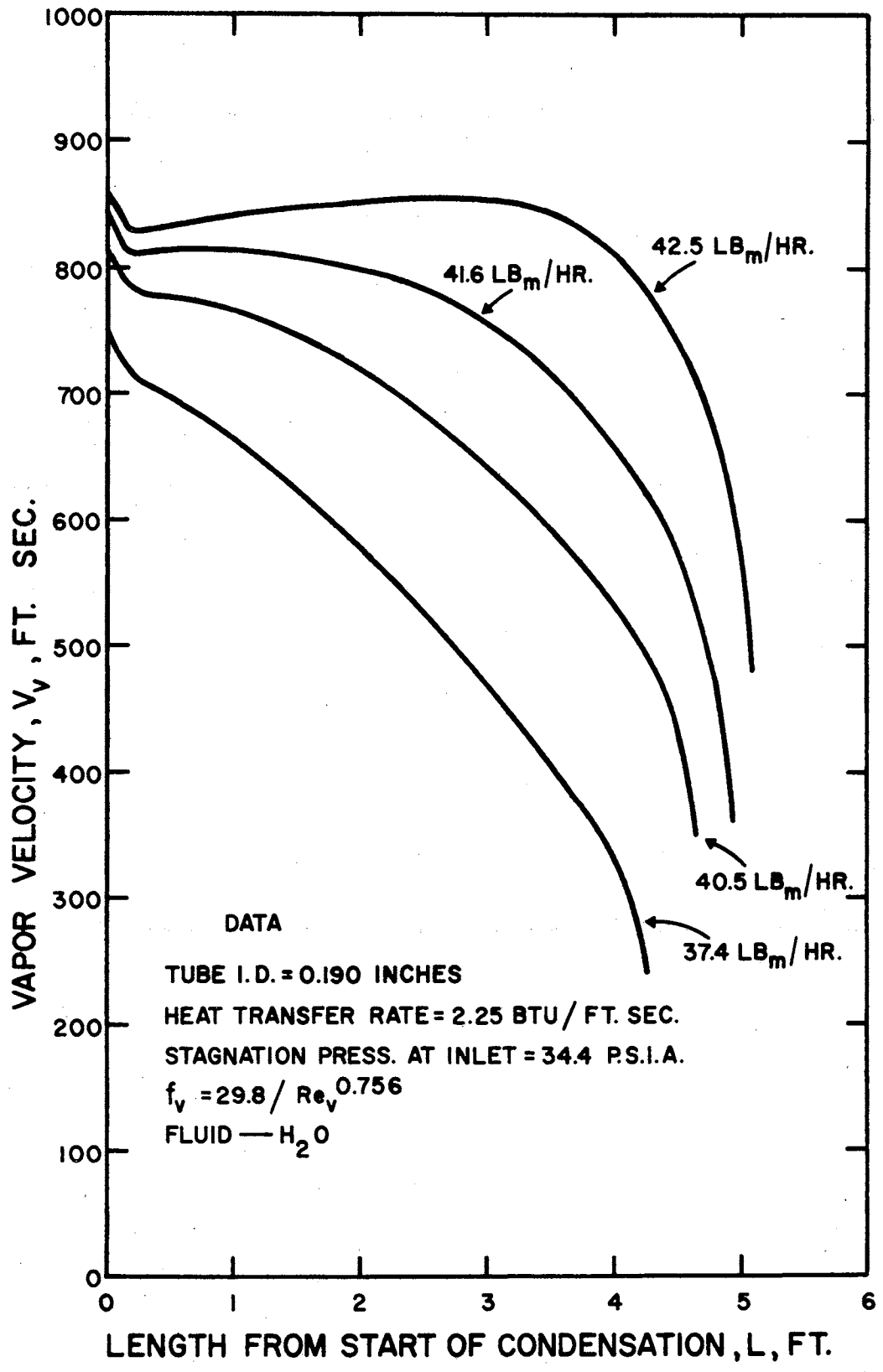
Figure 15. Effect of Total Mass Flow on Local Vapor
Velocity for 0.190 Inch I.D. Tube
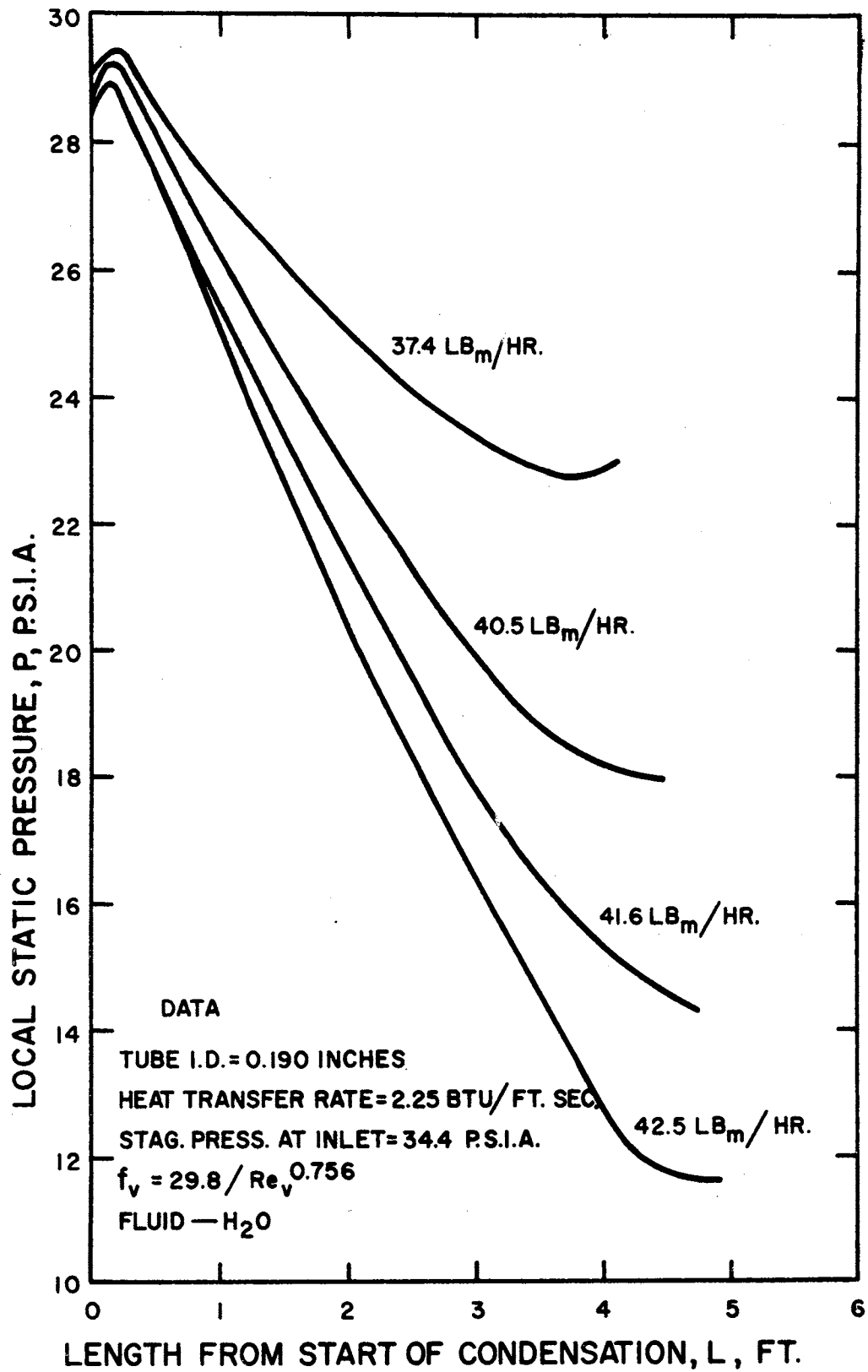
Figure 16. Effect of Total Mass Flow on Local Static
Pressure for 0.190 Inch I.D. Tube
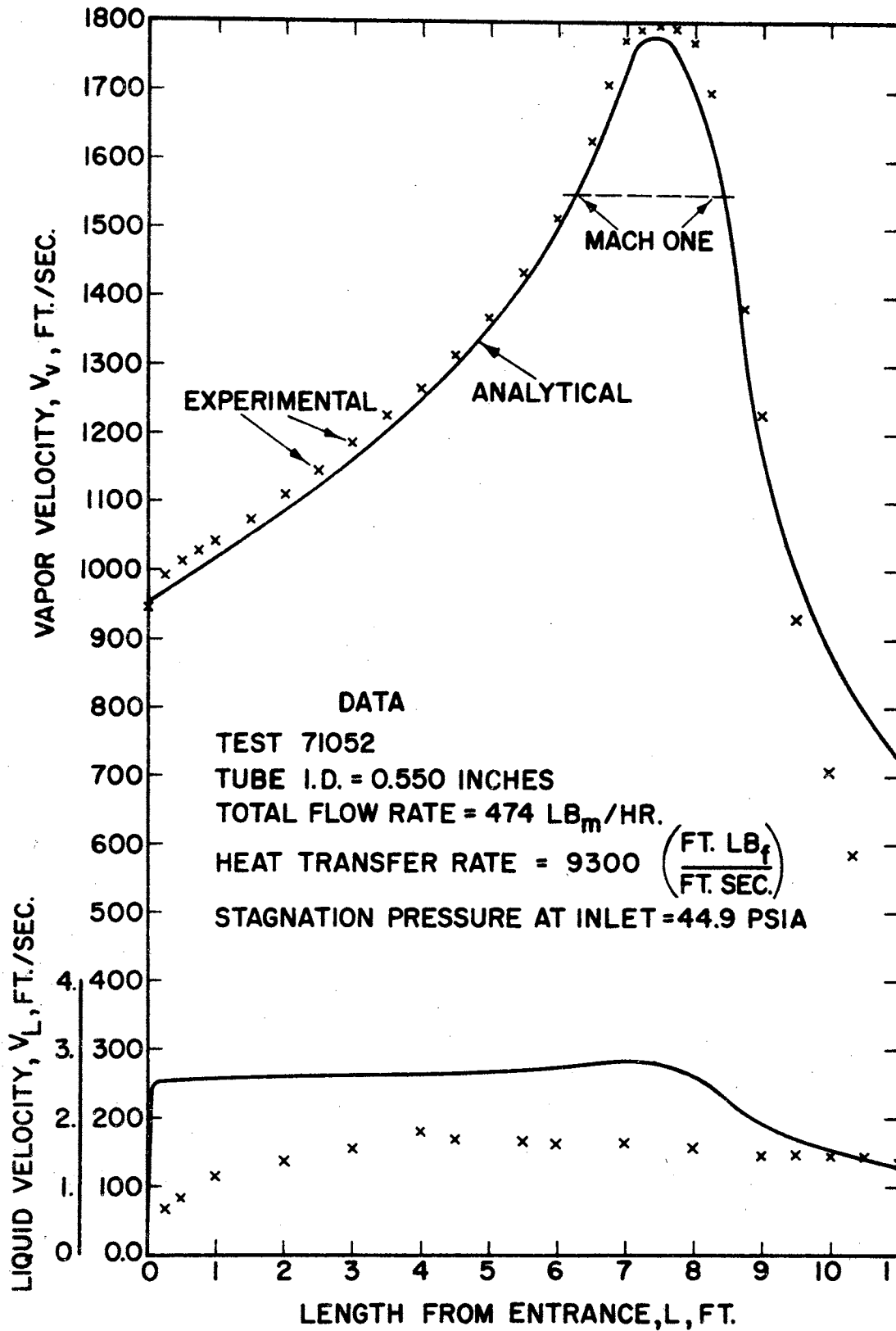
Figure 17. Comparison of Analytical and Experimental Vapor and Liquid Velocities for 0.550 Inch I.D. Tube
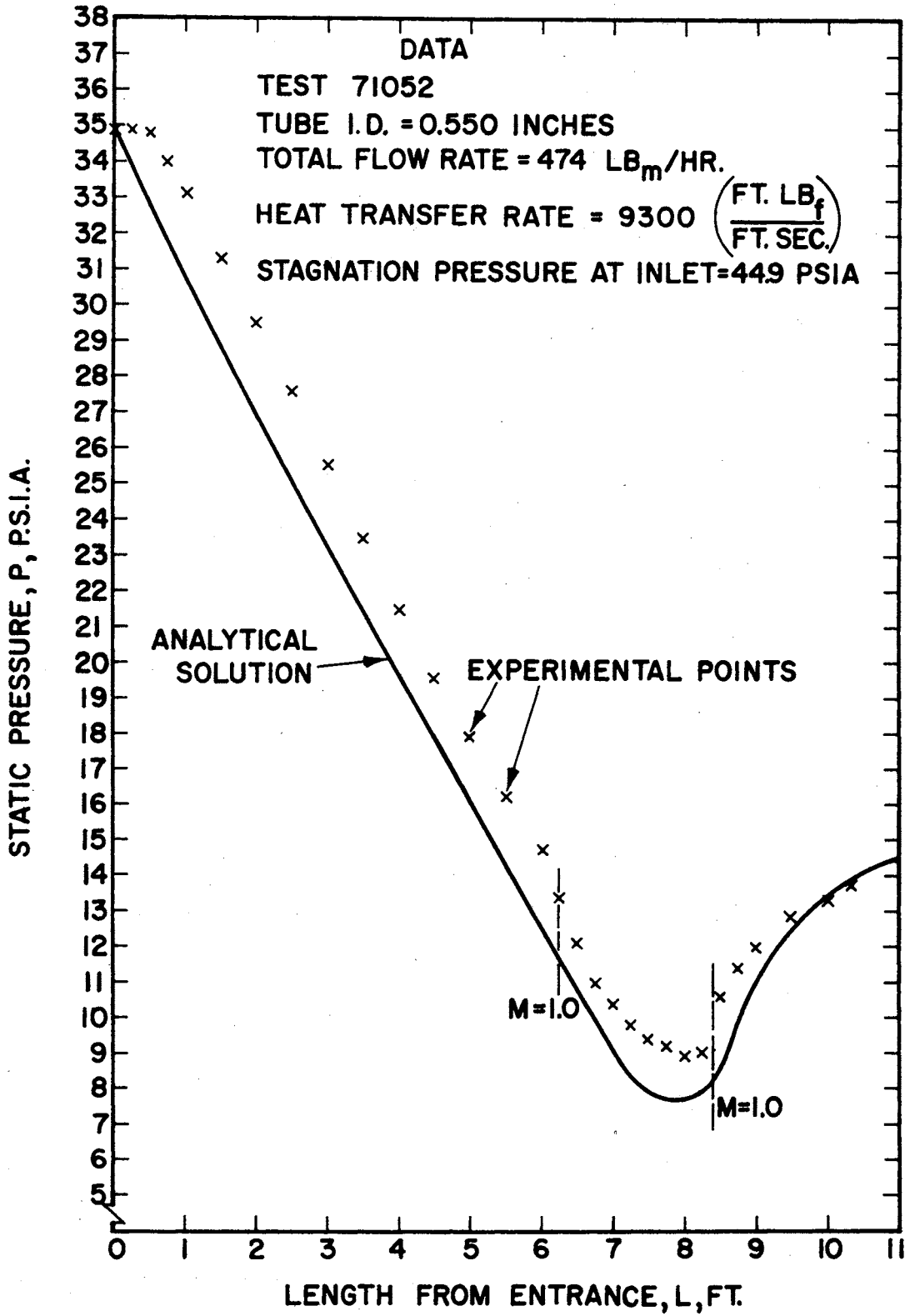
Figure 18. Comparison of Analytical and Experimental Static
Pressures for 0.550 Inch I.D. Tube
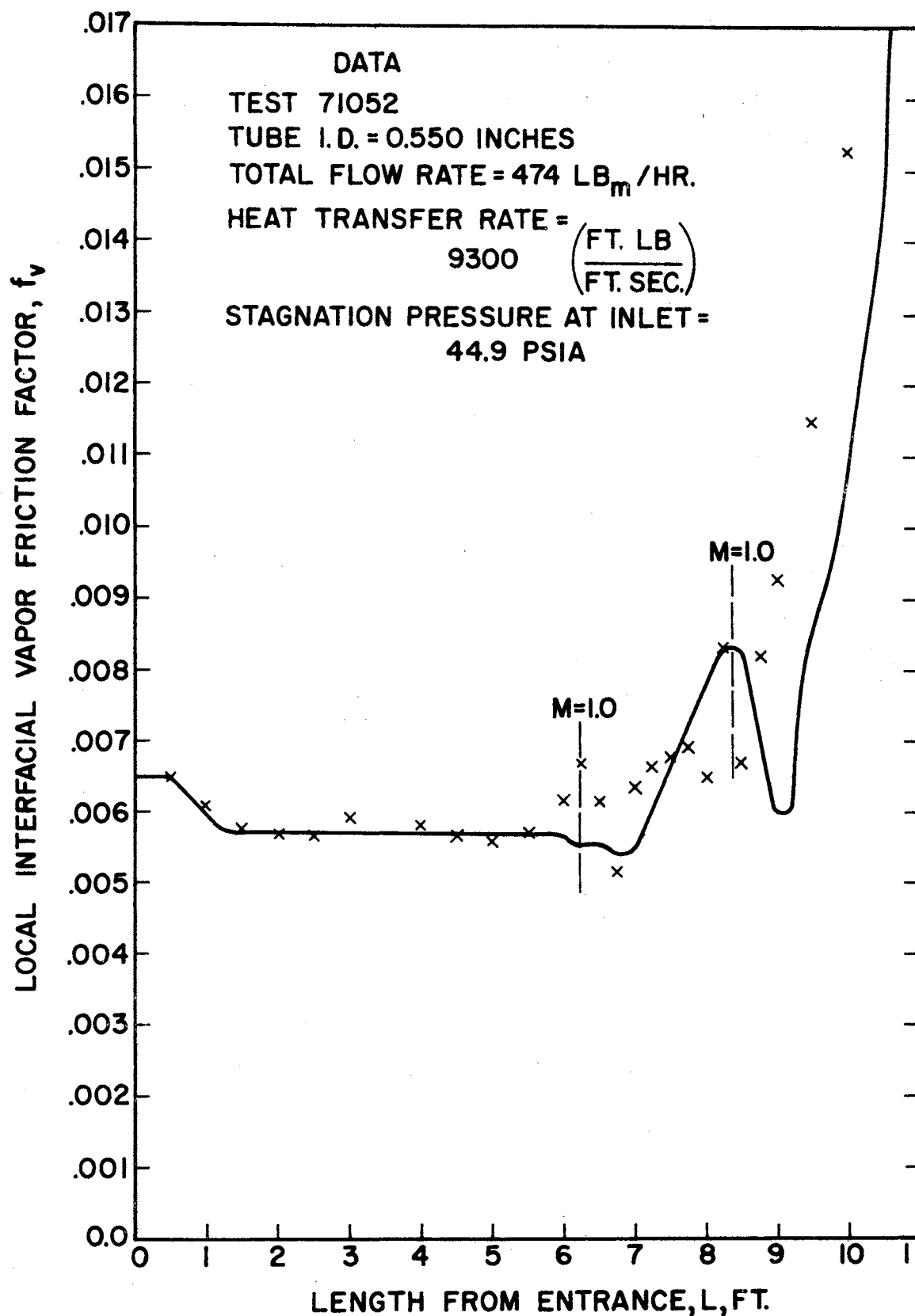
Figure 19.   Comparison of Analytical and Experimental Inter-
facial Friction Factors for 0.550 Inch I.D. Tube
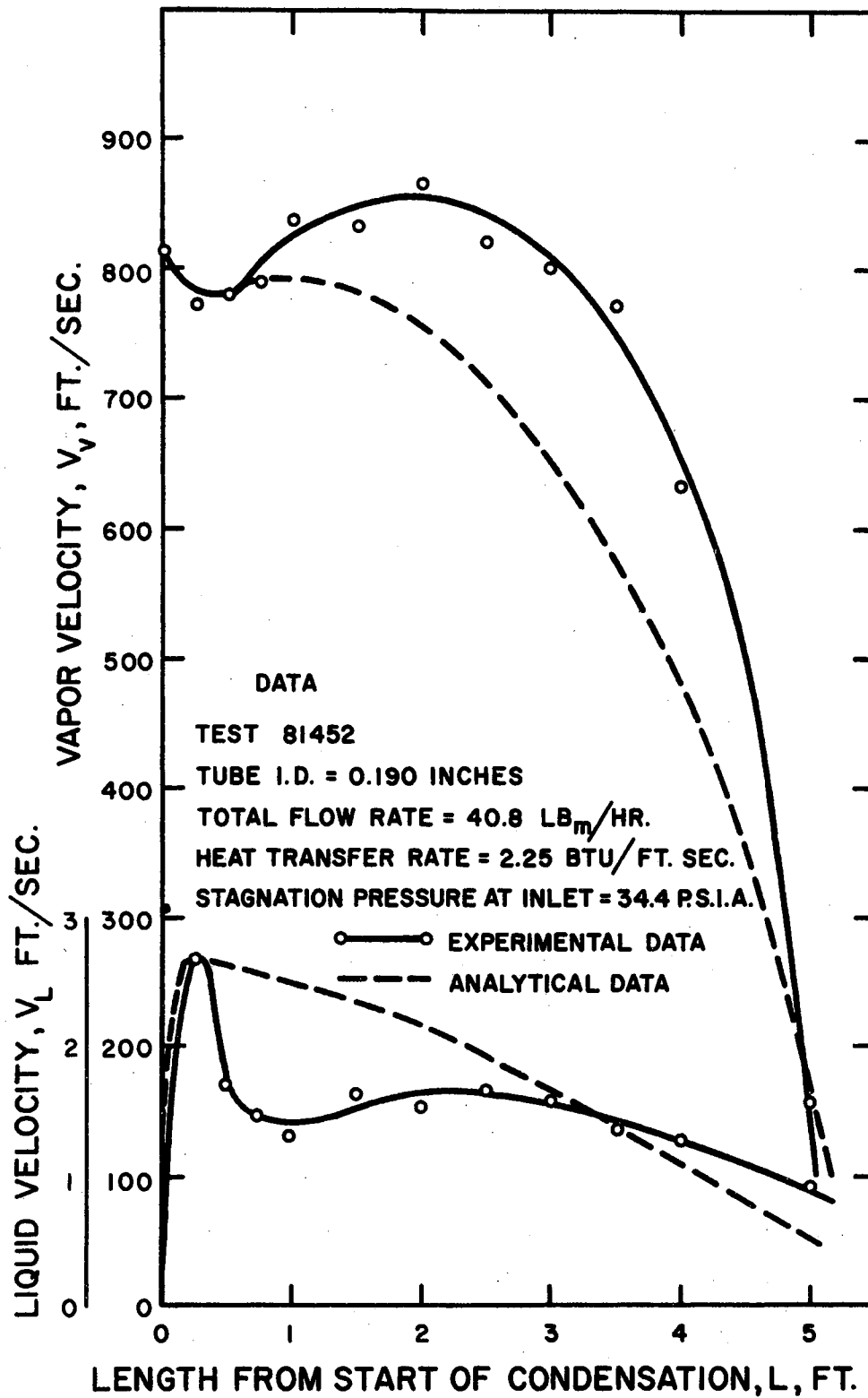
Figure 20.   Comparison of Analytical and Experimental Vapor
and Liquid Velocities for 0.190 Inch I.D. Tube
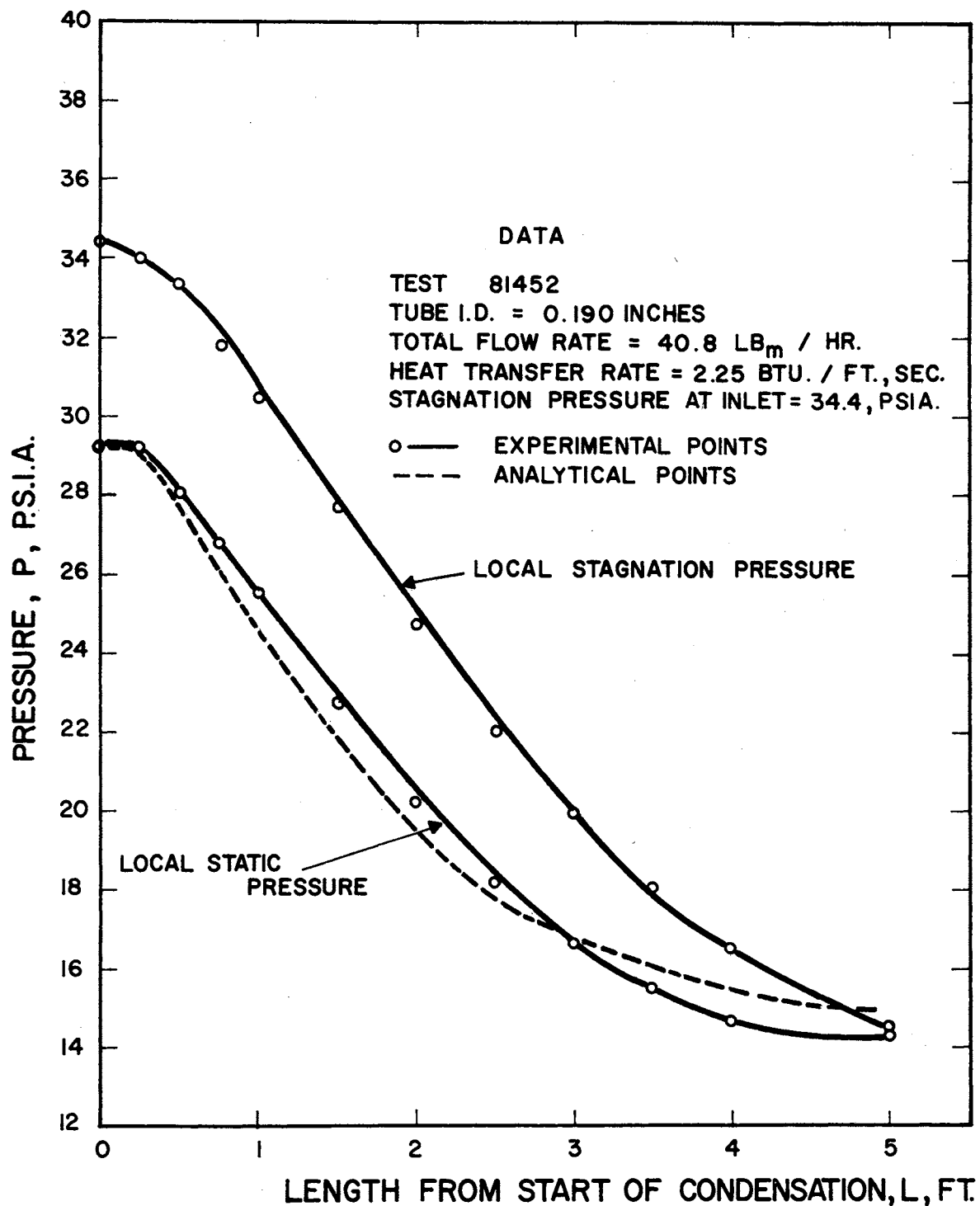
Figure 21.   Comparison of Analytical and Experimental Pressures for
0.190 Inch I.D. Tube
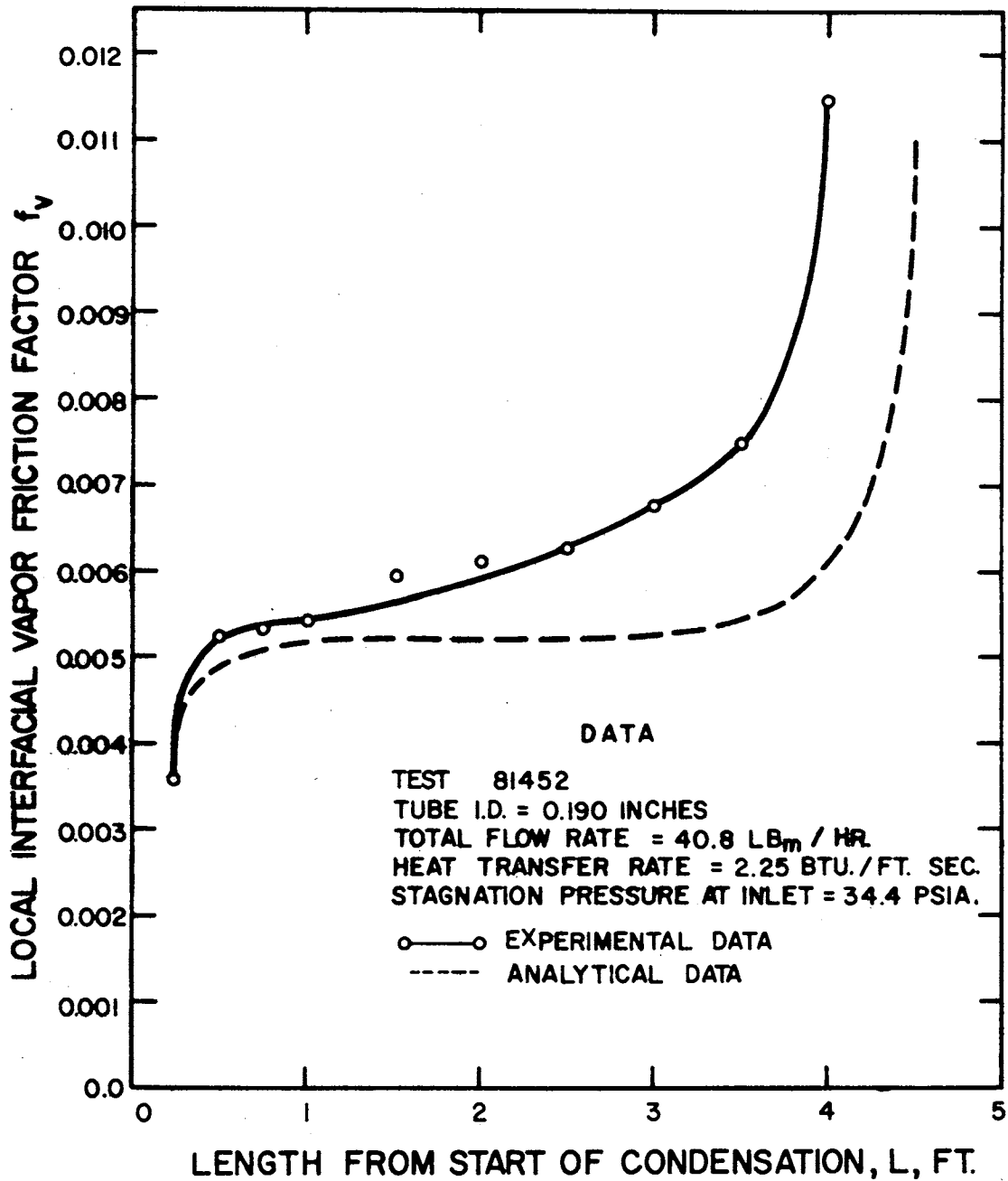
Figure 22. Comparison of Analytical and Experimental Inter-
facial Friction Factors for 0.190 Inch I.D.
Tube
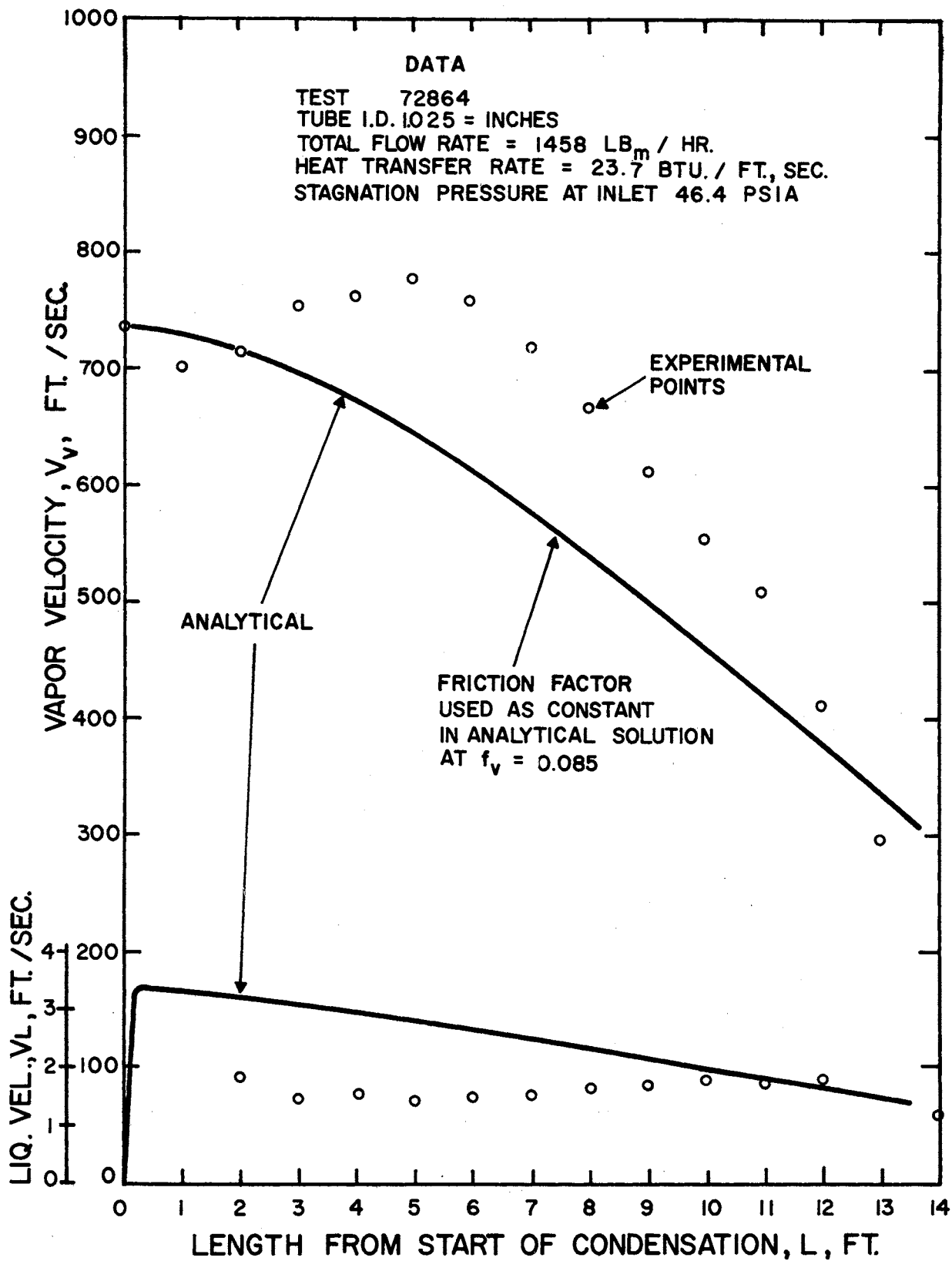
Figure 23. Comparison of Analytical and Experimental Vapor and
Liquid Velocities for 1.025 Inch I.D. Tube
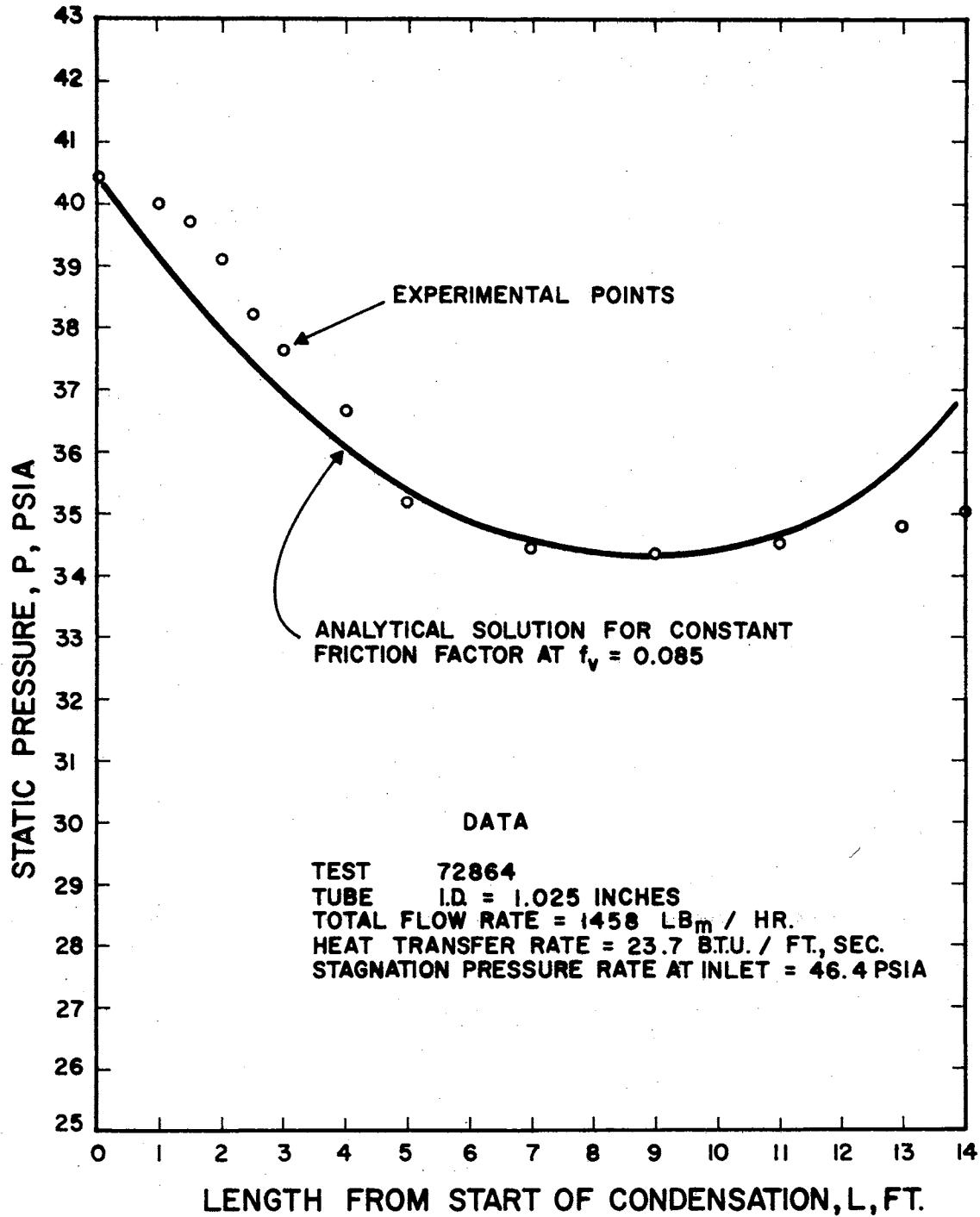
Figure 24. Comparison of Analytical and Experimental Pressures for
1.025 Inch I.D. Tube
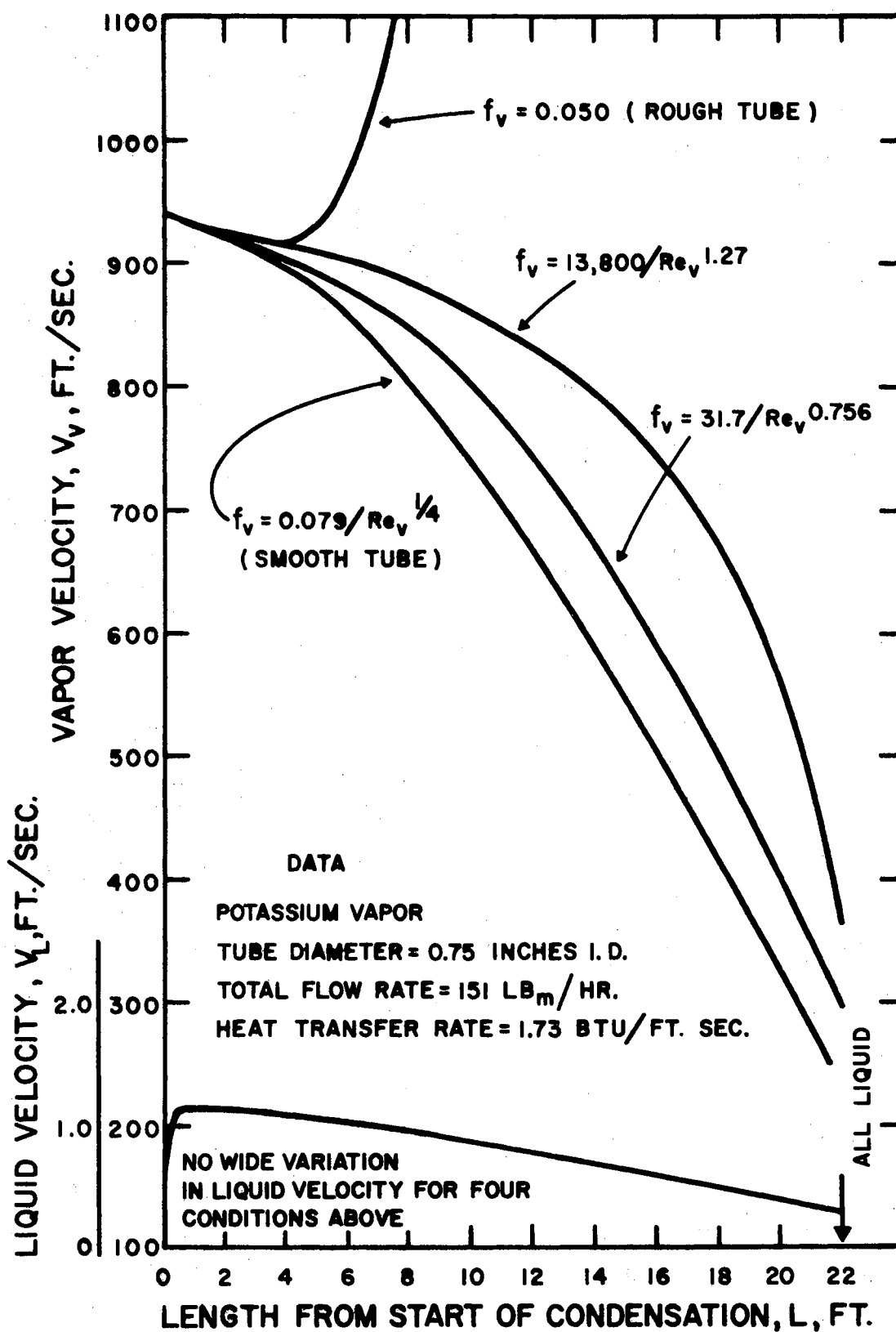
Figure 25. Analytical Vapor and Liquid Velocities Versus
Condensing Length for Potassium
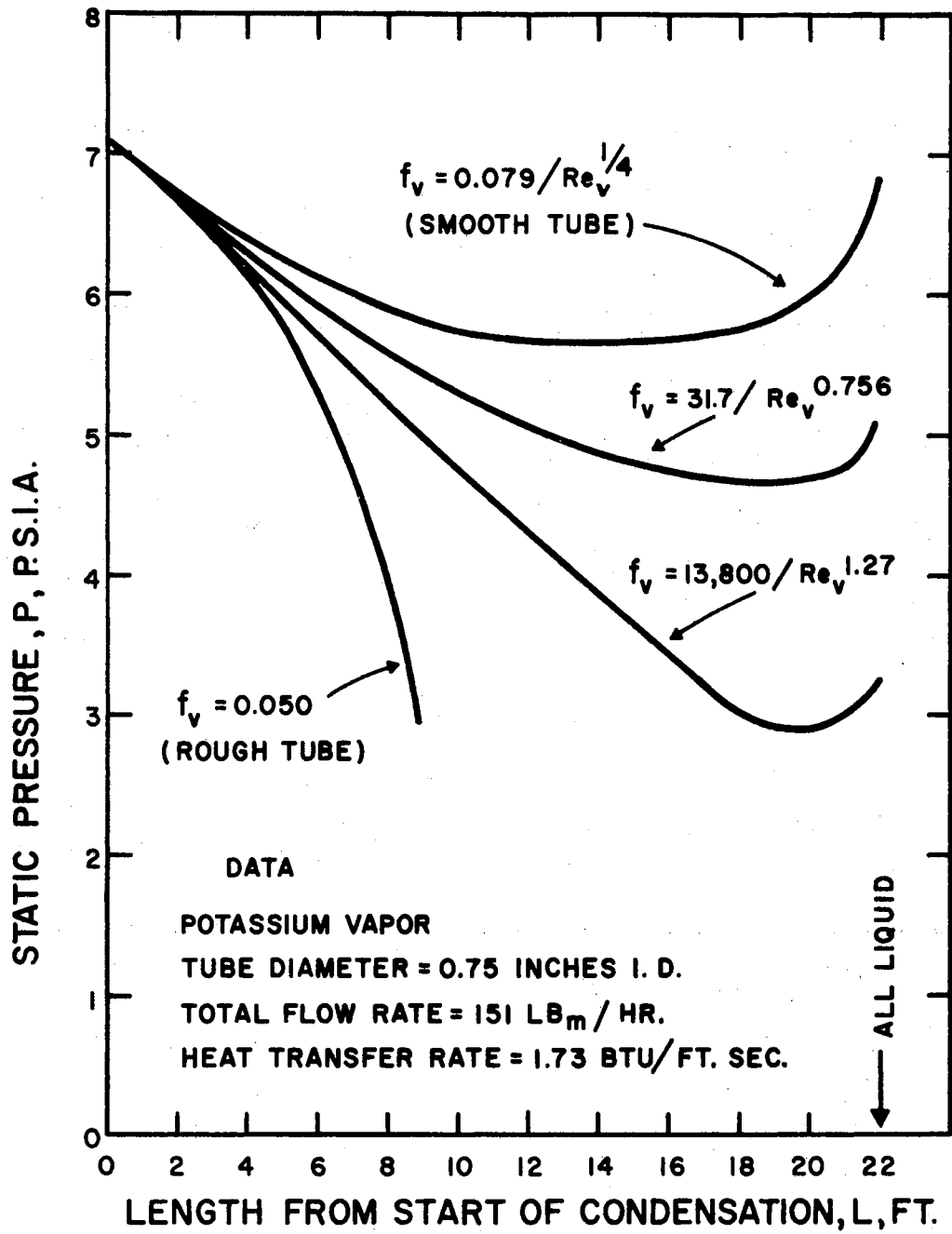
Figure 26. Analytical Static Pressure Versus Condensing
Length for Potassium

several points in this paper, it is recognized that this mathematical model is inexact in several ways. For example, the presence of liquid droplets in the vapor core has been ignored in the analytical development. In addition the two-phase flow is certainly not a simple-coupled one-dimensional system as it has been treated analytically in this paper. The excellent analytical-experimental agreement obtained in spite of these analytical simplifications is gratifying. The success of the present analytical treatment points the way to the development of a more precise analytical attack, which would include consideration of the variable liquid droplet entrainment in the vapor as well as two-dimensional effects of velocity variation of liquid and vapor over the tube cross section. The intermittent interfacial wave action, which is a most complicated phenomenon, also needs to be treated analytically.

One of the most serious obstacles to the success of this work that has been encountered is the problem of the empirical correlation of either the interfacial or wall shear stresses which occur with the condensation of a high velocity pure vapor in a tube. The results of the analysis of this problem (which has been taken up at length in Appendix I) indicate that further investigation of the flow mechanics of the wavy liquid layer, including the laminar sublayer, must be undertaken before a completely satisfactory evaluation of the local wall shear stress for condensing flow can be made. The data presented give a clear indication of the very high degree of turbulence which occurs in the wavy annular liquid layer (see Figs. 46 and 47, pages 154 and 157). The empirical correlation (Fig. 49) obtained from this boundary layer analysis makes possible the prediction of the local wall shear stress of the correct order of magnitude, but a still more precise correlation is needed.

The need for precision in the determination of either the interfacial or wall shear stresses is emphatically demonstrated by Figs. 12 and 14, which show the very sharp change in overall pressure loss that can occur in a condenser tube as a result of a small change in interfacial or wall shear stress. For example, Fig. 14 shows that for a constant wall friction factor of $f_w = 0.004$ an overall pressure loss of 7 psi from 29 psi at entrance is calculated for complete condensation. For $f_w = 0.006$ an overall pressure loss of 18 psi from 29 psi at entrance is calculated for the same condensing length. Thus, an increase in wall friction factor of 50 percent resulted in an increase in overall pressure loss of about 250 percent. This unfavorable effect is directly related to the higher vapor velocities resulting from the decrease in vapor density accompanying the fall in pressure caused by the increase in wall friction. The wall shear stress in turn is almost directly proportional to the square of the vapor velocity. Thus a circle of events is created which tends to magnify the effect of a change in wall friction on the pressure losses occurring with a high velocity condensing vapor. Such sensitivity to wall friction factor would never be encountered in the flow of an incompressible homogeneous fluid. This result clearly demonstrates how important it is to predict the wall shear stress precisely in two-phase condensing flow.

Conclusions

1. In the high velocity condensing flow of a vapor, the vapor velocity and the static pressure may both rise and fall along the condensing length. The local position derivatives of these flow properties may, therefore, be both positive and negative at different axial

locations. Consequently, considerable variation of the local interfacial and wall shear stresses may occur over the length of a condenser tube. For this reason, the use of overall average axial flow properties to estimate overall pressure drop in such a system will be likely to give unreliable results. By the analytical methods developed in this investigation, the pressure distribution over the full axial length of a condenser tube may be determined. Hence, it is analytically possible to determine and compare the effect on pressure distribution of the variation of such factors as: 1) total mass flow rate of fluid, 2) local heat transfer rate, and 3) the apparent roughness of the wavy interfacial surface. Figs. 12,14, and 16 have been included to demonstrate the sharp effect on pressure distribution and overall pressure loss, caused by small variations of these variables.

2. The condensation of a high velocity vapor in annular two-phase flow results in a momentum change which plays a significant role in the determination of both the local interfacial and wall shear stresses. This factor is not usually present in adiabatic, two-component, two-phase flow.

3. The presence of a very high level of turbulence (e.g., $I_T \simeq 1$) in the annular liquid layer surrounding a high velocity condensing vapor has been demonstrated (see Appendix I, page 163). As a result of this turbulence, a thin laminar liquid sublayer of a thickness of the order of $y^+ \simeq 1$ evidently exists over the major portion of the condensing length. Because of the high turbulence and the resulting thin laminar sublayer, both the local wall shear stress and the surface coefficient of heat transfer have values as much as an order of magnitude, or more, greater than those found in single phase flow in a smooth tube for the same mass

flow rate of fluid per unit cross section.

4. An empirical correlation for wall shear stress has been de-
veloped (Fig. 49, page 161) which may be used to predict the local wall
shear stress necessary for a stepwise analytical solution of
the mechanics of the complete condensing process.

5. An empirical correlation for the local heat transfer co-
efficient in high velocity condensation is presented (Fig. 50, page 170).
However, the correlation applies specifically to the condensation of
H_2O vapor in the two tube sizes for which data are given. Additional
work needs to be done to generalize the correlation to other vapors and
a wider range of tube sizes.

6. The effect of the acceleration and/or deceleration of vapor and
liquid, as well as momentum change during condensation, on the mechanics
of two-phase flow with high vapor velocities needs to be investigated.

7. Under certain conditions of high velocity flow with boiling, it
has been shown that annular two-phase flow can occur. For these condi-
tions the analytical methods developed in this investigation could
also be applied with some modifications. The method of numerical in-
tegration of the system of equations developed can proceed equally well
in either direction--i.e., for either condensing or boiling flow. It
remains to be demonstrated whether the annular mathematical model, em-
ployed with reasonable success for condensing flow in this investigation,
can also give useful results for boiling flow.

BIBLIOGRAPHY

(1) Bergelin, O. P., and C. Gazley, Jr., "Co-Current Gas Liquid Flow,
        I. Flow in Horizontal Tubes," Heat Transfer and Fluid Mechan-
        ics Institute, 1949, pp. 5-18.

(2) Bergelin, O. P., P. K. Kegel, F. G. Carpenter, and C. Gazley, Jr.,
        "Co-Current Gas Liquid Flow, II. Flow in Vertical Tubes,"
        Heat Transfer and Fluid Mechanics Institute, 1949, pp. 19-28.

(3) Boelter, L. M. K., and R. H. Kepner, "Pressure Drop Accompanying
        Two-Component Flow Through Pipes," Industrial Engineering
        Chemistry, No. 31, 1939, pp. 426-434.

(4) Burbank, A., and W. E. Hilding, "The Initial Boundary Layer Equa-
        tion With Wall Shear Stress Expressed as a Function of the
        Vapor Reynolds Number," Technical Note, Mechanical Engineering
        Department, the University of Connecticut, March 1963, 6 pp.

(5) Calvert, S., "Vertical Upward, Annular, Two-Phase Flow in Smooth
        Tubes," Ph.D. thesis, University of Michigan, 1952.

(6) Carpenter, F. G., "Heat Transfer and Pressure Drop for Condensing
        Pure Vapors Inside Vertical Tubes at High Vapor Velocities,"
        Ph.D. thesis, University of Delaware, 1948.

(7) Charvonia, D. A., "A Study of the Mean Thickness of the Liquid
        Film and the Characteristics of the Interfacial Surface in
        Annular Two-Phase Flow in a Vertical Pipe," Jet Propulsion
        Center, Report No. I-59-I, Purdue University, May 1959.

(8) Chien, S. F., and W. Ibele, "Pressure Drop and Liquid Film Thick-
        ness of Two-Phase Annular and Annular-Mist Flows," Journal of
        Heat Transfer, Trans. ASME, Series C, vol. 86, 1964, pp. 89-96.

(9) Coogan, C. H. Jr., and W. E. Hilding, "A Study and Analysis of the
        Problem of Condensing the Maximum Amount of Steam in Small
        Diameter Long Tubes," Report to Pratt & Whitney Aircraft,
        Division of United Aircraft Co., June 17, 1952, 35 pp.

(10) Coogan, C. H. Jr., and W. E. Hilding, "Heat Transfer Studies on
        Steam Condensation in Small Tubes," Final Summary Report to
        Pratt & Whitney Aircraft, Division of United Aircraft Co.,
        from the University of Connecticut, October 1952.

(11) Coogan, C. H. Jr., and W. E. Hilding, "Heat Transfer Studies on
Steam Condensation in Small Tubes," Final Summary Report to
Pratt & Whitney Aircraft, Division of United Aircraft Co.,
from the University of Connecticut, November 1953.

(12) Dukler, A. E., "Dynamics of Vertical Falling Film Systems," Chemi-
cal Engineering Progress, vol. 55, No. 10, 1959, October 1959,
pp. 62-67.

(13) Dukler, A. E., and O. P. Bergelin, "Characteristics of Flow in
Falling Liquid Films," Chemical Engineering Progress, vol. 48,
1952, pp. 557-563.

(14) Dukler, A. E., M. Wicks, III, and R. G. Cleveland, "Frictional
Pressure Drop in Two-Phase Flow: Part B, An Approach Through
Similarity Analysis," A.I.Ch.E. Journal, vol. 10, No. 1, 1964,
p. 44.

(15) Dussourd, J. L., "A Theoretical and Experimental Investigation of
a Deceleration Probe for Measurement of Several Properties of
a Droplet Laden Stream," Sc.D. thesis, M.I.T., October 1954.

(16) Fauske, H., "Critical Two-Phase Steam Water Flow," Heat Transfer
and Fluid Mechanics Institute, 1961.

(17) Gazley, C. Jr., "Co-Current Gas Liquid Flow, III. Interfacial
Shear and Stability," Heat Transfer and Fluid Mechanics
Institute, 1949, pp. 29-40.

(18) Hilding, W. E., et al., "Final Report on an Experimental and
Analytical Study of the Heat Transfer and Pressure Drop of
Vapor Condensing at High Velocities in Small Straight Tubes,"
Report to NASA from the University of Connecticut, October 31,
1963, 265 pp.

(19) Hilding, W. E., et al., "Experimental Determination of the Quantity
of Liquid Particle Entrainment in the Vapor Core in Annular
Two-Phase Flow," Interim Progress Report to NASA from the
University of Connecticut, June 1965, pp. 6-11.

(20) Hughmark, G. S., "Heat Transfer in Horizontal Annular Gas-Liquid
Flow," Chemical Engineering Progress Symposium Series, 57,
vol. 61, 1965, p. 176.

(21) Jacowitz, L. A., "An Analysis of the Geometry and Pressure Drop for
the Annular Flow of Gas-Liquid Systems," Doctoral Dissertation,
Ohio State University, 1962.

(22) Jakob, M., Heat Transfer, vol. I, John Wiley and Sons, New York,
1949.

(23) Keenan, J. H., and F. G. Keyes, Thermodynamic Properties of Steam,
John Wiley and Sons, New York, 1952.

(24) Kegel, P. K., "Two-Phase Flow in a Vertical Column," B.Ch.E. thesis, University of Delaware, 1948.

(25) Kutateladze, S. S., Fundamentals of Heat Transfer, Second Edition, English Translation, Academic Press, New York, 1963.

(26) Levy, S., "Theory of Pressure Drop and Heat Transfer for Annular Steady-State, Two-Phase, Two-Component Flow in Pipes," Second Midwestern Conference on Fluid Mechanics, Proceedings, 1952.

(27) Levy, S., "Steam Slip-Theoretical Prediction From Momentum Model," Journal of Heat Transfer, Trans. ASME, Series C, vol. 82, 1960, p. 113.

(28) Levy, S., "Prediction of Two-Phase Pressure Drop and Density Distribution From Mixing Length Theory," Journal of Heat Transfer, Trans. ASME, vol. 85, Series C, 1963, pp. 137-152.

(29) Lockhart, R. W., and R. C. Martinelli, "Proposed Correlation of Data for Isothermal Two-Phase, Two-Component Flow in Pipes," Chemical Engineering Progress, vol. 45, 1949, pp. 39-48.

(30) Powell, C. K., "Condensation Inside a Horizontal Tube With High Vapor Velocity," Masters thesis, Purdue University, 1961.

(31) Robson, F. L., and W. E. Hilding, "Experimental Measurements of the Wave Characteristics of Condensing Flow in a Horizontal Tube," Part I of Final Report to NASA from the University of Connecticut, December 1965, 119 pp.

(32) Schlichting, H., Boundary Layer Theory, Fourth Edition, McGraw Hill, New York, 1960.

(33) Shapiro, A. H., The Dynamics and Thermodynamics of Compressible Fluid Flow, vol. I, The Ronald Press, New York, 1953.

APPENDIX A

EMPIRICAL EXPRESSIONS FOR THE PHYSICAL PROPERTIES OF

SATURATED VAPOR AND OF SATURATED LIQUID

For the two-phase system with condensing pure vapors, it was assumed
that the two phases present were continuously in equilibrium at the satu-
ration state of the respective phase. For a rapidly expanding vapor
near the entrance of a condenser tube this assumption may not always be
true. It is well known that a dry saturated vapor may expand well into
the saturated region before condensation begins at the so-called "Wilson
Line." In the normal condenser tube this condition of supersaturation
may or may not exist near the entrance to the tube. The qualit1tive ex-
perimental evidence observed during this investigation indicated that the
region of supersaturation will usually constitute a very short section
near the mouth of the condenser tube, and therefore a detailed examination
of this very local phenomenon was not included in this investigation.
After condensation has begun, the presence of liquid droplets as fog or
mist in the vapor tends to insure a continuous, near equilibrium state for
the saturated vapor.

For the liquid layer on the inside tube surface, it is necessary that
a temperature gradient exist in the direction normal to the tube surface.
The degree of subcooling in the liquid layer will depend on the thickness
of the layer, the rate of heat transfer, and the degree of turbulence in
the layer. Since the physical properties of the liquid are not sharply

60

affected by small variations in pressure or temperature, the effect of subcooling on the physical properties in the liquid layer has been neglected.

By plotting the available data on logarithmic graph paper it was discovered that simple empirical functions could be used to represent the physical and thermodynamic properties of the pure saturated vapor and liquid over moderate pressure ranges with satisfactory accuracy. The various properties have been expressed as simple power functions of the saturation pressure in each case. The value of the resulting pressure exponent for a particular property is not necessarily constant over a large range of pressures. Examination of such exponents, plotted in Figs. 27 through 29 for H_2O and Figs. 30 through 34 for potassium, indicates that no significant error will be incurred over the range of pressures encountered in any normal condenser tube by use of a mean value of the empirical exponent for the particular range of pressures involved (see also the discussion on page 18, Chapter II). The necessary functions are listed below.

(1) <u>Specific Enthalpy of Saturated Liquid</u>

Assuming the empirical function

$$h_L = C_1 P^a \tag{1A}$$

therefore,

$$h_L/h_{Le} = P/P_e{}^a \equiv \phi^a \tag{2A}$$

where the term ϕ has been introduced as the non-dimensional local pressure ($\phi = P/P_e$). Equation (2A) may also be written in the form

$$h_L = h_{Le}\phi^a \tag{3A}$$
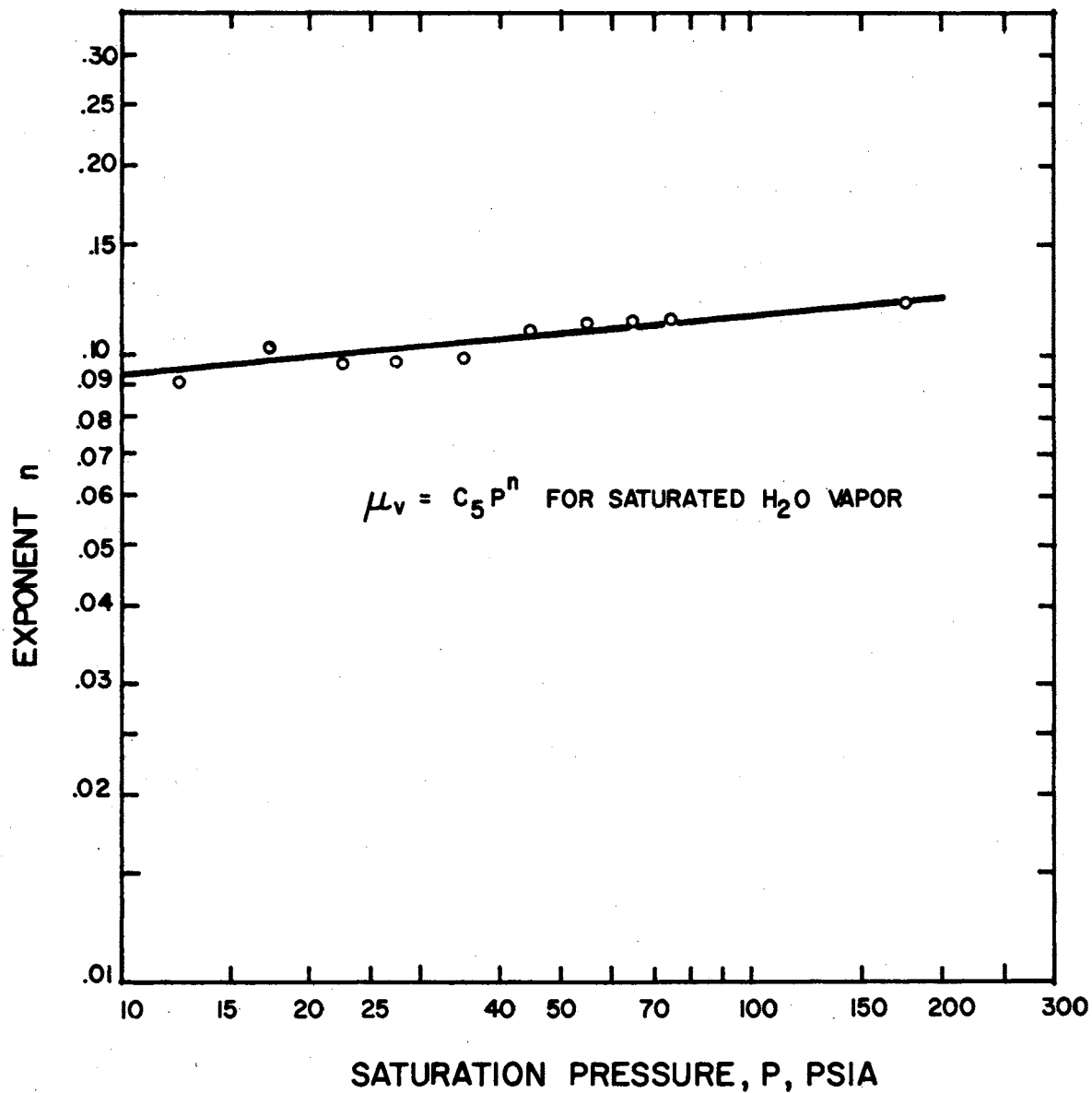
Figure 27. Exponent for Pressure Function for Vapor Viscosity of Saturated Water Vapor
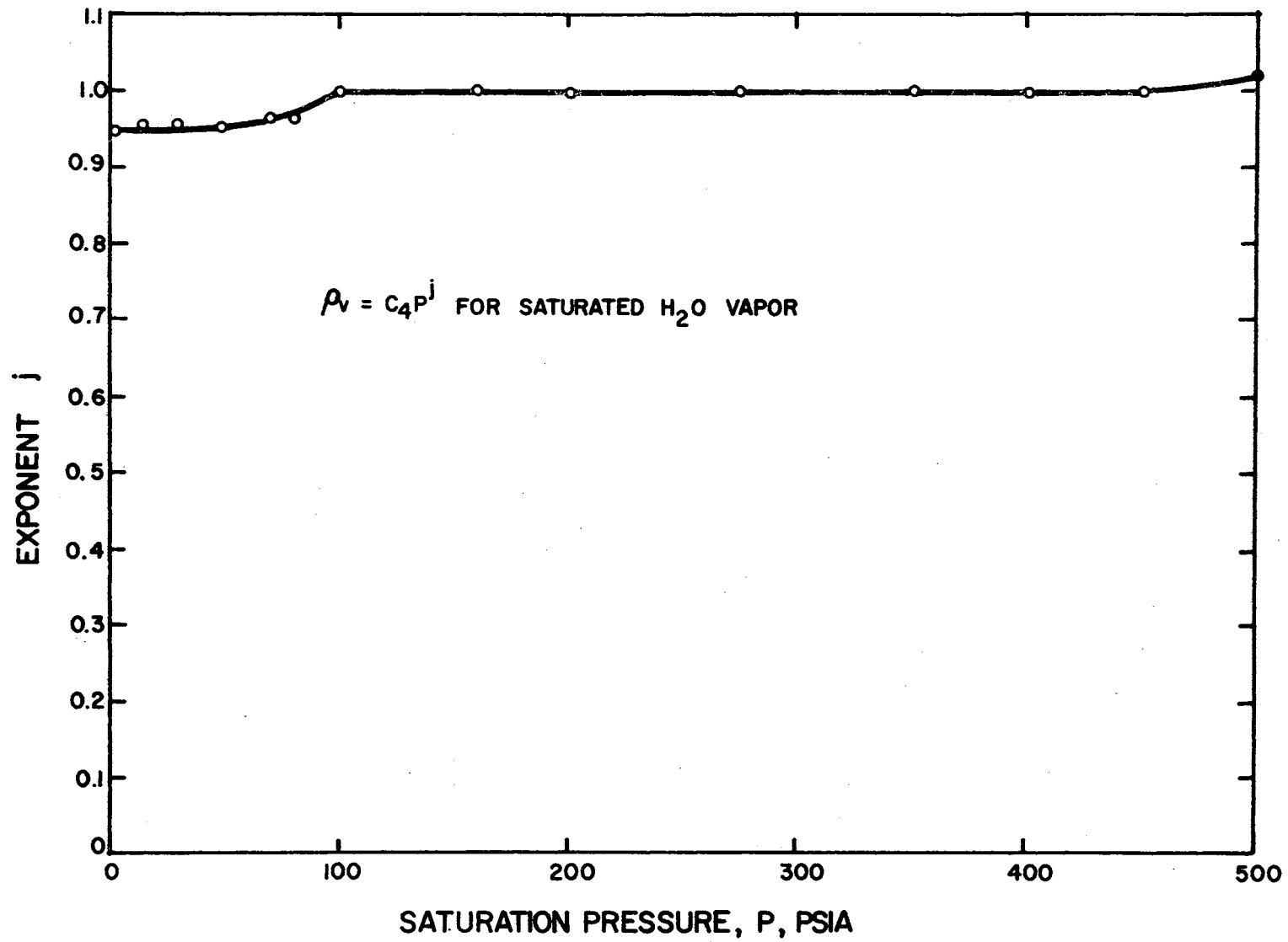
Figure 28. Exponent for Pressure Function for Vapor Density of Saturated Water Vapor
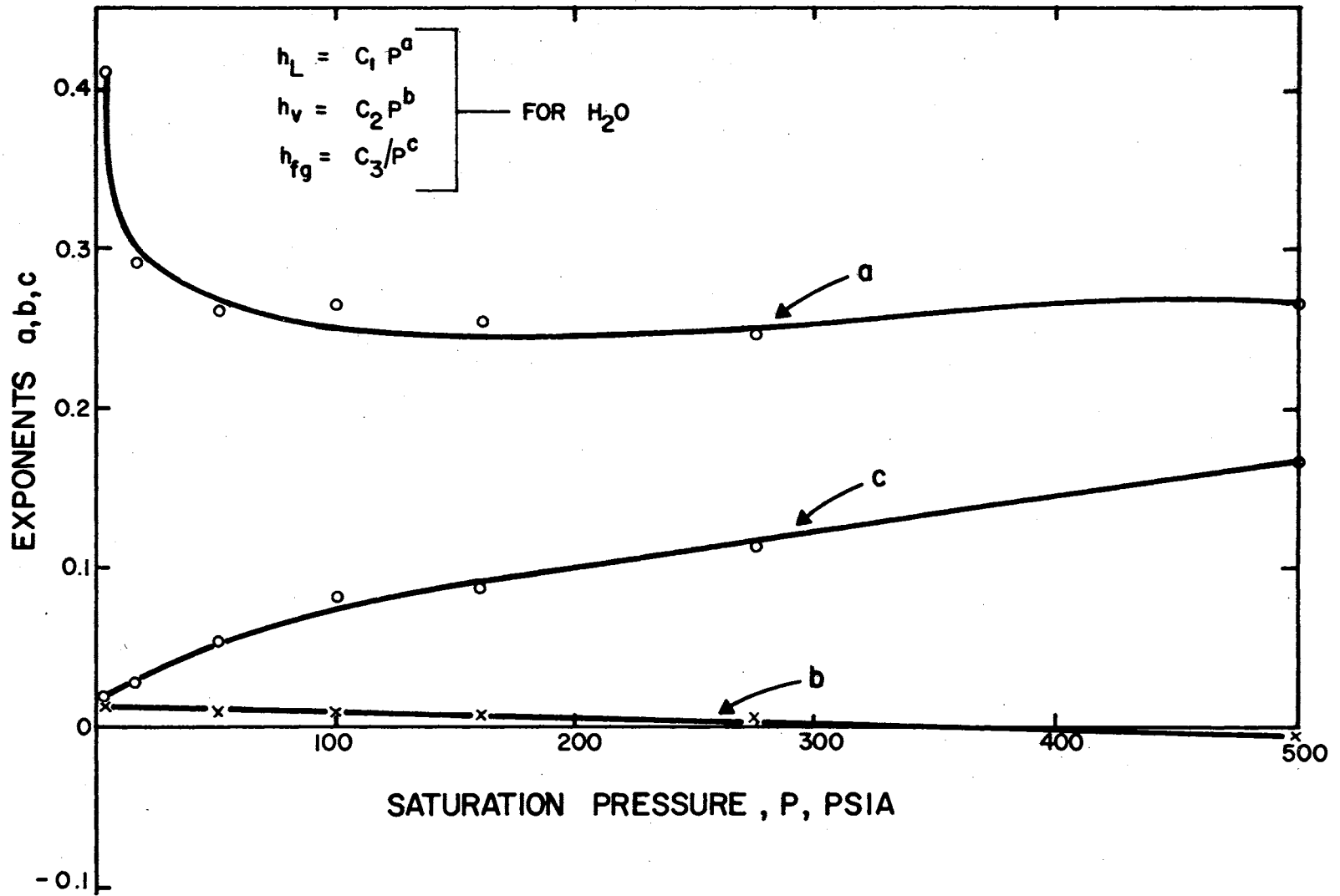
Figure 29. Exponents for Enthalpy-Pressure Functions for Water
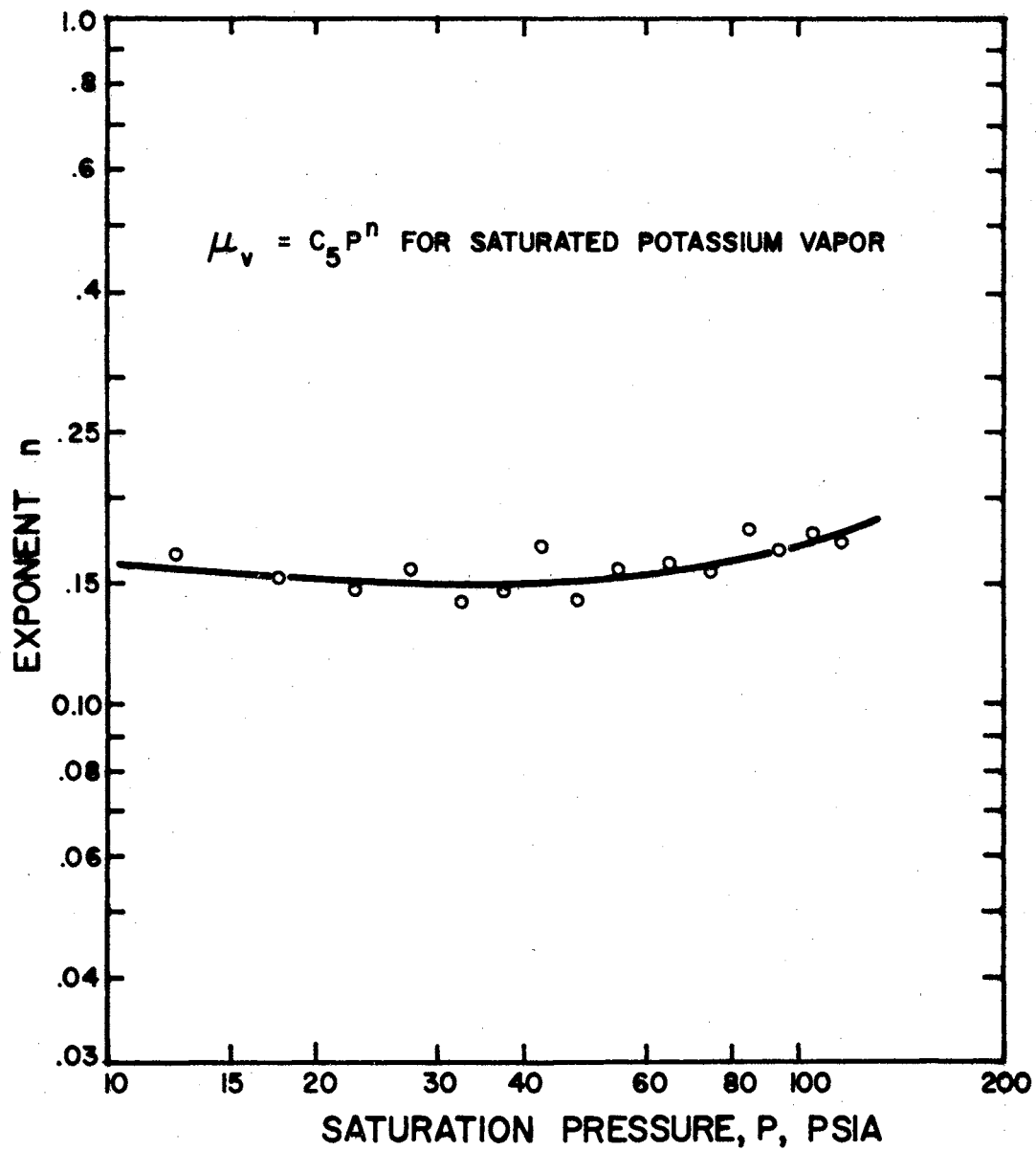
Figure 30. Exponent for Pressure Function for Vapor
Viscosity of Saturated Potassium Vapor
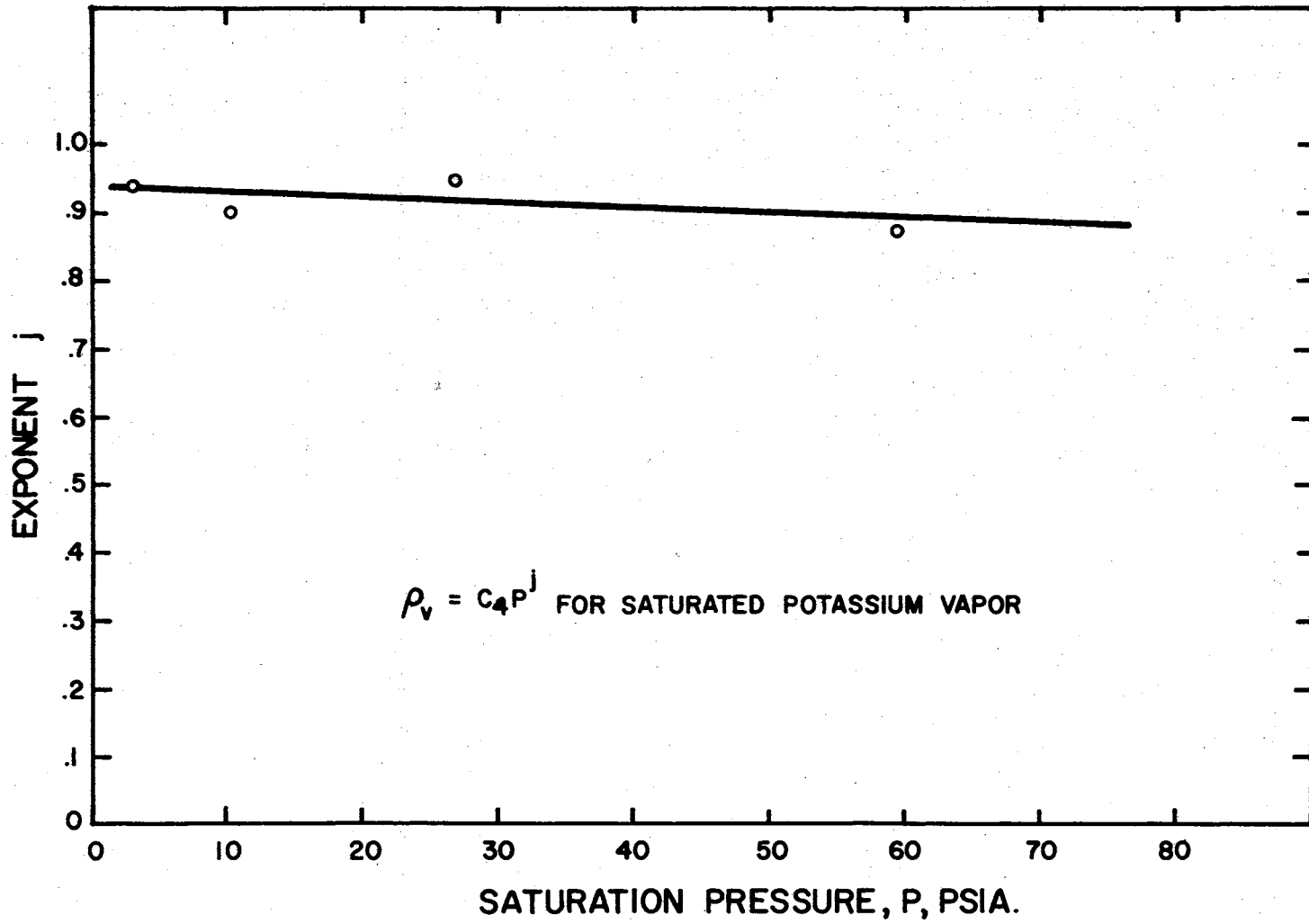
Figure 31. Exponent for Pressure Function for Vapor Density of Saturated Potassium Vapor
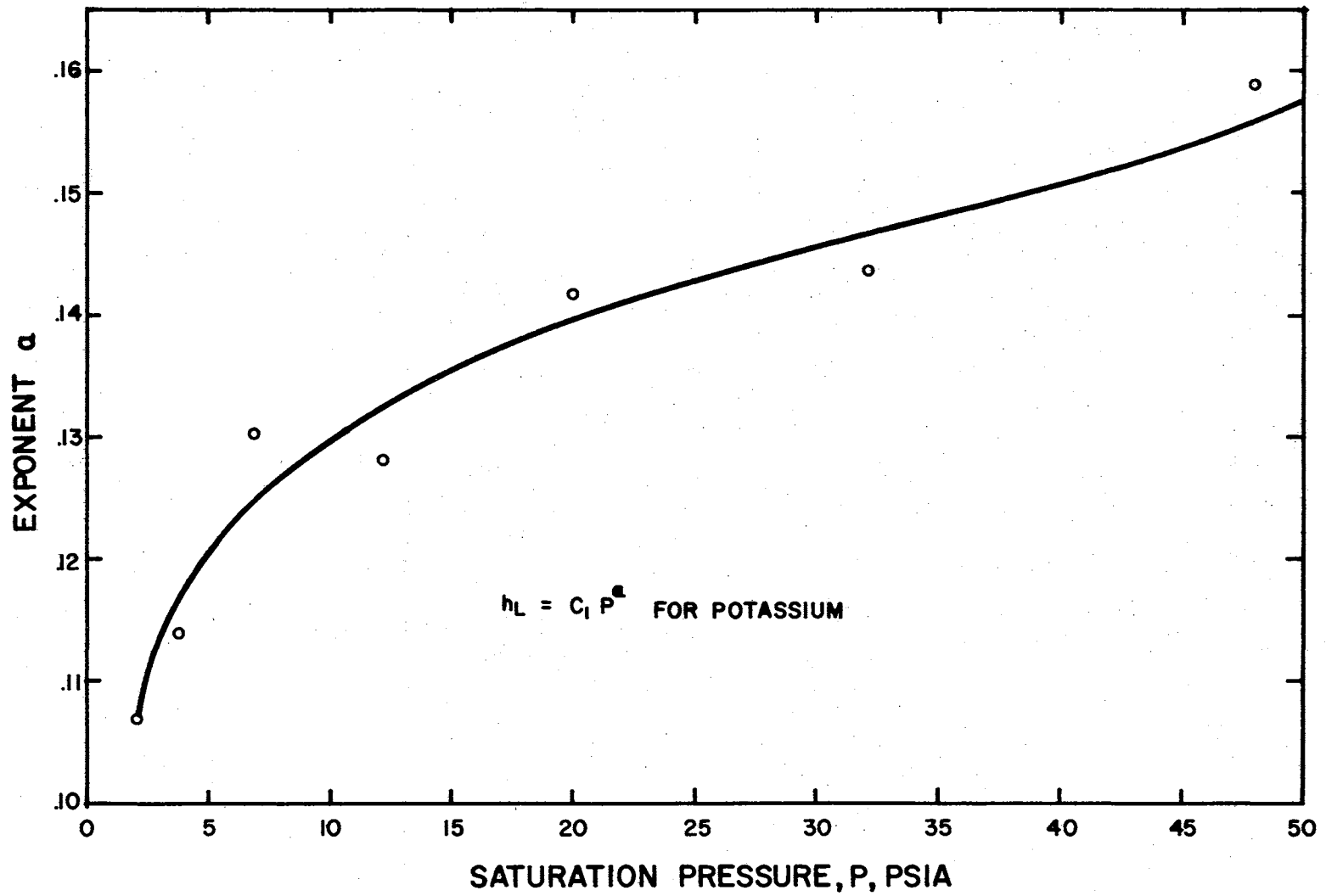
Figure 32.   Exponent for Pressure Function for Enthalpy of Saturated Potassium Liquid
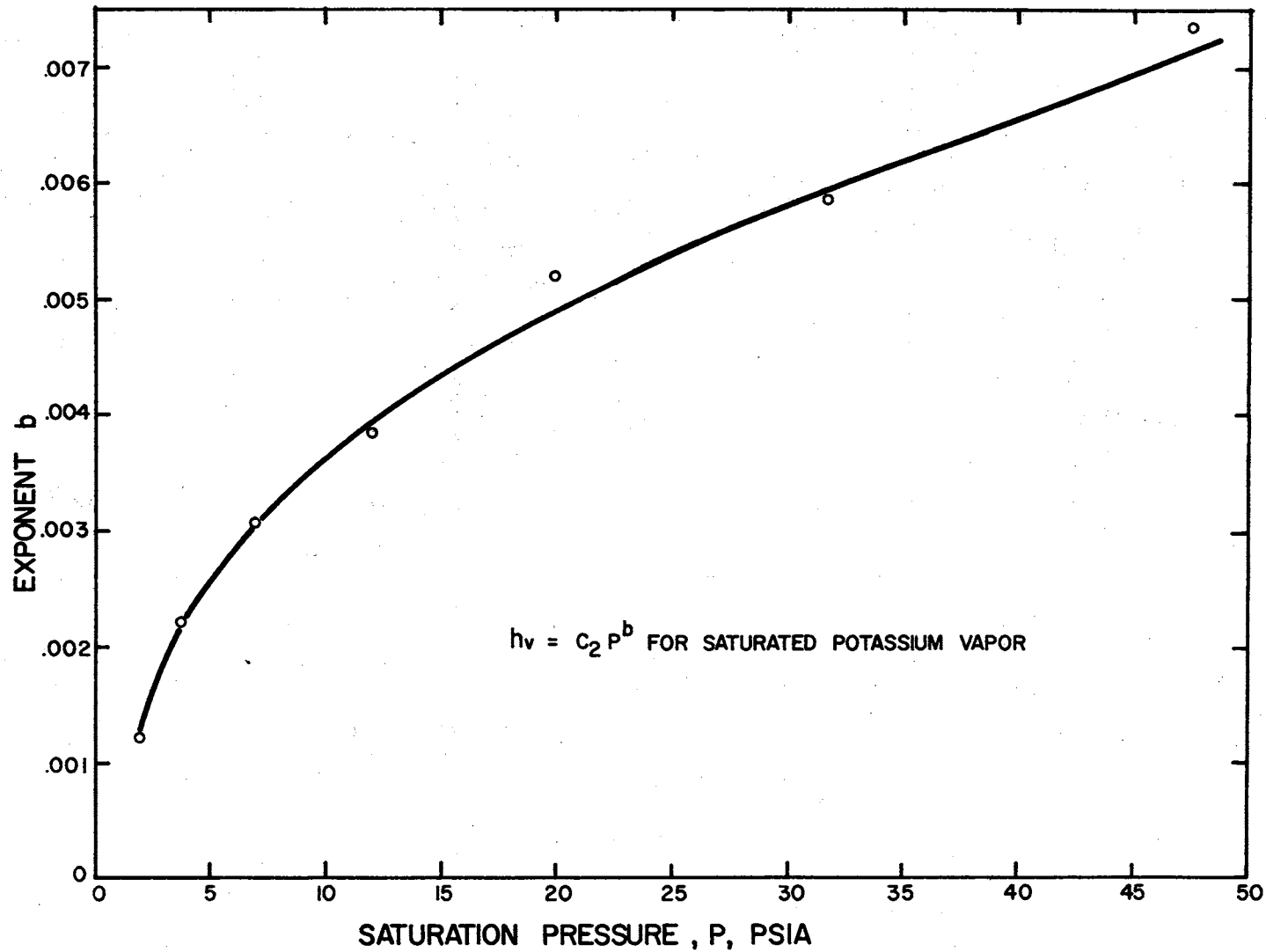
Figure 33. Exponent for Pressure Function for Enthalpy of Saturated Potassium Vapor
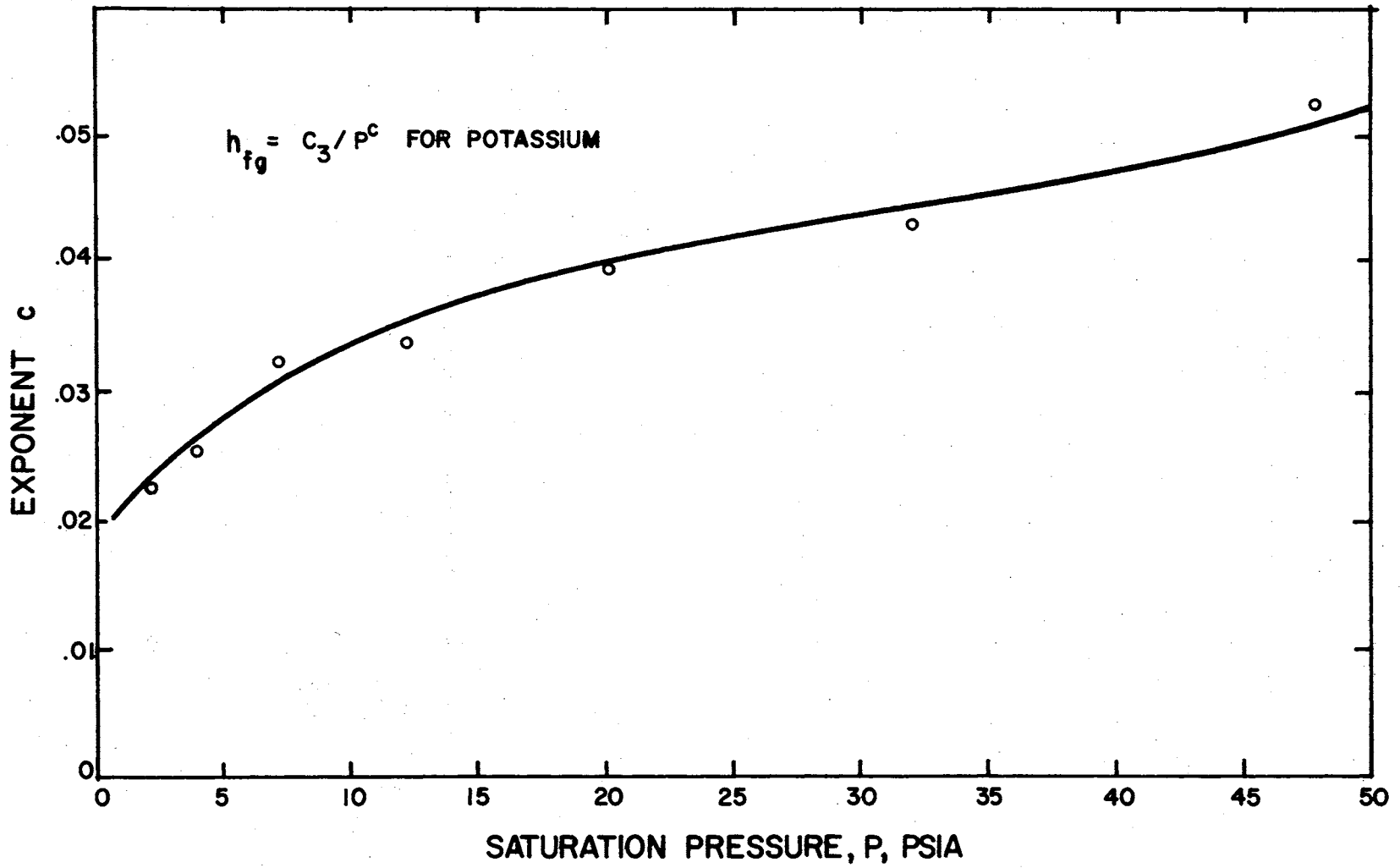
Figure 34. Exponent for Pressure Function for Latent Heat of Potassium

By introducing the non-dimensional constant

$$\eta \equiv \frac{h_{L_e}}{V_{ve}^2} \tag{4A}$$

it is possible to obtain the useful ratio

$$\frac{h_L}{V_{ve}^2} = \eta \phi^a \tag{5A}$$

(2) Specific Enthalpy of Saturated Vapor

Assuming the empirical function

$$h_v = C_2 P^b \tag{6A}$$

therefore,

$$h_v / h_{ve} = P/P_e{}^b = \phi^b \tag{7A}$$

or

$$h_v = h_{ve} \phi^b \tag{8A}$$

Introducing the non-dimensional constant

$$\epsilon \equiv \frac{h_{ve}}{V_{ve}^2} \tag{9A}$$

leads to

$$\frac{h_v}{V_{ve}^2} = \epsilon \phi^b \tag{10A}$$

(3) Latent Heat of Evaporation of Saturated Liquid

Assuming the empirical function

$$h_v - h_L = h_{fg} = C_3 / P^c \tag{11A}$$

therefore

$$h_{fg}/h_{fge} = (P/P_e)^{-c} \tag{12A}$$

or

$$h_{fg} = \frac{h_{fge}}{\phi^c} \tag{13A}$$

Introducing the non-dimensional constant

$$\lambda \equiv \frac{h_{fge}}{V_{ve}^2} \tag{14A}$$

results in

$$\frac{h_v - h_L}{V_{ve}^2} = \frac{h_{fg}}{V_{ve}^2} = \lambda/\phi^c \tag{15A}$$

(4) Density of Saturated Vapor

Assuming the empirical function

$$\rho_v = C_4 P^j \tag{16A}$$

therefore

$$\rho_v/\rho_{ve} = P/P_e^{\ j} = \phi^j \tag{17A}$$

or

$$\rho_v = \rho_{ve}\phi^j \tag{18A}$$

Introducing the non-dimensional constant

$$\sigma \equiv \rho_{ve}/\rho_L \tag{19A}$$

where ρ_L, the density of the liquid, is very nearly constant in the range

of temperatures normally encountered in a condenser tube,

therefore

$$\rho_v/\rho_L = \frac{\rho_{ve}}{\rho_L} \phi^j = \sigma\phi^j \qquad (20A)$$

(5) <u>Viscosity of Saturated Vapor</u>

Assuming the empirical function

$$\mu_v = C_5 P^n \qquad (21A)$$

therefore

$$\frac{\mu_v}{\mu_{ve}} = P/P_e{}^n = \phi^n \qquad (22A)$$

or

$$\mu_v = \mu_{ve}\phi^n \qquad (23A)$$

(6) <u>Viscosity of Saturated Liquid</u>

Assuming the empirical function

$$\mu_L = C_6 P^m \qquad (24A)$$

therefore

$$\frac{\mu_L}{\mu_{Le}} = P/P_e{}^m = \phi^m \qquad (25A)$$

or

$$\mu_L = \mu_{Le}\phi^m \qquad (26A)$$

APPENDIX B

THE DIFFERENTIAL EQUATIONS FOR CONTINUITY OF TWO-PHASE

STEADY FLOW IN A STRAIGHT TUBE

Assumptions   (see Fig. 2, page 6):

   (a)   Flow is steady and one-dimensional in each phase.

   (b)   Pressure is constant across the tube at any point, i.e., at

any radius.

Applying the continuity equation first to the liquid phase and then

to the vapor phase at any axial position leads to

$$(\text{liquid}) \quad W_L = A_L V_L \rho_L \tag{1B}$$

$$(\text{vapor}) \quad W_v = A_v V_v \rho_v \tag{2B}$$

Differentiating equations (1B) and (2B) logarithmically, dividing by

the differential length dL and assuming the liquid density constant,

equations (1B) and (2B) become:

$$\frac{1}{W_L} \frac{dW_L}{dL} = \frac{1}{A_L} \frac{dA_L}{dL} + \frac{1}{V_L} \frac{dV_L}{dL} \tag{3B}$$

and

$$\frac{1}{W_v} \frac{dW_v}{dL} = \frac{1}{A_v} \frac{dA_v}{dL} + \frac{1}{V_v} \frac{dV_v}{dL} + \frac{1}{\rho_v} \frac{d\rho_v}{dL} \tag{4B}$$

The continuity equation applied to the length dL, requires that

$$W_T = W_L + W_v = W_L + dW_L + W_v + dW_v \tag{5B}$$

therefore

$$dW_L = - dW_v \tag{6B}$$

and similarly for the tube of constant cross-sectional area

$$A = A_L + A_v = A_L + dA_L + A_v + dA_v \tag{7B}$$

therefore

$$dA_L = - dA_v \tag{8B}$$

Combining equations (6B), (7B), and (8B) into (3B) leads to

$$\frac{A_L/A_v}{V_L} \frac{dV_L}{dL} + \frac{A_L/A_v}{W_L} \frac{dW_v}{dL} - \frac{1}{A_v} \frac{dA_v}{dL} = 0 \tag{9B}$$

Rearrangement of (4B) results in the form

$$\frac{1}{\rho_v} \frac{d\rho_v}{dL} + \frac{1}{V_v} \frac{dV_v}{dL} - \frac{1}{W_v} \frac{dW_v}{dL} + \frac{1}{A_v} \frac{dA_v}{dL} = 0 \tag{10B}$$

Adding equations (9B) and (10B) leads to the continuity equation in differential form for combined liquid and vapor flow

$$\frac{A_L/A_v}{V_L} \frac{dV_L}{dL} + \frac{1}{V_v} \frac{dV_v}{dL} + \left[\frac{A_L/A_v}{W_L} - \frac{1}{W_v}\right] \frac{dW_v}{dL} + \frac{1}{\rho_v} \frac{d\rho_v}{dL} = 0 \tag{11B}$$

In order to write the combined continuity equation in non-dimensional form, the following substitutions are now made in equation (11B)

$$X = L/D \text{ (Local tube length to diameter ratio)} \tag{12B}$$

therefore,

$$dL = DdX \tag{13B}$$

From Appendix A, equation (20A) is given as

$$\rho_v/\rho_L = (\rho_{ve}/\rho_L)\phi^j = \sigma\phi^j \qquad (14B)$$

Differentiating (14B) logarithmically leads to

$$d\rho_v/\rho_v = j(d\phi/\phi) \qquad (15B)$$

Introducing a non-dimensional variable for the local average velocity in the annular liquid layer as follows:

$$\alpha \equiv V_L/V_{ve} \qquad (16B)$$

By differentiating equation (16B) logarithmically, one obtains

$$dV_L/V_L = d\alpha/\alpha \qquad (17B)$$

Introducing a non-dimensional variable for the local average vapor velocity in the vapor core

$$\beta \equiv V_v/V_{ve} \qquad (18B)$$

therefore

$$\frac{dV_v}{V_v} = \frac{d\beta}{\beta} \qquad (19B)$$

Introducing a non-dimensional expression for the local, total vapor quality

$$\theta \equiv W_v/W_T \qquad (20B)$$

therefore

$$\frac{dW_v}{W_v} = \frac{d\theta}{\theta} \qquad (21B)$$

Combining equations (1B) and (2B) results in the relation

$$A_L/A_v = \frac{W_L \rho_v V_v}{W_v \rho_L V_L} = \frac{(W_T - W_v)\rho_v V_v}{W_v \rho_L V_L} \qquad (22B)$$

Now substituting from the non-dimensional equations (17A), (19A), (16B), (18B), and (20B) leads to the ratio

$$A_L/A_v = \frac{1 - \theta}{\theta} \frac{\sigma\beta\phi^j}{\alpha} \qquad (23B)$$

Equation (22B) may also be written in the form

$$\frac{A_L/A_v}{W_L} = \frac{\rho_v V_v}{W_v \rho_L V_L} \qquad (24B)$$

Combining equations (23B) and (24B) leads to the useful expression

$$\frac{A_L/A_v}{W_L} - \frac{1}{W_v} = \frac{1}{W_v}\left[\frac{\sigma\beta\phi^j}{\alpha} - 1\right] \qquad (25B)$$

By making use of the several expressions developed above, equation (11B) can now be written in non-dimensional form as a function of the four dependent variables α, β, θ, and ϕ as follows:

$$\left[\frac{1 - \theta}{\theta}\right]\frac{\sigma\beta\phi^j}{\alpha^2}\frac{d\alpha}{dX} + \frac{1}{\beta}\frac{d\beta}{dX} + \frac{1}{\theta}\left[\frac{\sigma\beta\phi^j}{\alpha} - 1\right]\frac{d\theta}{dX} + \frac{j}{\phi}\frac{d\phi}{dX} = 0 \qquad (26B)$$

Equation (26B) is then the normalized general form for the combined continuity equation in annular two-phase flow with mass interchange between phases.

APPENDIX C

THE DIFFERENTIAL EQUATIONS OF MOMENTUM FOR TWO-PHASE STEADY

FLOW IN A STRAIGHT TUBE WITHOUT GRAVITY FORCES

Vapor Phase Analysis

Summation of forces acting in the axial flow direction for the vapor

core   (Gravity forces neglected, other assumptions same as in Appendix B,

see Fig. 35.):

Positive Forces   Negative Forces

1. PA_v 1. $(P + dP) (A_v - dA_v)$

2. $W_v V_v$ 2. $(W_v + dW_v) (V_v + dV_v)$

                               3. $V_{vi} (dW_L)$ (1C)

                               4. $(P + dP/2) (dA_v)$

                               5. $\tau_v \pi (D_v - dD_v/2)dL$

Summing up the positive and negative forces, eliminating differen-

tials of higher order, and dividing throughout by dL leads to the differ-

ential equation for vapor momentum:

$$V_{vi} \frac{dW_L}{dL} + V_v \frac{dW_v}{dL} + W_v \frac{dV_v}{dL} + A_v \frac{dP}{dL} = - \tau_v \pi D_v \qquad (2C)$$
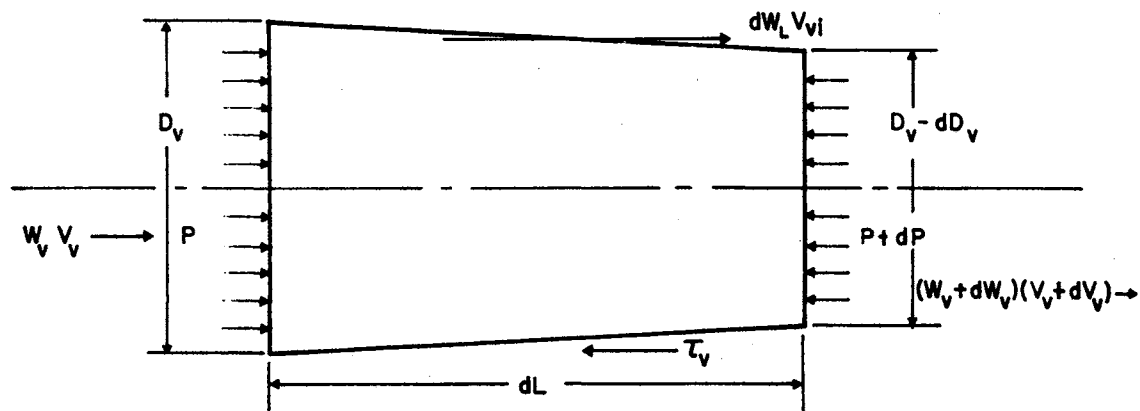
Figure 35.   Control Volume for the Vapor Phase
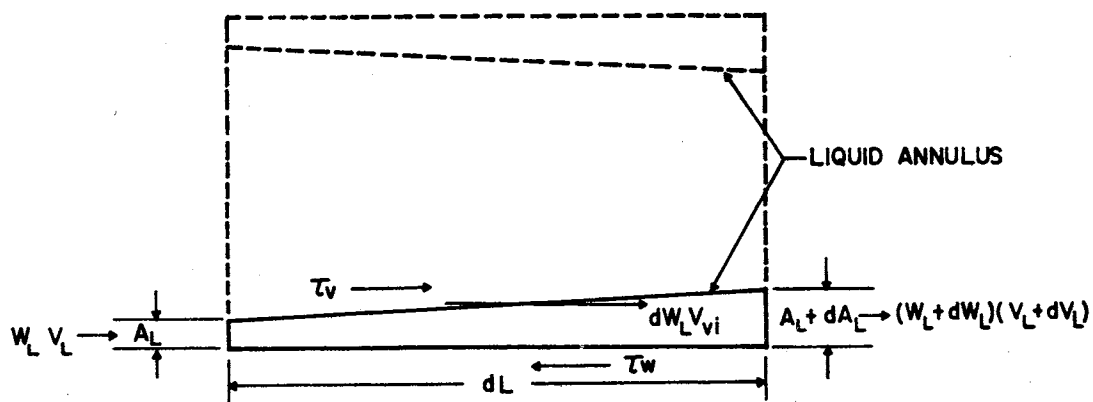
Figure 36.   Control Volume for the Liquid Phase

Liquid Phase Analysis

Summation of forces acting in the axial flow direction for the annular liquid layer   (see Fig. 36):

Positive Forces	Negative Forces

1. PA_L

2. $W_L V_L$

3. $(V_{vi})(dW_L)$

4. $(P + dP/2)dA_L$

5. $\tau_v \pi (D_v - dD_v/2)dL$

1. $(P + dP)(A_L + dA_L)$

2. $(W_L + dW_L)(V_L + dV_L)$

3. $\tau_w \pi D dL$

(3C)

Again summing up the positive and negative forces, eliminating differentials of higher order, and dividing throughout by dL results in the following expression:

$$W_L \frac{dV_L}{dL} + A_L \frac{dP}{dL} + V_L \frac{dW_L}{dL} - V_{vi} \frac{dW_L}{dL} = (\tau_v \pi D_v - \tau_w \pi D)$$

(4C)

In the above equation, V_{vi} is the time average axial component of the velocity at which the condensed liquid particles or diffusional vapor molecules leave the vapor core and enter the liquid layer. This velocity could be anywhere between the vapor velocity in the core center and the interfacial liquid velocity. In this analysis it has been assumed that this interfacial velocity has a value of the order of magnitude of the time average interfacial axial liquid velocity. The chief support for this assumption is based on the fact that the diffusional molecules leaving the vapor core and entering the liquid layer could only travel a

distance of one mean free path since their last molecular impact in the vapor. For saturated steam vapor at 212°F, the mean free path of the vapor molecules is about 2×10^{-6} inches.

The experimental evidence shown in Figs. 3 and 4 indicates that liquid layer wave amplitudes are of the order of 0.020 inches or greater at vapor axial velocities of 300 to 1000 feet per second. Comparing the liquid wave amplitude to the mean free path of the vapor molecule, it is seen that the vapor molecule would suffer a minimum of 10,000 molecular impacts if it traveled strictly in a radial direction through this interfacial region of wave activity before entering the liquid layer. Considering these facts, it seems reasonable to conclude that the diffusional vapor molecule entering the liquid layer does so with an axial component of velocity of the same order of magnitude as the interfacial liquid wave velocity.

For want of more exact knowledge of the interfacial wave velocity, the following relation has been used:

$$V_{vi} = 2V_L \tag{5C}$$

where V_L is, of course, the time and area average liquid layer velocity. A more precise evaluation of the interfacial velocity V_{vi} remains to be accomplished. Since the time average vapor velocity is of the order of one hundred times greater than the similar liquid velocity the exact value of V_{vi} may not be of critical importance in equation (4C).

Defining an interfacial vapor friction factor by the expression

$$f_v \equiv \frac{\tau_v}{\rho_v V_v^2 / 2} \tag{6C}$$

then making use of the relations

$$dW_L = -dW_v \qquad (6B)$$

$$A_v = W_v/\rho_v V_v \qquad (7C)$$

and

$$\pi D^2 = 4A = 4 W_T/\rho_{ve} V_{ve} \qquad (8C)$$

also introducing the non-dimensional constant

$$N = P_e/\rho_{ve} V_{ve}^2 \qquad (9C)$$

again introducing the necessary non-dimensional terms of Appendix A, it is possible to write equation (2C) for vapor momentum in the form

$$\theta \frac{d\beta}{dX} + (\beta - 2\alpha) \frac{d\theta}{dX} + \frac{\theta N}{\beta \phi^j} \frac{d\phi}{dX} = - 2f_v \beta^{3/2} \sqrt{\theta \phi^j} \qquad (10C)$$

where all terms are non-dimensional and are as previously defined.

Adding equations (2C) and (4C) leads to

$$W_L \frac{dV_L}{dL} + W_v \frac{dV_v}{dL} + (V_v - V_L) \frac{dW_v}{dL} + A \frac{dP}{dL} = -\tau_w \pi D \qquad (11C)$$

which can then be expressed in the non-dimensional form

$$(1 - \theta) \frac{d\alpha}{dX} + \theta \frac{d\beta}{dX} + (\beta - \alpha) \frac{d\theta}{dX} + N \frac{d\phi}{dX} = -4N\Psi \qquad (12C)$$

This is the combined differential equation for momentum change in non-dimensional form where $\Psi \equiv \tau_w/P_e$ and Ψ is a non-dimensional wall shear stress. The other non-dimensional terms are as previously defined.

If a wall friction factor is defined by

$$f_w \equiv 2\tau_w/\rho_v V_v^2 \qquad (13C)$$

then equation (12C) can be written in the form

$$(1 - \theta) \frac{d\alpha}{dX} + \theta \frac{d\beta}{dX} + (\beta - \alpha) \frac{d\theta}{dX} + N \frac{d\phi}{dX} = - 2f_w \beta^2 \phi^j \qquad (14C)$$

Equation (14C) is the same as (12C) except that the non-dimensional wall shear stress Ψ has been replaced by the more common wall friction factor f_w.

Either the vapor momentum equation (10C) or the combined momentum equation (14C) may be used as one equation in the system of four fundamental equations necessary to find a solution to the values of the flow properties over the condensing length. The choice of equations will depend on the quality of the available empirical data for the local friction factors f_v or f_w.

APPENDIX D

THE DIFFERENTIAL EQUATION OF ENERGY TRANSFER FOR STEADY HIGH

SPEED ANNULAR TWO-PHASE FLOW IN A STRAIGHT TUBE

The total flow rate of energy E of the two-phase stream at any

position L in the flow direction may be expressed by

$$E = \frac{W_L V_L^2}{2} + \frac{W_v V_v^2}{2} + W_L h_L + W_v h_v \tag{1D}$$

This equation can be rewritten in non-dimensional form by dividing

through by $W_T V_{ve}$, thus

$$\frac{E}{W_T V_{ve}^2} = \frac{1 - \theta}{2} \alpha^2 + \frac{\theta \beta^2}{2} + (1 - \theta) \frac{h_L}{V_{ve}^2} + \theta \frac{h_v}{V_{ve}^2} \tag{2D}$$

Differentiating with respect to the tube length L and introducing

$dE/dL \equiv Q'$, where Q' is the energy abstracted per unit length of tube at L,

leads to the non-dimensional differential equation for energy transfer

$$- DQ'/W_T V_{ve}^2 = \alpha(1 - \theta) \frac{d\alpha}{dX} + \beta\theta \frac{d\beta}{dX} + \left[\frac{\beta^2 - \alpha^2}{2} + \frac{h_v - h_L}{V_{ve}^2} \right] \frac{d\theta}{dX}$$

$$+ \left[\frac{1 - \theta}{V_{ve}^2} \right] \frac{dh_L}{dX} + \frac{\theta}{V_{ve}^2} \frac{dh_v}{dX} \tag{3D}$$

But from Appendix A

$$\frac{h_L}{V_{ve}^2} = \eta \phi^a \tag{5A}$$

83

therefore

$$\frac{1}{V_{ve}^2} \frac{dh_L}{dX} = a\eta\phi^{a-1} \frac{d\phi}{dX} \qquad (4D)$$

Also from Appendix A,

$$\frac{h_v}{V_{ve}^2} = \epsilon\phi^b \qquad (12A)$$

therefore

$$\frac{1}{V_{ve}^2} \frac{dh_v}{dX} = b\epsilon\phi^{b-1} \frac{d\phi}{dX} \qquad (5D)$$

Again from Appendix A

$$\frac{h_v - h_L}{V_{ve}^2} = \frac{h_{fg}}{V_{ve}^2} = \lambda/\phi^c \qquad (15A)$$

Introducing a non-dimensional expression for the rate of heat transfer through the tube wall

$$H = DQ'/W_T V_{ve}^2 \qquad (6D)$$

and substituting from the above terms into equation (3D), leads to

$$(1 - \theta)\alpha \frac{d\alpha}{dX} + \theta\beta \frac{d\beta}{dX} + \left[\frac{\lambda}{\phi^c} + \tfrac{1}{2}(\beta^2 - \alpha^2)\right] \frac{d\theta}{dX}$$

$$+ \left[\frac{b\epsilon\theta}{\phi^{(1-b)}} + \frac{a\eta(1-\theta)}{\phi^{(1-a)}}\right] \frac{d\phi}{dX} = -H \qquad (7D)$$

This is the normalized differential equation for energy change with axial distance in the total two-phase flow. Note that the term H is usually variable. If such is the case, an expression H = H(X) must be introduced to make possible a solution to the equation set.

APPENDIX E

THE DIFFERENTIAL EQUATION RELATING THE VELOCITY PRESSURES

IN THE LIQUID AND VAPOR FLOW REGIMES

Experimental investigation of the variation in both stagnation and

stream (static) pressure in the interfacial region between the liquid

and vapor phase in annular two-phase flow, indicated that in the radial

direction normal to the axial streamline, no discontinuity in the dynamic

pressure occurred as the pressure probe passed from the vapor core into

the annular liquid layer. Fig. 37 shows the radial variation in the

dynamic pressure across the diameter of a 0.550 I.D. condenser tube

measured by a hypodermic pressure probe. The evidence of Fig. 37 indi-

cates that no sharp change in the quantity $(P_o - P)$ occurred as the probe

was moved in a radial direction from the vapor core across the inter-

facial region into the liquid layer and toward the tube wall.

The determination of the relative magnitudes and variation of the

quantity $(P_o - P)$ across the condenser tube is an important factor in the

development of the mathematical model for this annular flow system. When

the evidence cited in the previous paragraph is compared with the inde-

pendent analysis of the wall shear stress and velocity distribution in the

liquid layer as developed in Appendix I, it is possible to construct a

physical model for the annular two-phase system which leads to a mathe-

matical treatment that can be incorporated with the system of equations of

heat, mass, and momentum conservation already developed in Appendixes B, C,

and D.

TUBE I.D. = 0.550 inches

Liquid Layer Thickness = 0.050 Inches

Test 32453

DATA FOR TEST 32453

W_T = 265 lb$_m$/hr W_V = 100 lb$_m$/hr. $\overline{V}_V$ = 200 ft/sec

$\overline{V}_L$ = 1.45 ft/sec. P = 52.0 psia Quality θ = 38%

Liquid Layer Thickness = 0.040 Inches

Test 33053

RADIAL DISTANCE FROM TUBE CENTER IN INCHES

DATA FOR TEST 33053

W_T = 270 lb$_m$/hr W_V = 115 lb$_m$/hr P_{static} = 28.0 psia

$\overline{V}_V$ = 400 ft/sec $\overline{V}_L$ = 1.64 ft/sec   Quality θ = 43%
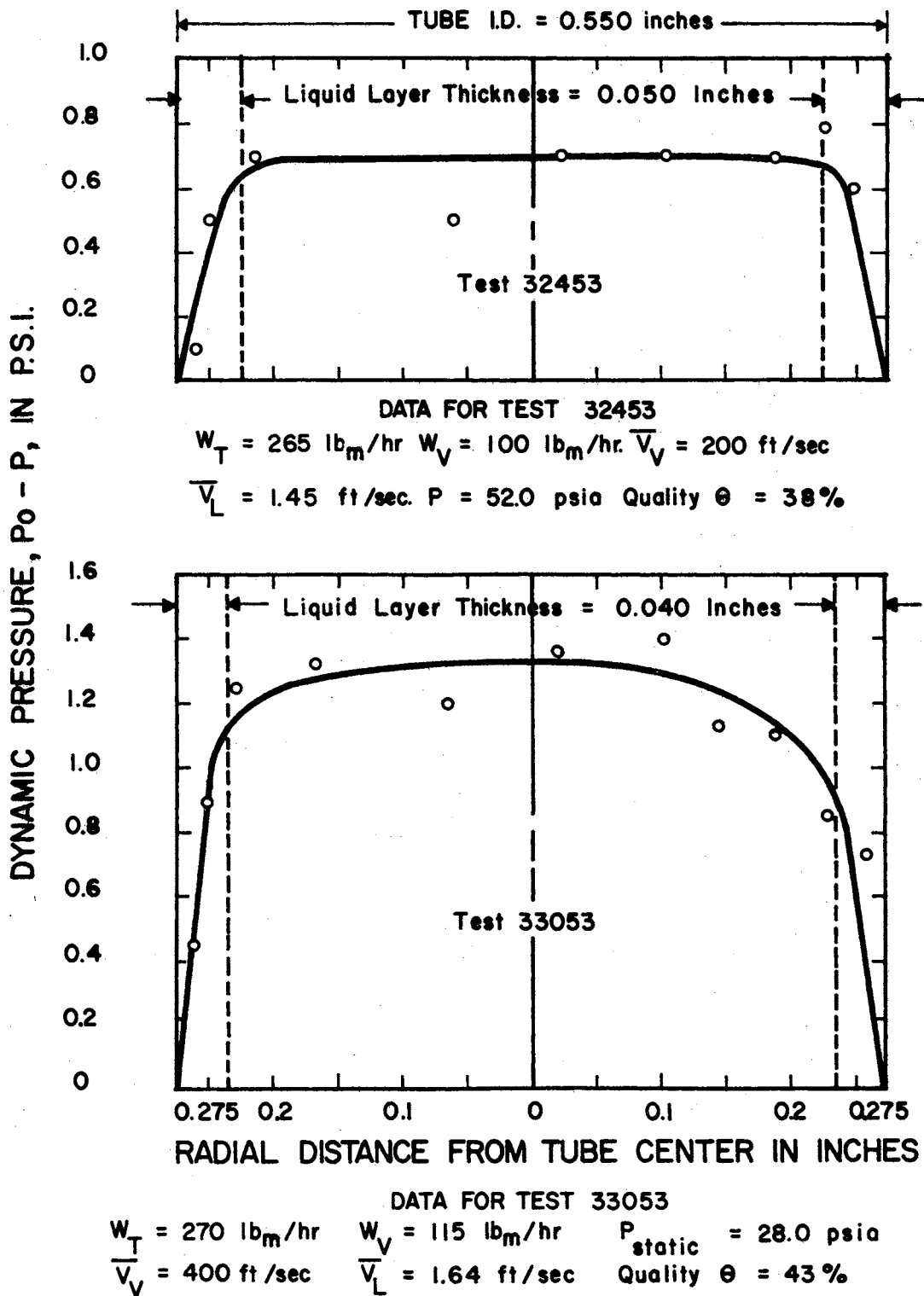
Figure 37. The Radial Variation of Dynamic Pressure for Annular Two-Phase Flow in a 0.550 Inch I.D. Tube

In accordance with the information reviewed in the two previous paragraphs it is now considered that the magnitude of the velocity pressure (P_o - P) in the annular two-phase system decreases without discontinuity in the radial direction from the axial center line of the tube to zero at the inside tube wall.

For a vapor flowing at moderate velocities of up to several hundred feet per second, a form of the Bernoulli equation can be used to represent the relation between the stagnation pressure P_o and stream pressure P as follows:

$$\frac{V^2}{2} + \frac{P}{\rho} = \frac{P_o}{\rho} \tag{1E}$$

which may be written

$$P_o - P = \rho V^2/2 \tag{2E}$$

Equation (2E) is therefore an expression for the velocity pressure for incompressible flow. For incompressible flow, the ratio

$$\frac{P_o - P}{\rho V^2/2} = 1 \tag{3E}$$

will be exact. Therefore, up to a vapor Mach number of about M = 0.3 the velocity pressure of the liquid and of the vapor at the annular interface may be related with sufficient accuracy by the expression

$$\rho_L V_{Li}^2 = \rho_v V_{vi}^2 \tag{4E}$$

where V_{Li} and V_{vi} are the time and mass average interfacial liquid and vapor velocities repectively.

Considering the experimental measurements of wave speeds and wave heights reported by Robson and Hilding (31), it appears that the effective

liquid layer thickness should be taken at the crest height of the liquid waves at a particular axial location. The wavy annular interface may be likened to the wall of a corrugated pipe with respect to the vapor flow. The mass average vapor velocity in the vapor core will then be determined by the available cross section area between the liquid wave crests. Because of the severe fluid turbulence generated by the interfacial waves in both the liquid and vapor regions, it appears that except at the tube wall, there is no sharp radial variation of the mass average axial velocity of either vapor or liquid in its respective layer. This condition would appear to imply that a sharp discontinuity between vapor and liquid velocities must exist at the annular liquid-vapor interface. Such a discontinuity would be impossible in a uniform continuum. The actual interface, of course, consists only of the peak of a traveling liquid wave; the peak of this wave having zero axial width. In the trough between the waves is a region of greatly reduced vapor velocity which serves as a kind of boundary layer to the vapor core and so evidently permits the existence of a mass average vapor velocity at the wave crest considerably in excess of either the wave velocity or the mass average liquid velocity at that location.

The analysis of Appendix I strongly indicates that for turbulent flow, i.e., $\delta^+ \geq 1$, the mass average velocity in the liquid layer is virtually constant for a radial traverse from the liquid-vapor interface, i.e., wave crest, to the very thin laminar sublayer of $y^+ = 1$; thus $V_{Li} \simeq V_L$.

Introducing the constants

$$C_L \equiv V_{Li}/V_L \text{ and } C_v \equiv V_{vi}/V_v \tag{5E}$$

where $C_L \geq 1$ and $C_v \leq 1$ are assumed to vary insignificantly relative to changes in the average axial velocities V_L and V_v, and substituting in (4E) leads to

$$\rho_L (C_L V_L)^2 = \rho_v (C_v V_v)^2 \qquad \text{(6aE)}$$

which may be written in the form

$$K_p \equiv \frac{C_L}{C_v} = \frac{V_v}{V_L} \sqrt{\rho_v / \rho_L} \qquad \text{(6bE)}$$

If $C_L \equiv \frac{V_{Li}}{V_L} \backsim 1$ then $K_p = \frac{1}{C_v} \geq 1$. Values of the ratio K_p have been plotted against the total liquid fraction $(1 - \theta)$ over the condensing length for the several different tube sizes in Fig. 38. It should be noted that because of the wide differences between the density of the vapor and of the liquid, rather small errors in the experimental determination of the average velocity of the vapor will be reflected in quite large errors in the resulting determination of the average velocity in the liquid layer. Such errors are magnified even more at the start of condensation when the liquid layer is very thin. Fig. 38 gives rather inconclusive support to the assumption of a constant ratio of K_p over the condensing length of a particular condenser tube.

Assuming the liquid density to be nearly constant and differentiating (6bE) logarithmically leads to the expression

$$\frac{2dV_L}{V_L} = \frac{d\rho_v}{\rho_v} + \frac{2dV_v}{V_v} \qquad \text{(7E)}$$

Again, introducing the non-dimensional expressions of Appendix A for the above variables in equation (7E) leads to the form

$$\frac{1}{\alpha} \frac{d\alpha}{dX} - \frac{1}{\beta} \frac{d\beta}{dX} - \frac{j}{2\phi} \frac{d\phi}{dX} = 0 \qquad \text{(8E)}$$
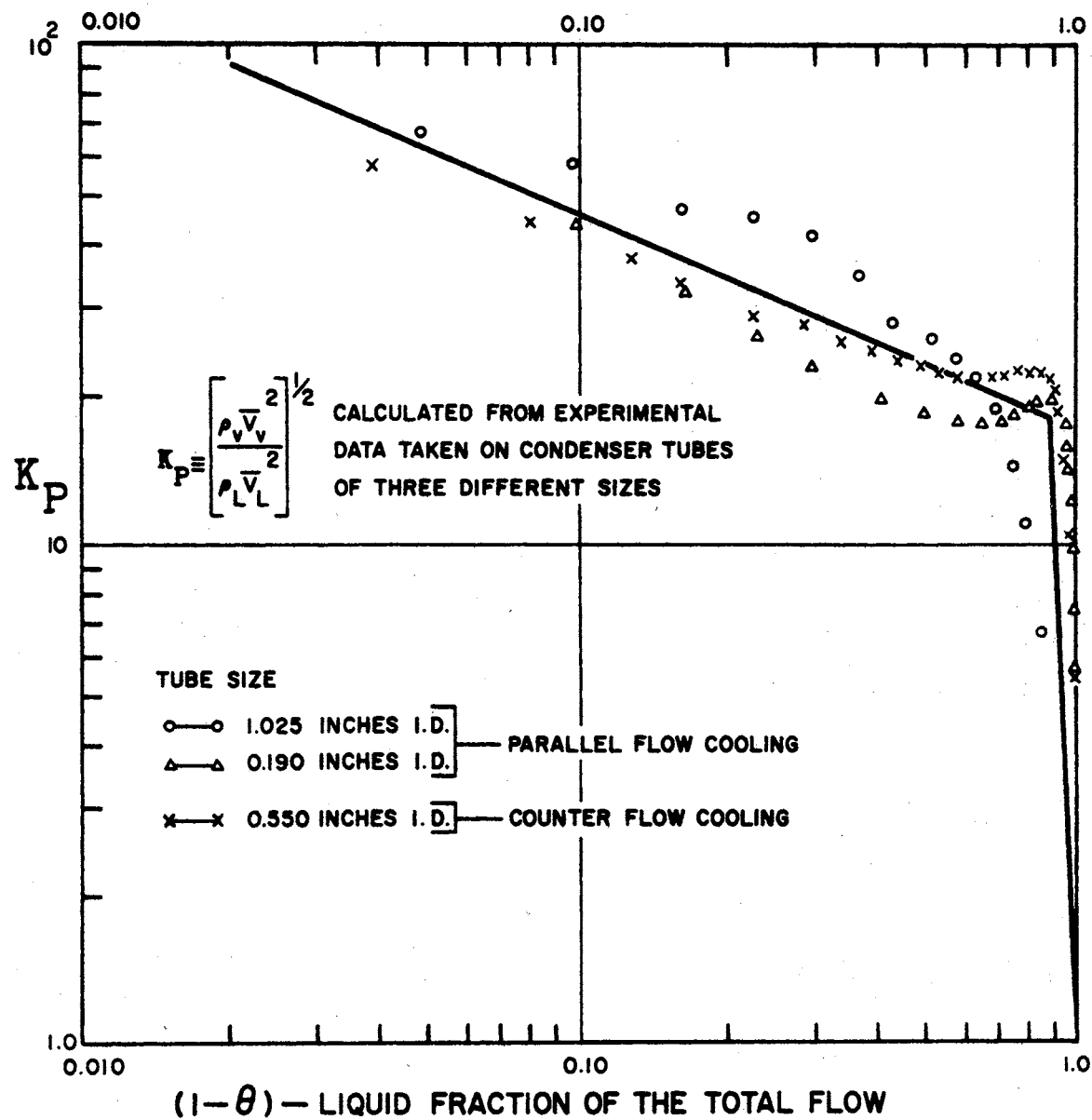
Figure 38.   Variation of Ratio K_p With Liquid Fraction of the Total Flow

Equation (8E) is the normalized differential equation relating vapor and liquid velocity pressure at the interface between the two-flow regimes for low subsonic vapor velocities (M ≤ 0.3).

Equation (8E) and its compressible form (28E) have been applied in the analysis of the flow characteristics in the region of fully developed vapor and liquid turbulence. For the region of the developing laminar annular liquid layer at the beginning of vapor condensation, a different analytical approach has been followed. For the analysis of the developing laminar annular liquid layer, see Appendix F.

For compressible fluids, the ratio

$$\frac{P_o - P}{\rho V^2/2}$$

will increase steadily from unity as a function of the Mach number. The ratio has been plotted in Fig. 39 as a function of the Mach number for saturated steam vapor. The values of Fig. 39 were calculated from data taken from the tables of Thermodynamic Properties of Steam by Keenan and Keyes (23). Isentropic compression from saturated vapor at the stream pressure P, to the stagnation pressure P_o, is assumed in this calculation.

In order to relate the velocity pressures of a liquid and a compressible vapor, it was expected that it would be necessary to represent the curve of Fig. 39 by an empirical polynomial function of the vapor Mach number and then to incorporate this function into the differential equation derived from the expression for equal velocity pressures. It was discovered, however, that an expression derived from perfect gas relations would accurately describe the actual ratio for saturated steam vapor up to quite high pressures or densities (see Fig. 39). Starting

$$\frac{P_o - P}{\rho_v V_v^2 / 2} = \frac{2}{kM^2}\left[\left(1 + \frac{k-1}{2}M^2\right)^{k/k-1} - 1\right]$$

⎯⎯⎯ FROM ABOVE EQ. FOR k = 1.31

o ⎯ FROM STEAM TABLES FOR SAT. STEAM AT 10 PSIA

x ⎯ FROM STEAM TABLES FOR SAT. STEAM AT 100 PSIA

$\dfrac{P_o - P}{\rho_v V_v^2 / 2}$

M — MACH NUMBER OF THE VAPOR
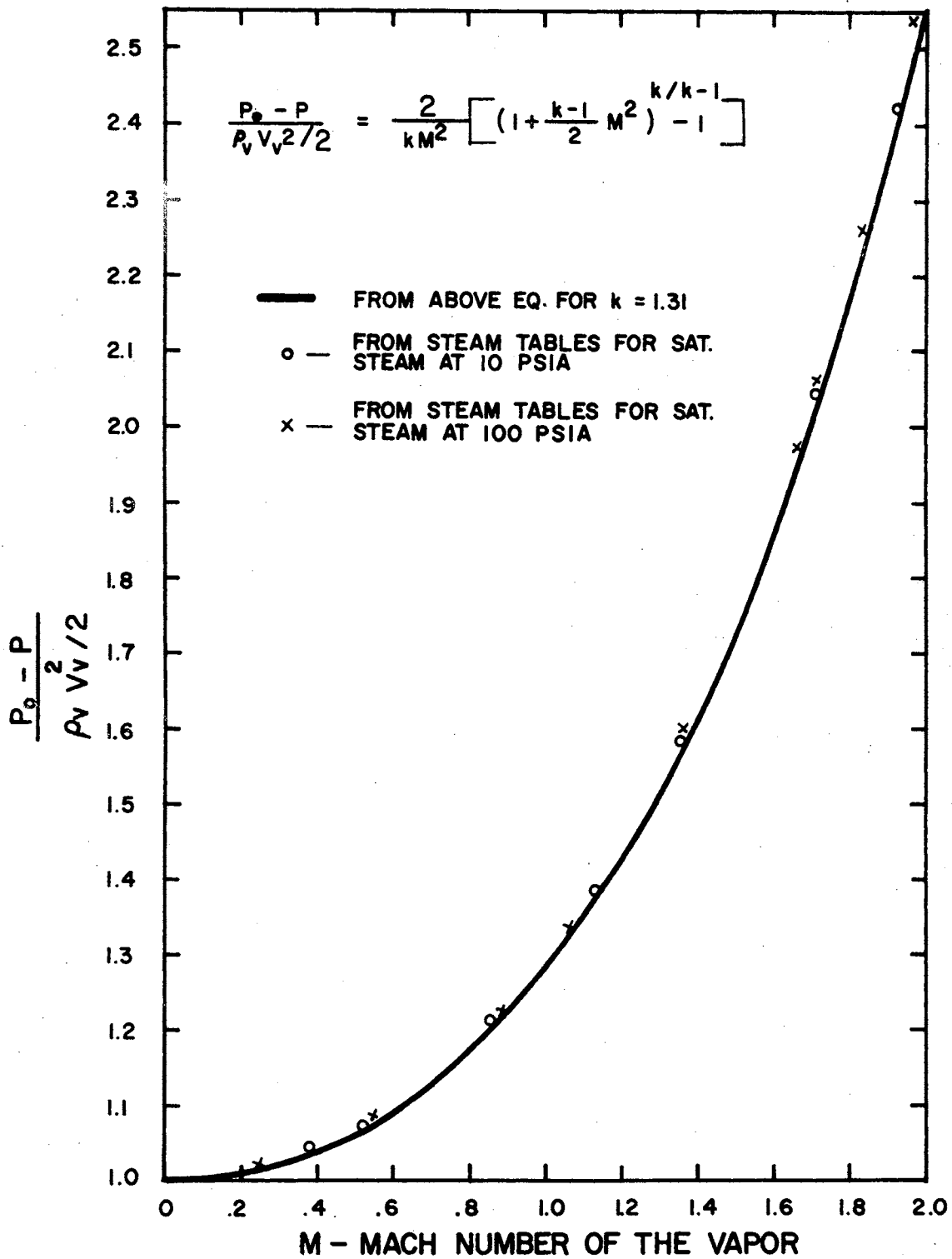
. Figure 39. Non-Dimensional Dynamic Pressure in Saturated Vapor Versus Mach Number

from the well-known relation for isentropic flow of a perfect gas, a functional relation has been derived for a compressible vapor. For isentropic flow of a perfect gas

$$P_o/P = (1 + \frac{k-1}{2} M^2)^{k/k-1} \tag{9E}$$

or

$$P_o = P(1 + \frac{k-1}{2} M^2)^{k/k-1} \tag{10E}$$

where k is the isentropic exponent and is not necessarily constant for all pressure ranges of the pure vapor. Subtracting P from both sides and also dividing by P results in the equation

$$\frac{P_o - P}{P} = \left[(1 + \frac{k-1}{2} M^2)^{k/k-1} - 1\right] \tag{11E}$$

For a perfect gas $M \equiv \frac{V}{C}$, where the sonic velocity $C = \sqrt{kRT}$; therefore, $M^2 = V^2/kRT$. Now dividing both sides of equation (11E) by M^2 and also substituting the perfect gas equation $P = \rho RT$ leads to the equation

$$\frac{P_o - P}{\rho_v V_v^2/2} = \frac{2}{kM^2} \left[(1 + \frac{k-1}{2} M^2)^{k/k-1} - 1\right] \tag{12E}$$

By use of l'Hospital's rule, it is easily shown that when $M \to 0$, equation (12E) reduces to

$$\frac{P_o - P}{\rho_v V_v^2/2} = 1 \tag{3E}$$

which is identical to equation (3E), as is required. Values of the ratio

$$\frac{P_o - P}{\rho_v V_v^2/2}$$

have been calculated by equation (12E) for saturated steam vapor up to M = 2.0 for a pressure P = 10 psia and also P = 100 psia (see Fig. 39).

The agreement is surprisingly close between the values calculated from steam table data and by use of the perfect gas based equation (12E). Evidently equation (12E) gives a satisfactory expression for the velocity pressure of pure saturated steam vapor up to a Mach number of 2 and a vapor pressure of at least 100 psia.

Again making use of the experimentally observed phenomenon of the equality of velocity pressures across the liquid-vapor interface in annular two-phase flow (see Fig. (37), thus

$$(P_o - P) \text{ (liquid phase)} = (P_o - P) \text{ (vapor phase)} \tag{13E}$$

For the incompressible liquid

$$P_o - P = \rho_L C_L^2 V_L^2 / 2$$

and also substituting from equations (5E) and (12E) into (13E), leads to the expression

$$\rho_L C_L^2 V_L^2 = \rho_v C_v^2 V_v^2 \left\{ \frac{2}{kM^2} \left[(1 + \frac{k-1}{2} M^2)^{k/k-1} - 1 \right] \right\} \tag{14E}$$

where the constants C_L and C_v are defined the same as before and are assumed to vary insignificantly relative to the time average velocities V_L and V_v over the condensing length.

Considering the terms C_L, C_v, ρ_L, and k as constant and differentiating (14E) logarithmically results in the equation

$$2 \frac{dV_L}{V_L} = \frac{d\rho_v}{\rho_v} + 2 \frac{dV_v}{V_v} - \frac{2dM}{M} + \frac{k(1 + \frac{k-1}{2} M^2)^{1/k-1} MdM}{(1 + \frac{k-1}{2} M^2)^{k/k-1} - 1} \tag{15E}$$

The vapor Mach number, M, as defined previously is

$$M \equiv \frac{V_v}{C} \tag{16E}$$

where C is the sound speed in the vapor. Differentiating (16E) logarithmically gives

$$\frac{dM}{M} = \frac{dV_v}{V_v} - \frac{dC}{C}$$ (17E)

which also may be written

$$MdM = \frac{V_v dV_v}{C^2} - \frac{V_v^2 dC}{C^3}$$ (18E)

Substituting (18E) in (15E) leads to

$$\frac{2dV_L}{V_L} = \frac{d\rho_v}{\rho_v} + \frac{2dC}{C} + \frac{k(1 + \frac{k-1}{2}M^2)^{1/k-1}}{(1 + \frac{k-1}{2}M^2)^{k/k-1} - 1}\left[\frac{V_v dV_v}{C^2} - \frac{V_v^2 dC}{C^3}\right]$$ (19E)

Fig. 40 shows the variation of sound speed versus pressure in dry saturated steam. This curve can be approximated by the function

$$C = 1432P^{0.030}$$ (20E)

where C is the velocity in feet per second and P the saturation pressure in psia. From a pressure of 1 psia to a pressure of 100 psia, this expression (20E) has a maximum error of about ± 4 feet per second or ± 0.25 percent. In general, therefore,

$$C = BP^t$$ (21E)

where B and t are constants.

Differentiating equation (21E) logarithmically gives

$$\frac{dC}{C} = t\frac{dP}{P} = t\frac{d\phi}{\phi}$$ (22E)

where ϕ is the normalized pressure as defined in Appendix A.

Making use of the definition $M \equiv \frac{V_v}{C}$ leads to the identity

The y-axis is labeled "SONIC VELOCITY, C, FT./SEC." with values 1400, 1500, 1600 and sub-gridlines 20, 40, 60, 80.

The x-axis is labeled "SATURATION PRESSURE FOR STEAM, PSIA" with values 0, 10, 20, 30, 40, 50, 60, 70, 80, 90, 100, 110.

SONIC VELOCITY, $C = \sqrt{\left(\dfrac{\partial P}{\partial \rho}\right)_s} = \sqrt{k \, V \, P}$

FOR THIS CURVE THE VALUE OF k HAS BEEN DETERMINED FROM FIGURE 8, PAGE 82, REF. 23
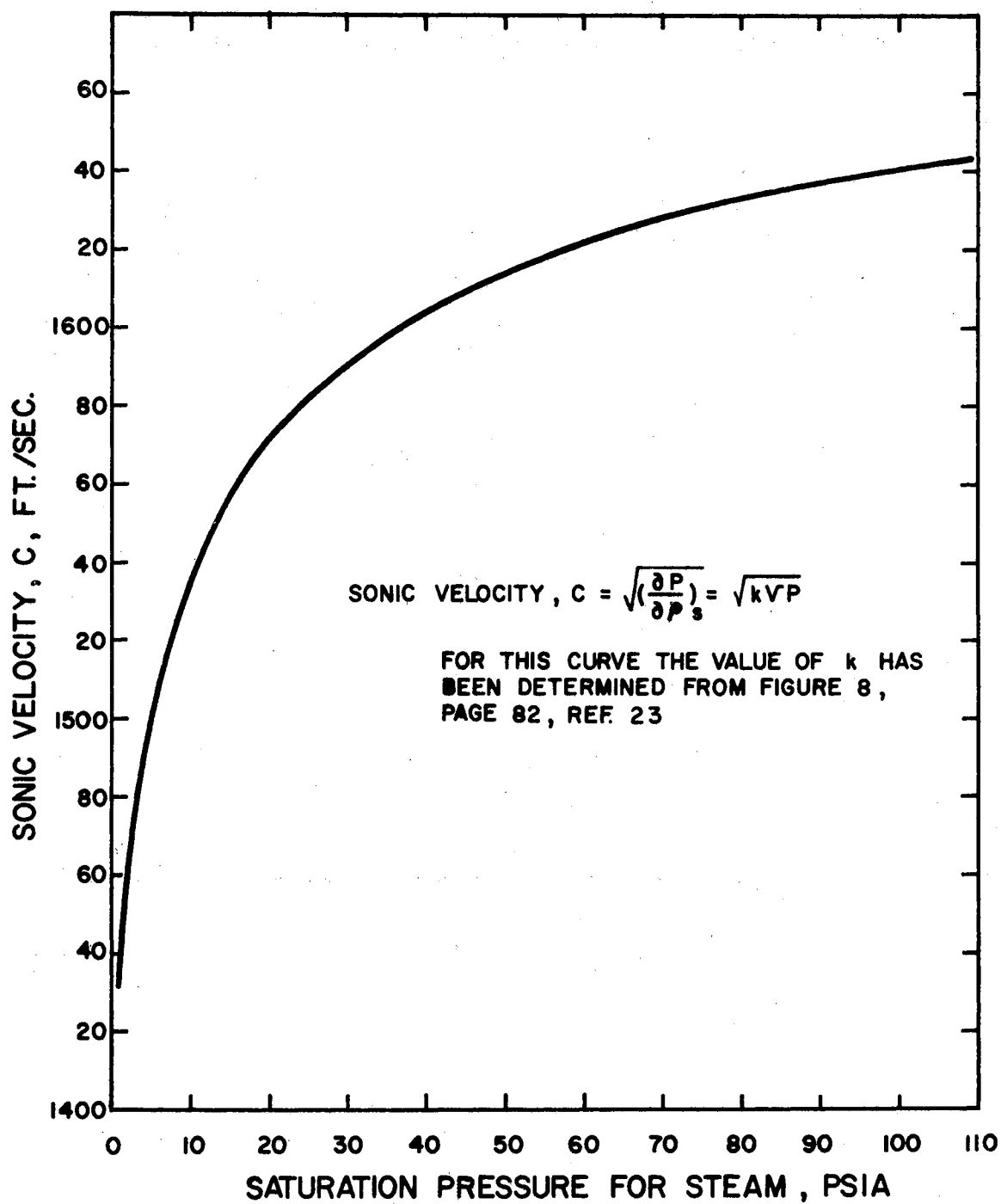
Figure 40. Sonic Velocity in Saturated Vapor Versus Pressure

$$V_v dV_v/C^2 = M^2 \frac{d\beta}{\beta} \qquad (23E)$$

where $\beta = V_v/V_{ve}$ and is the normalized vapor velocity.

Equation (22E) may also be written in the form

$$V_v^2 dC/C^3 = tM^2 \frac{d\phi}{\phi} \qquad (24E)$$

Again drawing on the empirical property functions of Appendix A for the vapor density,

$$\rho_v = \rho_{ve} \phi^j \qquad (17A)$$

where ρ_{ve} is the particular inlet vapor density. Differentiating (17A) logarithmically yields

$$d\rho_v/\rho_v = j \frac{d\phi}{\phi} \qquad (25E)$$

For purposes of simplification, it is useful to define a secondary variable

$$S \equiv \frac{k(1 + \frac{k-1}{2} M^2)^{\frac{1}{k-1}}}{\left[(1 + \frac{k-1}{2} M^2)^{k/k-1} - 1\right]} \qquad (26E)$$

Now substituting equations (23E), (24E), (25E), and (26E) into equation (19E) results in the normalized form

$$\frac{2d\alpha}{\alpha} = j \frac{d\phi}{\phi} + 2t \frac{d\phi}{\phi} + SM^2 \left[\frac{d\beta}{\beta} - t \frac{d\phi}{\phi}\right] \qquad (27E)$$

Rearranging (27E) and dividing through by dX where $X = \frac{L}{D}$, the local length to diameter ratio for the tube finally results in

$$\frac{2}{\alpha} \frac{d\alpha}{dX} - \frac{SM^2}{\beta} \frac{d\beta}{dX} + \left[\frac{SM^2 t - 2t - j}{\phi}\right] \frac{d\phi}{dX} = 0 \qquad (28E)$$

The quantity SM^2 is a secondary dependent variable which is a function

of the local vapor velocity and the particular isentropic exponent of

the vapor. For saturated pure vapor, the isentropic exponent may be

taken at an average value over the range of pressures encountered in a

particular condenser tube. By use of l'Hospital's rule, it can be shown

that at low velicities $(M \rightarrow 0)$ the variable SM^2 reduces to $SM^2 = 2$. The

differential equation (28E) then reduces to

$$\frac{1}{\alpha} \frac{d\alpha}{dX} - \frac{1}{\beta} \frac{d\beta}{dX} - \frac{j}{2} \frac{d\phi}{dX} = 0 \tag{8E}$$

This is identical to equation (8E) derived at the beginning of this

Appendix for an incompressible vapor.

Equation (28E) must be applied in the analysis of two-phase flow

characteristics for fully developed turbulent flow whenever the vapor

velocity is such that the ratio

$$\frac{P_o - P}{\rho_v V_v^2 / 2}$$

is significantly greater than unity.

APPENDIX F

INITIAL LIQUID BOUNDARY LAYER EQUATION

Assuming that liquid condensate flows in an annular cross section with an area A_L and a thickness δ, then

$$A_L = \frac{\pi}{4} \left[D^2 - (D - 2\delta)^2 \right] \tag{1F}$$

which reduces to

$$A_L = \pi(D\delta - \delta^2) = \pi(D - \delta)\delta \tag{2F}$$

The rate of flow of liquid condensate W_L can then be expressed

$$W_L = \pi(D - \delta)\delta \rho_L V_L \tag{3F}$$

Differentiating (3F) logarithmically and assuming ρ_L varies insignificantly results in

$$\frac{dW_L}{W_L} = \frac{d\delta}{\delta} + \frac{dV_L}{V_L} - \frac{d\delta}{(D - \delta)} \tag{4F}$$

When δ is small relative to D, i.e., $\delta \ll D$, (4F) reduces to

$$\frac{dW_L}{W_L} = \frac{d\delta}{\delta} + \frac{dV_L}{V_L} \tag{5F}$$

The f o l l o w i n g well-known non-dimensional universal distribution functions are now introduced:

$$y^+ \equiv (y/\mu_L) \sqrt{\tau_w/\rho_L} \tag{6F}$$

and

$$V_L^+ \equiv V_L \sqrt{\rho_L/\tau_w} \tag{7F}$$

In the present analysis the upper limit of y^+ will be $y^+ = \delta^+$ at $y = \delta$, where δ is the local liquid layer thickness for the annular liquid layer. In Appendix I it is shown that $y^+ = V_L^+$ up to $y^+ \simeq 1$. For the region where $y^+ = \delta^+ \leqq 1$, therefore

$$V_{Li} = \frac{\delta \tau_w}{\mu_L} \tag{8F}$$

where V_{Li} is the time average interfacial liquid velocity. This linear relation (8F) requires that the time and area average liquid velocity V_L equal one-half the time average interfacial liquid velocity. V_{Li} for the very thin laminar liquid layer, thus

$$V_{Li} = 2V_L \tag{9F}$$

The laminar liquid boundary layer thickness may, therefore, be expressed by

$$\delta = \frac{2\mu_L V_L}{\tau_w} \tag{10F}$$

Differentiating (10F) logarithmically gives

$$\frac{d\delta}{\delta} = \frac{dV_L}{V_L} - \frac{d\tau_w}{\tau_w} \tag{11F}$$

Equation (11F) may be substituted into (5F) to obtain

$$\frac{dW_L}{W_L} = 2\frac{dV_L}{V_L} - \frac{d\tau_w}{\tau_w} \tag{12F}$$

At the beginning of vapor condensation the total liquid flow W_L is a very small quantity with virtually negligible momentum. In this region,

therefore, it may be assumed that $\tau_v = \tau_w$. If the vapor flow begins to develop a boundary layer in either laminar or turbulent flow after inlet to a condenser tube, the vapor friction factor may be expressed in the form

$$f_v = C_f/(Re_{vx})^s \tag{13F}$$

where C_f and s are particular constants and the length Reynolds number is $Re_{vx} = V_v \rho_v L/\mu_v$. The wall shear stress may then be expressed in terms of the vapor friction factor as follows:

$$\tau_w = \tau_v = f_v \rho_v V_v^2/2 = C_f \rho_v V_v^2/2(Re_{vx})^s \tag{14F}$$

Differentiating (14F) logarithmically and neglecting the variation in dynamic viscosity leads to the expression

$$\frac{d\tau_w}{\tau_w} = (2 - s)\frac{dV_v}{V_v} + (1 - s)\frac{d\rho_v}{\rho_v} - s\frac{dL}{L} \tag{15F}$$

Now substituting (15F) into (12F) gives

$$2\frac{dV_L}{V_L} - (2 - s)\frac{dV_v}{V_v} - \frac{dW_L}{W_L} - (1 - s)\frac{d\rho_v}{\rho_v} = -s\frac{dL}{L} \tag{16F}$$

Again normalizing the terms of (16F) and dividing by dL results in the differential equation

$$\frac{2}{\alpha}\frac{d\alpha}{dX} - \frac{(2 - s)}{\beta}\frac{d\beta}{dX} + \frac{1}{1 - \theta}\frac{d\theta}{dX} - \frac{j(1 - s)}{\phi}\frac{d\phi}{dX} = -\frac{s}{X} \tag{17F}$$

In most cases the region of the developing laminar annular liquid layer is so short, i.e., several diameters or less, that the variation in vapor velocity and density over this length may be neglected. Equation (17F) may then be simplified to the form

$$\frac{2}{\alpha}\frac{d\alpha}{dX} + \frac{1}{1 - \theta}\frac{d\theta}{dX} = -\frac{s}{X} \tag{18F}$$

If the initial vapor boundary layer develops in laminar flow from the
tube entrance, the constant s has the value s = ½. If the vapor layer
develops in turbulent flow, s = 1/5.

If the vapor flow enters the condensing region in fully developed
laminar or turbulent flow, the initial boundary layer equation will take
still another form. Burbank and Hilding (4) have derived an expression
for the liquid boundary layer equation for fully developed laminar or
turbulent vapor flow. For the turbulent flow of steam in smooth pipes
at moderate pressures, the equation given is

$$\frac{2}{\alpha} \frac{d\alpha}{dX} - \frac{1.75}{\beta} \frac{d\beta}{dX} + \frac{1}{1 - \theta} \frac{d\theta}{dX} - \frac{(0.732)}{\phi} \frac{d\phi}{dX} = 0 \qquad (19F)$$

For fully developed laminar vapor flow at the beginning of condensation,
the liquid boundary layer equation given is

$$\frac{2}{\alpha} \frac{d\alpha}{dX} - \frac{1}{\beta} \frac{d\beta}{dX} + \frac{1}{1 - \theta} \frac{d\theta}{dX} = 0 \qquad (20F)$$

If the variation in stream pressure and vapor velocity are neglected
over the short length of the developing liquid boundary layer, equations
(19F) and (20F) both simplifiy to the form

$$\frac{2}{\alpha} \frac{d\alpha}{dX} + \frac{1}{1 - \theta} \frac{d\theta}{dX} = 0 \qquad (21F)$$

Except for the right-hand term of (18F), equations (18F) and (21F) are
identical. In equation (18F), the term $\frac{s}{X}$ plays a strong role since the
value becomes infinite at the tube entrance where $X = \frac{L}{D} = 0$.

For the integrated solutions presented in this paper, equation
(17F), with $\frac{d\beta}{dX} \backsimeq 0$, has been used for the region up to $\delta^+ = 1$. The
value s = ½ has been assumed for a laminar development of the flow in

the vapor core starting at zero tube length. For turbulent development of the vapor core the value s = 1/5 has been used.

Either form of the initial liquid boundary layer equation must be limited in application to the region of developing laminar liquid flow, i.e., $\delta^+ \leq 1$. In the numerical solution of the system of equations, it is necessary, therefore, to determine the axial position at which the liquid interface will begin to become turbulent. From this point, the equation of equal interfacial velocity pressures may be employed (see Appendix E).

Rearranging equation (6F) and, since $y^+ = \delta^+$ at $y = \delta$, then

$$\delta^2 = \frac{\mu_L^2 \, \delta^{+2}}{\rho_L \tau_w} \tag{22F}$$

At the start of condensation a linear development of the velocity distribution in the very thin liquid layer has been assumed. Thus equation (9F) gives $V_{Li} = 2V_L$ and equation (10F) relates the liquid layer thickness with the average liquid layer velocity as follows:

$$\delta = 2\mu_L V_L / \tau_w \tag{10F}$$

In addition, the continuity equation for the very thin annular liquid layer, equation (3F), may be simplified to

$$W_L \simeq \pi D \delta \rho_L V_L \tag{23F}$$

Combining equations (10F), (22F), and (23F), the local liquid flow rate can be expressed as a function of the dimensionless liquid layer thickness δ^+, thus

$$W_L = \pi D \mu_L (\delta^+)^2 / 2 \tag{24F}$$

An expression for the local liquid flow rate as a function of the axial tube length after start of condensation is given in Appendix G, as follows:

$$\Delta W_L = \frac{Q' \Delta L}{h_{fge} + V_{ve}^2/2J} \tag{2G}$$

Assuming this equation holds with sufficient accuracy over the first few diameters of the condensing length, i.e., $W_L = \Delta W_L$ in this region, and equating (24F) and (2G) leads to the equation

$$X = L/D = \pi \mu_L (\delta^+)^2 (h_{fge} + V_{ve}^2/2J)/2Q' \tag{25F}$$

Equation (25F) may be solved for the initial dimensionless distance X over which the developing liquid layer remains in a laminar flow. The value $\delta^+ = 1$ has been used in the solutions presented in this thesis.

APPENDIX G

CALCULATION OF INITIAL CONDITIONS NECESSARY FOR DIGITAL COMPUTER

SOLUTION OF THE DIFFERENTIAL EQUATIONS OF CHANGE

A direct analytical integration of the system of non-linear

differential equations of change developed in this investigation and

summarized in Table II, page 20, is not known. However, it is possible

to find approximate solutions of sufficient accuracy by employing numer-

ical methods of solution. Beginning with dry saturated vapor at the

entrance of a condenser tube, the system of equations of Table II may be

solved numerically by use of a digital computer. The following informa-

tion must be specified to permit programming a solution for a proposed

condenser tube:

1. Tube I.D. (D)

2. Local heat transfer rate per unit length (Q')

3. Inlet static pressure of saturated vapor (P)

4. Inlet average steam velocity or total mass flow rate (W_T)

5. A suitable correlation for determining the local interfacial

shear stress (τ_V) or local wall shear stress (τ_W)

6. Empirical data on the thermo-physical properties of the parti-

cular saturated vapor and its saturated liquid

Examination of the equations of Table II reveals that singularities

in the values of several of the coefficients will exist at the beginning

105

of condensation when the total quality is unity ($\theta = 1$) and the liquid velocity is zero. This situation presents no difficulty for a direct integration process, but cannot be handled with a numerical solution on a digital computer. It is possible to avoid the problem of coefficient singularities by establishing finite values of these coefficients at a very short length increment after the beginning of condensation by the method outlined below. It should be pointed out that ordinarily it is not possible to begin the numerical solution in the middle of a condenser tube since the values of the normalized dependent variables are always related to the conditions at a total quality of unity at the onset of condensation. A condenser tube which is expected to receive wet vapor may, of course, be designed from the point at which the expected total inlet quality corresponds to the quality of the analytical solution.

In order to establish finite coefficients at the start of the numerical solution process, the equation of energy conservation is applied to the process of condensation of a small fraction of saturated inlet vapor, thus

$$Q' \Delta L = \Delta W_L \left[(h_{ve} - h_L) + \frac{V_{ve}^2 - V_L^2}{2J} \right] \tag{1G}$$

where Q' is the heat transfer rate per unit axial tube length and ΔL is a small but finite increment of length usually a tenth of a diameter or less. Solving for the condensed liquid fraction results in

$$\Delta W_L \simeq \frac{Q' \Delta L}{h_{fge} + \frac{V_{ve}^2}{2J}} \tag{2G}$$

where h_{fge} is the latent heat of condensation taken at the inlet saturation pressure. The local quality θ at ΔL will, therefore, be

$$\theta = \frac{W_v}{W_T} = \frac{W_T - W_L}{W_T} = 1 - \frac{Q' \Delta L}{W_T (h_{fge} + \frac{V_{ve}^2}{2J})} \tag{3G}$$

From the equation of continuity

$$\rho_L V_L A_L = W_L \tag{4G}$$

and for the thin annular liquid layer near the tube entrance the cross section area is

$$A_L \simeq \pi D \delta \tag{5G}$$

For the developing laminar liquid layer,

$$\tau_w = \mu_L \frac{dV_L}{dy} \tag{6G}$$

Assuming a linear development of the velocity in the very thin liquid layer at the beginning of condensation, the mean liquid velocity is

$$V_{mean} = V_L = V_{Li}/2 \tag{7G}$$

where V_{Li} is the time average interfacial liquid velocity and, therefore,

$$\tau_w = \mu_L 2 V_L / \delta \tag{8G}$$

If it is assumed that a laminar vapor layer begins to develop from the leading edge of the tube mouth, the local interfacial vapor shear stress can be expressed as

$$\tau_v = 0.332 \frac{V_{ve} \mu_{ve}}{\Delta L} \left[\frac{V_{ve} \rho_{ve} \Delta L}{\mu_{ve}} \right]^{\frac{1}{2}} \tag{9G}$$

At the start of condensation the small amount of low velocity liquid has

virtually negligible momentum and, therefore, $\tau_w \simeq \tau_v$.

Combining equations (4G), (5G), and (8G) leads to the following expression for liquid velocity:

$$V_L = \left[\frac{W_L \tau_w}{2\pi D \rho_L \mu_L} \right]^{\frac{1}{2}} \tag{10G}$$

The normalized local velocity in the developing laminar liquid layer may then be represented by

$$\alpha = \frac{V_L}{V_{ve}} = \frac{1}{V_{ve}} \left[\frac{W_L \tau_w}{2\pi D \rho_L \mu_L} \right]^{\frac{1}{2}} \tag{11G}$$

As indicated above $\tau_w \simeq \tau_v$; this quantity is given by either equation (9G) or whatever equation is suitable for the starting vapor shear stress. The mass flow rate of vapor is expressed by the equation

$$\rho_v A_v V_v = W_v = W_T - W_L \tag{12G}$$

The vapor core cross section is related to the tube cross section area by

$$A_v = A - A_L \tag{13G}$$

It is, therefore, possible to find an expression for the local vapor velocity in its normalized form, thus

$$\beta = \frac{V_v}{V_{ve}} = \frac{W_T - W_L}{\rho_v A_v V_{ve}} = \frac{W_T - W_L}{\rho_v V_{ve}(A - A_L)} \tag{14G}$$

Actually the vapor velocity changes very little over the very short increment near the tube entrance, i.e., $\beta \simeq 1$.

For a developing laminar vapor layer near the tube entrance, it may be shown by simple integration that the average shear stress over an interval beginning at zero length is twice the local value, thus

$$\overline{\tau}_v = 2\tau_v = 0.664 \frac{V_v \mu_v}{\Delta L} \sqrt{\frac{V_v \rho_v L}{\mu_v}} \tag{15G}$$

Writing the momentum equation over the short increment ΔL, leads to

$$(P_e - P_L)A - \overline{\tau}_v \pi D \Delta L = W_L(V_L - V_{ve}) \tag{16G}$$

This expression neglects any small changes in the vapor velocity over the small increment ΔL.

Solving equation (16G) for the normalized pressure ϕ leads to

$$\phi = \frac{P_L}{P_e} = 1 - \frac{4\pi D \bar{\tau}_v \Delta L}{P_e A} + \frac{W_L(V_{ve} - V_L)}{P_e A} \tag{17G}$$

In order to establish a numerical value for ϕ from equation (17G) it is first necessary to evaluate $\bar{\tau}_v$ numerically by use of equation (15G).

For a very short, finite, initial increment ΔL, equations (3G), (11G), (14G), and (17G) may be used to establish finite values for the normalized dependent variables α, β, θ, and ϕ. The coefficients of each term of the several differential equations of change given in Table II will then have finite values, and the numerical solution may be started on a digital computer.

If the vapor is in fully developed laminar or turbulent flow at the start of condensation, a similar analysis can be made using the proper expression for the interfacial vapor shear stress at the beginning of condensation.

APPENDIX H

ANALYSIS OF EXPERIMENTAL DATA FOR HIGH VELOCITY

STEAM CONDENSATION IN SMALL TUBES

Most of the useful experimental data gathered during this investigation, as well as the information calculated from the data, is included in Tables IV through XVII, at the end of this Appendix. The data were recorded for the condensation of water vapor entering the condenser tube at pressures from about 20 to 100 psia in the saturated vapor state. The vapor was usually condensed to liquid water at exit pressures of about one atmosphere or higher. Condensing test data are included for condenser tubes of 0.190, 0.550, and 1.025 inches I.D. (see Table III for complete dimensions). The required length for complete condensation varied from about 5 to 20 feet. Vapor velocities up to and in excess of sonic velocity in saturated water vapor were calculated.

For each test, experimental data on local pressure and temperature measurements over the condensing length are reported for the condensing vapor. Also, temperature measurements in the cooling water over the condensing length are given, as well as the flow rates of both condensate and cooling water. From the heat balance on the cooling water taken at axial intervals along the condensing length, the total energy removed from the vapor Q_L, up to each axial position L, was calculated.

From the primary experimental data described above, a number of secondary calculations were made to determine local values of the

110

desired variables. The details of these computations are described in the following pages. A list of the recorded and computed data is given on the following page.

Recorded and Computed Data

For the experimental tests conducted on condensing steam, the following data were recorded in most tests:

1. axial distance along tube from onset of condensation (L)

2. local static pressure (P)

3. local stagnation pressure (P_o)

4. local condenser tube wall temperature (T_w)

5. local cooling water temperature (T_c)

6. total flow rate of condensate at exit (W_T)

7. total flow rate of cooling water (W_c)

From the above data the following information was computed for most tests:

1. local heat transfer rate (Q')

2. local liquid flow rate (W_L)

3. local vapor flow rate (W_v)

4. local vapor velocity (V_v)

5. local average liquid velocity (V_L)

6. local vapor cone cross section (A_v)

7. local liquid layer thickness (δ)

8. local interfacial vapor friction factor (f_v) and shear stress (τ_v)

9. local superficial wall friction factor (f_w) and shear stress (τ_w)

10. local vapor Reynolds number (Re_v)

11. local superficial vapor Reynolds number (Re_v')

12. local surface coefficient of heat transfer of the condensing vapor ($\overset{*}{h}_i$)

Method of Computation

1. Local Vapor Velocity - (V_v)

For the local saturation pressure P the local saturated vapor enthalpy h_v is determined from the steam tables of reference (23). Assuming isentropic compression of the saturated vapor in the mouth of the stagnation pressure probe from the static pressure P to the stagnation pressure P_o, the stagnation ehthalpy h_{vo} is then determined at P_o. The equation of energy conservation may be solved explicitly for the vapor velocity, thus

$$V_v = \sqrt{2J(h_{vo} - h_v)} \tag{1H}$$

This then is the local vapor velocity obtained from the pressure probe measurements.

2. Local Vapor Flow Rate - (W_v)

From the law of energy conservation

$$E_T = W_T h_{voe} = W_L h_L + W_v \left[h_v + \frac{V_v^2}{2J} \right] + Q_L \tag{2H}$$

where E_T is the total energy rate of the steam at the condenser tube entrance h_{voe} is the stagnation enthalpy of the supply steam and Q_L is the total rate of heat removed up to L feet. From the principle of conservation of mass

$$W_T = W_L + W_v \tag{3H}$$

and since W_T is a measured quantity, W_v is given by

$$W_v = \frac{W_T(h_{voe} - h_L) - Q_L}{h_v - h_L + V_v^2/2J} \qquad (4H)$$

which may be written in the form

$$W_v = \frac{W_T(h_{voe} - h_L) - Q_L}{h_{vo} - h_L} \qquad (5H)$$

Equation (4H) has been used to determine the local vapor flow rate W_v

of the remaining vapor in each case.

3. Local Vapor Cone Cross Section - (A_v)

From the equation of continuity

$$W_v = \rho_v A_v V_v \qquad (6H)$$

solving for the vapor area A_v gives

$$A_v = W_v/\rho_v V_v \qquad (7H)$$

4. Local Liquid Flow Rate and Local Liquid Cross Section Area - (W_L

and A_L)

The quantity W_L can now be determined directly by rearranging

equation (3H)

$$W_L = W_T - W_v \qquad (3H)$$

and the local liquid cross section A_L is calculated by use of the

relation

$$A_L = A - A_v \qquad (8H)$$

5. Local Mean Liquid Velocity and Local Thickness of the Annular

Liquid Layer (V_L and δ)

Solving the equation for the mass flow rate of the liquid ex-

plicitly for V_L gives

$$V_L = W_L/A_L \rho_L \qquad (9H)$$

Equation (2F) may also be solved for the local thickness of the annular

liquid layer, and can then be written in the form

$$\delta = \frac{D - \sqrt{D^2 - 4A_L/\pi}}{2} \qquad (10H)$$

The necessary information for evaluating equations (9H) and (10H)

is given by equations (3H) and (8H) above.

6. Local Interfacial Vapor Friction Factor - (f_v)

The vapor friction factor is defined in Appendix C by the

expression

$$f_v \equiv \frac{\tau_v}{\rho_v V_v^2/2} \qquad (6C)$$

Solving the vapor momentum equation (2C) explicitly for the vapor fric-

tion factor f_v results in the expression

$$f_v = \frac{-1}{V_v} \left[\frac{W_v}{\pi \rho_v V_v} \right]^{1/2} \left[\frac{V_v - V_i}{W_v} \frac{dW_v}{dL} + \frac{dV_v}{dL} + \frac{1}{\rho_v V_v} \frac{dP}{dL} \right] \qquad (11H)$$

In order to compute local values of either the interfacial shear

stress τ_v from equation (2C), or f_v from equation (11H), from experi-

mental data, it is necessary to determine each of the terms occurring

in the above equation from the experimental data. The method of evalu-

ating local flow properties has been outlined earlier in this Appendix.

The local derivatives of the same properties must be found by graphical

means from suitable plots of the several properties or by curve fitting

approximation equations from which the derivatives can be found by differentiation.

7. Local Superficial Wall Friction Factor - (f_w)

The superficial wall friction factor is defined in Appendix C by the expression

$$f_w \equiv \frac{\tau_w}{\rho_v V_v^2/2} \qquad (13C)$$

Solving the combined momentum equation (11C) explicitly for the superficial wall friction factor f_w , leads to the expression

$$f_w = \frac{-2}{\pi D \rho_v V_v^2} \left[W_L \frac{dV_L}{dL} + W_v \frac{dV_v}{dL} + (V_v - V_L) \frac{dW_v}{dL} + A \frac{dP}{dL} \right] \qquad (12H)$$

Computation of τ_w and/or f_w from experimental data must be done by the same methods as used in computing the interfacial friction factor.

8. Local Vapor Reynolds Number - (Re_v)

The local vapor Reynolds number is defined by the expression

$$Re_v \equiv V_v D_v \rho_v / \mu_v \qquad (13H)$$

The quantities on the right-hand side of this equation are taken from the computed local flow properties and from tables of the physical properties of saturated vapor taken at the local static pressure.

9. Local Superficial Reynolds Number - (Re_v')

The local superficial vapor Reynolds number is defined by the expression

$$Re_v' \equiv V_v D \rho_v / \mu_v \qquad (14H)$$

This definition is identical to the definition of the ordinary vapor Reynolds number except that the inside tube diameter has replaced the

vapor cone diameter. This definition, used by many earlier investigators, is written as though the vapor fraction flows in the condenser tube without the liquid being present, thus

$$Re_v' = G_v D/\mu_v \qquad (15H)$$

In this definition the quantity G_v is the average local vapor mass flow rate per unit area, based on the tube cross section. In most experimental work conducted by other investigators, no attempt has been made to measure the actual vapor velocity and so no alternative to the use of the above Reynolds number definition (14H) was possible.

10. The Local Heat Transfer Coefficient of the Condensing Vapor - $(\overset{*}{h_i})$

Two methods were used for computing the local coefficient of heat transfer $\overset{*}{h_i}$ for the condensing vapor. The first method, which will be called the __direct__ method, requires measurement of the outside surface temperature of the inner or condenser pipe. Only heat exchangers No. 2 and No. 4 were instrumented so as to measure this temperature directly. The local rate of heat flow in the radial direction at any point along the pipe was determined by taking the product of the cooling water flow rate in the annulus and the local axial temperature gradient of the cooling water. The axial gradient was determined graphically and/or by a curve fitting technique from the recorded experimental data on the temperature of the cooling water. Using the well-known equation for radial heat flow through a cylindric wall, the temperature drop ΔT_{cu} across the wall was calculated. Adding the drop in temperature across the wall to the measured outside wall temperature gives the inner surface temperature of the condenser pipe.

Using the local heat transfer rate per foot of tube Q' as determined by the method outlined above, the local surface coefficient of heat transfer $\overset{*}{h}_i$ was then derived from the defining equation

$$Q' \equiv \overset{*}{h}_i \pi D_i (T_v - T_w) \qquad (16H)$$

Solving for $\overset{*}{h}_i$ gives

$$\overset{*}{h}_i = \frac{Q'}{\pi D_i (T_v - T_w)} \qquad (17H)$$

Note that Q' is the local radial heat transfer flux in BTU per hour, foot. D_i is the inner diameter of the condenser tube, T_v is the local saturation temperature of the condensing vapor, and T_w is the local inside wall temperature determined by the method outlined above.

The second method, which will be called the indirect method, requires the calculation of the temperature drop across the cooling water film on the outside of the condenser tube. The local temperature drop across the cooling water film was determined by dividing the local rate of radial heat flow per foot of tube by the local outside cooling water surface coefficient of heat transfer $\overset{*}{h}_o$. (See succeeding paragraphs for the method of determining $\overset{*}{h}_o$.) Having indirectly determined the outer surface temperature of the condenser tube, the procedure is then identical with that of the direct method of calculation described above.

For the two condenser heat exchangers (Nos. 1 and 3) not instrumented with condenser tube surface thermocouples, it was necessary to experimentally determine a correlation for the outside surface heat transfer coefficient $\overset{*}{h}_o$. For these two heat exchangers, tests were conducted using hot water in the condenser tube cooled by cold water in the annulus between the inner and outer tubes. It was assumed that the

dimensionless correlation for a hot liquid flowing inside the circular

condenser tube was known with good accuracy. For example, in turbulent

flow in a tube the correlation

$$Nu = 0.027(Re)^{0.80}(Pr)^{1/3}(\mu/\mu_i)^{0.14} \qquad (18H)$$

is well documented (22) for the conditions encountered in this test. The

local rate of radial heat flow can be determined from either the heated

or cooled stream, since the flow rate of both streams as well as the

local axial temperature distribution in each stream was recorded. Em-

ploying the common expression for fluid-to-fluid heat transfer through

a circular wall, the local coolant surface coefficient was calculated.

The equation is as follows:

$$Q' = \frac{\pi(T_h - T_c)}{\dfrac{1}{D_o \overset{*}{h}_o} + \dfrac{\ln(D_o/D_i)}{2k_w} + \dfrac{1}{D_i \overset{*}{h}_i}} \qquad (19H)$$

Solving for the outside cooling surface coefficient $\overset{*}{h}_o$ results in the

expression

$$\overset{*}{h}_o = \frac{1}{D_o \left[\dfrac{\pi(T_h - T_c)}{Q'} - \dfrac{\ln(D_o/D_i)}{2k_w} - \dfrac{1}{D_i \overset{*}{h}_i} \right]} \qquad (20H)$$

For the correlation of the outside surface coefficient $\overset{*}{h}_o$ the j

factor or Colburn number was used. This dimensionless heat transfer

number is defined by

$$Co \equiv j \equiv (\overset{*}{h}_o/V\rho C)(Pr)^{2/3}(\mu_w/\mu)^{0.14} = f(D_e \rho V/\mu) \qquad (21H)$$

where μ_w is taken at the outside wall surface temperature of the condenser

tube. The equivalent diameter is $D_e = (D_2 - D_o)$, where D_2 is the inside

diameter of the outer tube of the annulus and D_o is the outer diameter of the condenser tube.

TABLE IV

Test Data

Test 71052   0.550 inches I.D. Tube
Counterflow coolant   Coolant rate = 2.40 lb_m/sec.

Condensing length = 11.1 ft.

L	X	T_c	P	P_o	μ_v	μ_L
DIST (FEET)	L/D	TCOOL (DEGF)	PSTAT (PSIA)	PSTAG (PSIA)	VPVISC (LBF-SEC/SQFT)	LQVISC
0.000	0.000	105.20	36.40	44.87	0.2733E-06	0.4484E-05
0.125	2.727	104.11	35.99	44.85	0.2731E-06	0.4498E-05
0.250	5.455	103.05	35.58	44.78	0.2728E-06	0.4512E-05
0.375	8.182	102.02	35.17	44.66	0.2725E-06	0.4527E-05
0.500	10.910	101.00	34.75	44.49	0.2722E-06	0.4542E-05
0.750	16.365	99.03	33.91	44.03	0.2716E-06	0.4573E-05
1.000	21.820	97.14	33.06	43.43	0.2709E-06	0.4606E-05
1.250	27.275	95.32	32.18	42.71	0.2706E-06	0.4640E-05
1.500	32.730	93.56	31.29	41.90	0.2696E-06	0.4677E-05
1.750	38.185	91.85	30.38	41.01	0.2688E-06	0.4716E-05
2.000	43.640	90.18	29.44	40.08	0.2681E-06	0.4758E-05
2.250	49.094	88.56	28.49	39.10	0.2673E-06	0.4802E-05
2.500	54.549	86.96	27.51	38.11	0.2664E-06	0.4849E-05
2.750	60.004	85.40	26.52	37.10	0.2655E-06	0.4900E-05
3.000	65.459	83.86	25.50	36.09	0.2646E-06	0.4955E-05
3.500	76.369	80.84	23.43	34.10	0.2626E-06	0.5075E-05
4.000	87.279	77.87	21.33	32.18	0.2603E-06	0.5214E-05
4.500	98.189	74.95	19.21	30.36	0.2579E-06	0.5374E-05
5.000	109.099	72.06	17.14	28.64	0.2553E-06	0.5555E-05
5.500	120.009	69.22	15.15	27.03	0.2526E-06	0.5760E-05
6.000	130.919	66.42	13.30	25.50	0.2497E-06	0.5985E-05
6.500	141.828	63.70	11.67	24.03	0.2469E-06	0.6224E-05
6.750	147.283	62.38	10.95	23.32	0.2455E-06	0.6343E-05
7.000	152.738	61.08	10.32	22.62	0.2443E-06	0.6457E-05
7.250	158.193	59.82	9.78	21.93	0.2432E-06	0.6563E-05
7.500	163.648	58.61	9.35	21.24	0.2422E-06	0.6654E-05
7.750	169.103	57.44	9.03	20.57	0.2415E-06	0.6724E-05
8.000	174.558	56.33	8.84	19.90	0.2411E-06	0.6768E-05
8.250	180.013	55.29	9.02	19.25	0.2415E-06	0.6726E-05
8.500	185.468	54.31	10.65	18.61	0.2450E-06	0.6397E-05
8.750	190.923	53.41	11.40	17.99	0.2464E-06	0.6266E-05
9.000	196.378	52.61	12.02	17.40	0.2475E-06	0.6168E-05
9.250	201.833	51.90	12.52	16.83	0.2484E-06	0.6094E-05
9.500	207.288	51.31	12.92	16.31	0.2491E-06	0.6037E-05
9.750	212.743	50.83	13.25	15.84	0.2496E-06	0.5992E-05
10.000	218.198	50.49	13.52	15.43	0.2501E-06	0.5956E-05
10.250	223.653	50.30	13.75	15.10	0.2504E-06	0.5926E-05
10.500	229.108	50.25	13.98	14.87	0.2508E-06	0.5898E-05
10.750	234.563	50.18	14.20	14.76	0.2511E-06	0.5870E-05
11.000	240.017	50.16	14.46	14.75	—	—

TABLE V

Test Data

Test 71752
Counterflow coolant

0.550 inches I.D. Tube
Coolant rate = 2.52 lb$_m$/sec.

Condensing length = 9.7 ft.

L	X	T_c	P	P_o	μ_v	μ_L
DIST (FEET)	L/D	TCOOL (DEGF)	PSTAT (PSIA)	PSTAG (PSIA)	VPVISC	LQVISC
					(LBF-SEC/SQFT)	
0.000	0.000	94.00	26.80	34.70	0.2658E-06	0.4886E-05
0.125	2.727	92.58	26.76	34.69	0.2657E-06	0.4888E-05
0.250	5.455	91.24	26.71	34.67	0.2657E-06	0.4890E-05
0.375	8.182	89.97	26.59	34.60	0.2656E-06	0.4896E-05
0.500	10.910	88.77	26.40	34.50	0.2654E-06	0.4906E-05
0.750	16.365	86.57	25.60	34.19	0.2647E-06	0.4949E-05
1.000	21.820	84.60	24.95	33.77	0.2640E-06	0.4986E-05
1.250	27.275	82.84	24.14	33.25	0.2633E-06	0.5033E-05
1.500	32.730	81.26	23.33	32.65	0.2624E-06	0.5082E-05
1.750	38.185	79.83	22.51	31.97	0.2616E-06	0.5134E-05
2.000	43.640	78.53	21.70	31.22	0.2607E-06	0.5188E-05
2.250	49.094	77.33	20.89	30.43	0.2599E-06	0.5246E-05
2.500	54.549	76.23	20.08	29.59	0.2589E-06	0.5306E-05
2.750	60.004	75.18	19.26	28.72	0.2580E-06	0.5370E-05
3.000	65.459	74.19	18.45	27.84	0.2570E-06	0.5437E-05
3.250	70.914	73.24	17.64	26.94	0.2560E-06	0.5509E-05
3.500	76.369	72.31	16.83	26.04	0.2549E-06	0.5585E-05
3.750	81.824	71.38	16.01	25.15	0.2538E-06	0.5666E-05
4.000	87.279	70.46	15.20	24.26	0.2526E-06	0.5754E-05
4.500	98.189	68.58	13.58	22.56	0.2502E-06	0.5949E-05
5.000	109.099	66.62	12.20	20.97	0.2478E-06	0.6141E-05
5.250	114.554	65.60	12.12	20.24	0.2477E-06	0.6153E-05
5.500	120.009	64.55	12.15	19.54	0.2478E-06	0.6148E-05
5.750	125.464	63.48	12.20	18.89	0.2478E-06	0.6141E-05
6.000	130.919	62.39	12.26	18.29	0.2479E-06	0.6132E-05
6.250	136.374	61.28	12.33	17.74	0.2481E-06	0.6122E-05
6.500	141.828	60.16	12.41	17.23	0.2482E-06	0.6110E-05
6.750	147.283	59.04	12.51	16.78	0.2484E-06	0.6096E-05
7.000	152.738	57.93	12.62	16.37	0.2486E-06	0.6079E-05
7.250	158.193	56.84	12.75	16.01	0.2488E-06	0.6061E-05
7.500	163.648	55.78	12.90	15.70	0.2490E-06	0.6040E-05
7.750	169.103	54.77	13.06	15.44	0.2493E-06	0.6018E-05
8.000	174.558	53.83	13.23	15.21	0.2496E-06	0.5994E-05
8.250	180.013	52.97	13.42	15.03	0.2499E-06	0.5969E-05
8.500	185.468	52.22	13.61	14.88	0.2502E-06	0.5944E-05
8.750	190.923	51.59	13.81	14.76	0.2505E-06	0.5919E-05
9.000	196.378	51.12	13.99	14.67	0.2508E-06	0.5895E-05
9.250	201.833	50.82	14.17	14.59	0.2511E-06	0.5874E-05
9.500	207.288	50.72	14.31	14.53	0.2513E-06	0.5857E-05
9.625	210.015	50.70	14.37	14.50	-	-

TABLE VI

Test Data

Test 71852   0.550 inches I.D. Tube
Counterflow coolant   Coolant rate = 2.33 lb_m/sec.

Condensing length = 7.1 ft.

L	X	T_c	P	P_o	μ_V	μ_L
DIST (FEET)	L/D	TCOOL (DEGF)	PSTAT (PSIA)	PSTAG (PSIA)	VPVISC	LQVISC
					(LBF-SEC/SQFT)	
0.000	0.000	86.33	18.61	24.58	0.2572E-06	0.5423E-05
0.125	2.727	84.56	18.55	24.57	0.2571E-06	0.5428E-05
0.250	5.455	82.94	18.47	24.56	0.2570E-06	0.5436E-05
0.375	8.182	81.45	18.35	24.54	0.2569E-06	0.5445E-05
0.500	10.910	80.08	18.22	24.49	0.2567E-06	0.5457E-05
0.625	13.637	78.83	18.06	24.41	0.2565E-06	0.5471E-05
0.750	16.365	77.68	17.88	24.33	0.2563E-06	0.5487E-05
0.875	19.092	76.64	17.69	24.24	0.2560E-06	0.5504E-05
1.000	21.820	75.68	17.49	24.16	0.2558E-06	0.5522E-05
1.125	24.547	74.80	17.28	23.96	0.2555E-06	0.5542E-05
1.250	27.275	74.00	17.05	23.74	0.2552E-06	0.5563E-05
1.375	30.002	73.26	16.83	23.50	0.2549E-06	0.5585E-05
1.500	32.730	72.58	16.59	23.24	0.2546E-06	0.5607E-05
1.625	35.457	71.95	16.36	22.96	0.2543E-06	0.5631E-05
1.750	38.185	71.37	16.13	22.67	0.2540E-06	0.5655E-05
1.875	40.912	70.83	15.89	22.37	0.2563E-06	0.5679E-05
2.000	43.640	70.32	15.67	22.07	0.2533E-06	0.5703E-05
2.125	46.367	69.84	15.44	21.75	0.2530E-06	0.5727E-05
2.250	49.094	69.39	15.22	21.43	0.2527E-06	0.5751E-05
2.500	54.549	68.52	14.81	20.79	0.2521E-06	0.5798E-05
2.750	60.004	67.70	14.43	20.15	0.2515E-06	0.5842E-05
3.000	65.459	66.89	14.10	19.52	0.2510E-06	0.5882E-05
3.250	70.914	66.07	13.83	18.91	0.2506E-06	0.5916E-05
3.500	76.369	65.22	13.60	18.34	0.2502E-06	0.5945E-05
3.750	81.824	64.32	13.44	17.80	0.2499E-06	0.5966E-05
4.000	87.279	63.37	13.33	17.31	0.2498E-06	0.5981E-05
4.250	92.734	62.37	13.28	16.86	0.2497E-06	0.5987E-05
4.500	98.189	61.32	13.28	16.47	0.2497E-06	0.5987E-05
4.750	103.644	60.23	13.34	16.12	0.2498E-06	0.5980E-05
5.000	109.099	59.11	13.43	15.82	0.2499E-06	0.5968E-05
5.250	114.554	57.98	13.56	15.57	0.2501E-06	0.5951E-05
5.500	120.009	56.87	13.71	15.36	0.2504E-06	0.5932E-05
5.750	125.464	55.80	13.87	15.18	0.2506E-06	0.5911E-05
6.000	130.919	54.81	14.03	15.02	0.2509E-06	0.5891E-05
6.250	136.374	53.95	14.18	14.89	0.2511E-06	0.5873E-05
6.500	141.828	53.24	14.29	14.76	0.2513E-06	0.5859E-05
6.750	147.283	52.76	14.35	14.62	0.2514E-06	0.5852E-05
7.000	152.738	52.54	14.36	14.46	0.2514E-06	0.5850E-05
7.250	158.193	52.53	14.38	14.26	-	-

TABLE VII

Test Data

Test 80652
Counterflow coolant.

0.550 inches I.D. Tube
Coolant rate = 1.10 lb_m/sec.

Condensing length = 10.4 ft.

L	T_c	T_o	P	P_o	μ_V	μ_L
DIST (FEET)	TCOOL (DEGF)	TOUTWALL (DEGF)	PSTAT (PSIA)	PSTAG (PSIA)	VPVISC	LQVISC
					(LBF-SEC/SQFT)	
0.000	122.000	212.000	20.900	25.000	0.2599E-06	0.5245E-05
0.125	121.210	211.472	20.839	24.999	0.2598E-06	0.5249E-05
0.250	120.413	210.955	20.762	24.985	0.2597E-06	0.5255E-05
0.375	119.610	210.450	20.669	24.953	0.2596E-06	0.5262E-05
0.500	118.800	209.954	20.564	24.905	0.2595E-06	0.5269E-05
0.750	117.162	208.987	20.315	24.767	0.2592E-06	0.5288E-05
1.000	115.500	208.046	20.026	24.576	0.2589E-06	0.5310E-05
1.250	113.815	207.123	19.703	24.338	0.2585E-06	0.5335E-05
1.500	112.109	206.210	19.354	24.060	0.2581E-06	0.5362E-05
1.750	110.383	205.301	18.986	23.747	0.2577E-06	0.5392E-05
2.000	108.639	204.387	18.605	23.403	0.2572E-06	0.5424E-05
2.250	106.878	203.464	18.216	23.034	0.2567E-06	0.5457E-05
2.500	105.102	202.523	17.826	22.645	0.2562E-06	0.5492E-05
2.750	103.314	201.561	17.438	22.239	0.2557E-06	0.5527E-05
3.000	101.514	200.570	17.057	21.822	0.2552E-06	0.5563E-05
3.250	99.706	199.547	16.685	21.396	0.2547E-06	0.5599E-05
3.500	97.891	198.486	16.327	20.967	0.2542E-06	0.5634E-05
3.750	96.072	197.382	15.985	20.536	0.2538E-06	0.5669E-05
4.000	94.251	196.233	15.660	20.107	0.2533E-06	0.5703E-05
4.250	92.431	195.034	15.356	19.683	0.2529E-06	0.5736E-05
4.500	90.615	193.783	15.073	19.267	0.2525E-06	0.5768E-05
4.750	88.805	192.475	14.813	18.861	0.2521E-06	0.5797E-05
5.000	87.003	191.110	14.577	18.467	0.2517E-06	0.5825E-05
5.250	85.215	189.684	14.364	18.088	0.2514E-06	0.5850E-05
5.500	83.441	188.196	14.175	17.724	0.2511E-06	0.5873E-05
5.750	81.686	186.644	14.011	17.377	0.2508E-06	0.5893E-05
6.000	79.953	185.028	13.870	17.049	0.2506E-06	0.5911E-05
6.500	76.566	181.600	13.658	16.449	0.2503E-06	0.5938E-05
7.000	73.310	177.910	13.532	15.930	0.2501E-06	0.5954E-05
7.500	70.215	173.964	13.483	15.491	0.2500E-06	0.5961E-05
8.000	67.313	169.772	13.501	15.128	0.2500E-06	0.5958E-05
8.250	65.945	167.589	13.531	14.972	0.2501E-06	0.5955E-05
8.500	64.639	165.351	13.573	14.832	0.2501E-06	0.5949E-05
8.750	63.398	163.062	13.626	14.706	0.2502E-06	0.5942E-05
9.000	62.228	160.725	13.688	14.591	0.2503E-06	0.5934E-05
9.250	61.134	158.343	13.757	14.487	0.2504E-06	0.5925E-05
9.500	60.119	155.921	13.832	14.390	0.2506E-06	0.5916E-05
9.750	59.190	153.463	13.913	14.297	0.2507E-06	0.5906E-05
10.000	58.351	150.974	13.996	14.206	0.2508E-06	0.5895E-05
10.250	57.608	148.460	14.082	14.114	0.	0.

TABLE VIII

Test Data

Test 81352   0.190 inches I.D. Tube
Parallel flow coolant   Coolant rate = 0.101 lb_m/sec.

Condensing length = 10.2 ft.

L	X	T_c	P	P_o	μ_v	μ_L
DIST (FEET)	L/D	TCOOL (DEGF)	PSTAT (PSIA)	PSTAG (PSIA)	VPVISC	LQVISC (LBF-SEC/SQFT)
0.000	0.000	56.50	39.20	45.50	0.2752E-06	0.4393E-05
0.125	7.896	61.85	38.77	45.08	0.2750E-06	0.4406E-05
0.250	15.793	67.14	38.28	44.59	0.2746E-06	0.4422E-05
0.375	23.689	72.35	37.73	44.05	0.2743E-06	0.4440E-05
0.500	31.586	77.49	37.14	43.47	0.2739E-06	0.4459E-05
0.750	47.378	87.47	35.83	42.18	0.2730E-06	0.4504E-05
1.000	63.171	97.03	34.44	40.79	0.2719E-06	0.4554E-05
1.250	78.964	106.11	32.99	39.33	0.2709E-06	0.4609E-05
1.500	94.757	114.68	31.53	37.83	0.2697E-06	0.4667E-05
1.750	110.550	122.70	30.10	36.32	0.2686E-06	0.4728E-05
2.000	126.342	130.16	28.71	34.84	0.2674E-06	0.4792E-05
2.250	142.135	137.04	27.39	33.38	0.2663E-06	0.4856E-05
2.500	157.928	143.34	26.15	31.97	0.2652E-06	0.4920E-05
2.750	173.721	149.07	24.99	30.62	0.2641E-06	0.4983E-05
3.000	189.514	154.23	23.93	29.34	0.2630E-06	0.5046E-05
3.250	205.306	158.84	22.95	28.13	0.2621E-06	0.5106E-05
3.500	221.099	162.93	22.07	26.99	0.2611E-06	0.5163E-05
3.750	236.892	166.52	21.27	25.92	0.2603E-06	0.5218E-05
4.000	252.685	169.64	20.55	24.92	0.2595E-06	0.5270E-05
4.250	268.478	172.32	19.91	23.99	0.2587E-06	0.5319E-05
4.500	284.270	174.61	19.33	23.13	0.2581E-06	0.5364E-05
4.750	300.063	176.55	18.81	22.32	0.2574E-06	0.5407E-05
5.000	315.856	178.16	18.35	21.58	0.2569E-06	0.5446E-05
5.500	347.442	180.62	17.54	20.25	0.2558E-06	0.5518E-05
6.000	379.027	182.33	16.86	19.10	0.2550E-06	0.5582E-05
6.500	410.613	183.60	16.28	18.10	0.2542E-06	0.5639E-05
7.000	442.198	184.72	15.77	17.24	0.2535E-06	0.5692E-05
7.250	457.991	185.30	15.55	16.86	0.2531E-06	0.5616E-05
7.500	473.784	185.92	15.34	16.50	0.2528E-06	0.5738E-05
7.750	489.577	186.59	15.16	16.18	0.2526E-06	0.5758E-05
8.000	505.370	187.34	15.00	15.89	0.2523E-06	0.5776E-05
8.250	521.162	188.16	14.86	15.64	0.2521E-06	0.5792E-05
8.500	536.955	189.04	14.75	15.41	0.2520E-06	0.5804E-05
8.750	552.748	189.97	14.67	15.22	0.2519E-06	0.5814E-05
9.000	568.541	190.94	14.62	15.05	0.2518E-06	0.5820E-05
9.250	584.334	191.92	14.59	14.92	0.2517E-06	0.5823E-05
9.500	600.126	192.85	14.58	14.81	0.2517E-06	0.5825E-05
9.750	615.919	193.69	14.52	14.73	0.2516E-06	0.5831E-05
10.000	631.712	194.38	14.50	14.67	0.2516E-06	0.5835E-05
10.125	639.608	194.65	14.49	14.64	0.2516E-06	0.5836E-05

TABLE   IX

Test Data

Test 81452   0.190 inches I.D. Tube
Parallel flow coolant   Coolant rate = 0.206 lb_m/sec.

Condensing length = 4.5 ft.

L	X	T_c	P	P_o	μ_v	μ_L
DIST (FEET)	L/D	TCOOL (DEGF)	PSTAT (PSIA)	PSTAG (PSIA)	VPVISC	LQVISC (LBF-SEC/SQFT)
0.000	0.000	54.20	29.20	34.40	0.2679E-06	0.4769E-05
0.125	7.896	56.57	29.11	34.27	0.2678E-06	0.4773E-05
0.250	15.793	58.82	29.00	34.01	0.2677E-06	0.4778E-05
0.375	23.689	60.95	28.63	33.64	0.2674E-06	0.4795E-05
0.500	31.586	62.98	28.12	33.17	0.2669E-06	0.4819E-05
0.625	39.482	64.92	27.53	32.63	0.2664E-06	0.4849E-05
0.750	47.378	66.78	26.87	32.02	0.2658E-06	0.4882E-05
0.875	55.275	68.55	26.17	31.35	0.2652E-06	0.4918E-05
1.000	63.171	70.26	25.45	30.65	0.2645E-06	0.4957E-05
1.125	71.068	71.91	24.73	29.92	0.2638E-06	0.4998E-05
1.250	78.964	73.51	24.01	29.18	0.2631E-06	0.5040E-05
1.375	86.860	75.06	23.31	28.42	0.2624E-06	0.5083E-05
1.500	94.757	76.56	22.64	27.66	0.2617E-06	0.5126E-05
1.625	102.653	78.03	21.98	26.90	0.2610E-06	0.5169E-05
1.750	110.550	79.47	21.36	26.15	0.2604E-06	0.5212E-05
1.875	118.446	80.88	20.76	25.42	0.2597E-06	0.5255E-05
2.000	126.342	82.27	20.19	24.70	0.2591E-06	0.5297E-05
2.125	134.239	83.64	19.65	24.01	0.2584E-06	0.5339E-05
2.250	142.135	85.00	19.14	23.33	0.2578E-06	0.5379E-05
2.375	150.032	86.34	18.66	22.68	0.2573E-06	0.5419E-05
2.500	157.928	87.67	18.20	22.06	0.2567E-06	0.5459E-05
2.625	165.824	89.00	17.77	21.46	0.2561E-06	0.5497E-05
2.750	173.721	90.31	17.36	20.89	0.2556E-06	0.5534E-05
2.875	181.617	91.62	16.98	20.34	0.2551E-06	0.5570E-05
3.000	189.514	92.93	16.62	19.82	0.2546E-06	0.5605E-05
3.125	197.410	94.23	16.28	19.33	0.2542E-06	0.5639E-05
3.250	205.306	95.52	15.98	18.86	0.2537E-06	0.5670E-05
3.375	213.203	96.80	15.70	18.41	0.2533E-06	0.5700E-05
3.500	221.099	98.07	15.45	17.99	0.2530E-06	0.5727E-05
3.625	228.996	99.34	15.23	17.58	0.2527E-06	0.5751E-05
3.750	236.892	100.59	15.04	17.20	0.2524E-06	0.5772E-05
3.875	244.788	101.82	14.88	16.84	0.2522E-06	0.5789E-05
4.000	252.685	103.04	14.76	16.49	0.2520E-06	0.5803E-05
4.125	260.581	104.23	14.67	16.17	0.2519E-06	0.5814E-05
4.250	268.478	105.39	14.61	15.86	0.2518E-06	0.5821E-05
4.375	276.374	106.52	14.58	15.58	0.2517E-06	0.5824E-05

TABLE X

Test Data

Test 82852   0.190 inches I.D. Tube
Parallel flow coolant   Coolant rate = 0.253 lb$_m$/sec.
                          Condensing length = 12.0 ft.

L	X	T_c	P	P_o	μ_v	μ_L
DIST (FEET)	L/D	TCOOL (DEGF)	PSTAT (PSIA)	PSTAG (PSIA)	VPVISC	LQVISC
					(LBF-SEC/SQFT)	
0.000	0.000	53.50	87.00	99.50	0.2970E-06	0.3545E-05
0.125	7.896	57.04	85.56	98.61	0.2965E-06	0.3561E-05
0.250	15.793	60.48	84.08	97.54	0.2960E-06	0.3577E-05
0.375	23.689	63.82	82.58	96.30	0.2955E-06	0.3594E-05
0.500	31.586	67.07	81.05	94.94	0.2950E-06	0.3612E-05
0.750	47.378	73.30	77.93	91.89	0.2938E-06	0.3649E-05
1.000	63.171	79.18	74.76	88.57	0.2927E-06	0.3690E-05
1.250	78.964	84.73	71.56	85.11	0.2920E-06	0.3733E-05
1.500	94.757	89.97	68.37	81.63	0.2901E-06	0.3778E-05
1.750	110.550	94.90	65.21	78.20	0.2888E-06	0.3826E-05
2.000	126.342	99.56	62.09	74.91	0.2875E-06	0.3877E-05
2.500	157.928	108.07	56.06	68.90	0.2847E-06	0.3985E-05
3.000	189.514	115.63	50.39	63.82	0.2818E-06	0.4101E-05
3.500	221.099	122.33	45.16	59.70	0.2789E-06	0.4225E-05
4.000	252.685	128.27	40.41	56.41	0.2760E-06	0.4356E-05
4.500	284.270	133.54	36.16	53.75	0.2732E-06	0.4492E-05
5.000	315.856	138.22	32.40	51.49	0.2704E-06	0.4632E-05
5.500	347.442	142.40	29.11	49.35	0.2678E-06	0.4773E-05
6.000	379.027	146.13	26.25	47.13	0.2653E-06	0.4914E-05
6.500	410.613	149.47	23.78	44.62	0.2629E-06	0.5054E-05
6.750	426.406	151.02	22.68	43.23	0.2618E-06	0.5123E-05
7.000	442.198	152.49	21.66	41.73	0.2607E-06	0.5191E-05
7.250	457.991	153.88	20.71	40.12	0.2597E-06	0.5259E-05
7.500	473.784	155.21	19.82	38.41	0.2586E-06	0.5325E-05
7.750	489.577	156.48	19.00	36.59	0.2577E-06	0.5391E-05
8.000	505.370	157.68	18.24	34.69	0.2567E-06	0.5455E-05
8.250	521.162	158.83	17.53	32.72	0.2558E-06	0.5518E-05
8.500	536.955	159.93	16.87	30.71	0.2550E-06	0.5580E-05
8.750	552.748	160.97	16.26	28.67	0.2541E-06	0.5641E-05
9.000	568.541	161.97	15.70	26.64	0.2534E-06	0.5699E-05
9.250	584.334	162.92	15.36	24.64	0.2529E-06	0.5736E-05
9.500	600.126	163.82	15.00	22.71	0.2523E-06	0.5776E-05
9.750	615.919	164.68	14.60	20.89	0.2517E-06	0.5822E-05
10.000	631.712	165.49	14.20	19.21	0.2511E-06	0.5870E-05
10.250	647.505	166.26	14.00	17.69	0.2508E-06	0.5895E-05
10.500	663.298	166.97	13.80	16.38	0.2505E-06	0.5920E-05
10.750	679.090	167.64	13.64	15.29	0.2503E-06	0.5940E-05
11.000	694.883	168.26	13.52	14.46	0.2501E-06	0.5956E-05
11.250	710.676	168.82	13.49	13.89	0.2500E-06	0.5960E-05
11.500	726.469	169.33	13.47	13.60	-	-

TABLE XI

Test Data

Test 82952
Parallel flow coolant

Condensing length = 11.7 ft.

0.190 inches I.D. Tube
Coolant rate = 0.281 lb_m/sec.

L	X	T_c	P	P_o	μ_V	μ_L
DIST (FEET)	L/D	TCOOL (DEGF)	PSTAT (PSIA)	PSTAG (PSIA)	VPVISC	LQVISC (LBF-SEC/SQFT)
0.000	0.000	57.50	99.30	111.60	0.3009E-06	0.3425E-05
0.125	7.896	58.27	97.58	110.51	0.3004E-06	0.3440E-05
0.250	15.793	59.08	95.83	109.32	0.2999E-06	0.3457E-05
0.375	23.689	59.94	94.04	108.03	0.2993E-06	0.3474E-05
0.500	31.586	60.85	92.22	106.65	0.2987E-06	0.3492E-05
0.750	47.378	62.81	88.52	103.68	0.2975E-06	0.3529E-05
1.000	63.171	64.94	84.76	100.49	0.2963E-06	0.3570E-05
1.250	78.964	67.24	80.98	97.15	0.2949E-06	0.3591E-05
1.500	94.757	69.68	77.20	93.72	0.2936E-06	0.3658E-05
1.750	110.550	72.27	73.45	90.25	0.2922E-06	0.3707E-05
2.000	126.342	74.99	69.76	86.81	0.2907E-06	0.3758E-05
2.500	157.928	80.79	62.62	80.12	0.2877E-06	0.3868E-05
3.000	189.514	86.99	55.89	73.93	0.2846E-06	0.3988E-05
3.500	221.099	93.51	49.66	68.38	0.2814E-06	0.4118E-05
4.000	252.685	100.25	43.98	63.59	0.2782E-06	0.4256E-05
4.500	284.270	107.14	38.88	59.57	0.2750E-06	0.4403E-05
5.000	315.856	114.06	34.34	56.31	0.2719E-06	0.4557E-05
5.500	347.442	120.95	30.34	53.73	0.2688E-06	0.4718E-05
6.000	379.027	127.69	26.84	51.75	0.2658E-06	0.4884E-05
6.250	394.820	130.98	25.27	50.94	0.2643E-06	0.4968E-05
6.500	410.613	134.21	23.80	50.24	0.2629E-06	0.5053E-05
6.750	426.406	137.34	22.44	49.63	0.2615E-06	0.5139E-05
7.000	442.198	140.39	21.17	49.09	0.2602E-06	0.5225E-05
7.250	457.991	143.33	19.99	48.62	0.2588E-06	0.5312E-05
7.500	473.784	146.14	18.90	48.19	0.2576E-06	0.5399E-05
7.750	489.577	148.83	17.89	47.80	0.2563E-06	0.5486E-05
8.000	505.370	151.37	16.96	47.44	0.2551E-06	0.5572E-05
8.250	521.162	153.76	16.11	47.10	0.2539E-06	0.5657E-05
8.500	536.955	155.98	15.32	46.78	0.2528E-06	0.5740E-05
8.750	552.748	158.01	14.61	46.48	0.2518E-06	0.5821E-05
9.000	568.541	159.85	13.97	46.19	0.2508E-06	0.5898E-05
9.250	584.334	161.49	13.42	45.93	0.2499E-06	0.5970E-05
9.500	600.126	162.90	12.94	45.88	0.2491E-06	0.6034E-05
9.750	615.919	164.08	12.55	45.84	0.2485E-06	0.6089E-05
10.000	631.712	165.01	12.26	45.80	0.2480E-06	0.6131E-05
10.250	647.505	165.68	12.08	45.70	0.2476E-06	0.6158E-05
10.500	663.298	166.08	12.03	45.50	0.2475E-06	0.6167E-05
10.750	679.090	166.19	12.10	43.60	0.2477E-06	0.6156E-05
11.000	694.883	166.21	12.60	30.00	0.2485E-06	0.6082E-05
11.250	710.676	166.23	14.50	14.50	--	--

TABLE XII

Test Data

Test 62364   1.025 inches I.D. Tube
Counterflow coolant   Coolant rate = 3.03 lb_m/sec.
        Condensing length = 17.8 ft.

L	T_c	T_o	P	P_o
DIST (FEET)	TCOOL (DEGF)	TOUTWALL (DEGF)	PSTAT (PSIA)	PSTAG (PSIA)
0.000	125.500	204.000	19.710	23.032
0.125	125.104	203.843	19.708	23.025
0.250	124.703	203.683	19.706	23.018
0.375	124.297	203.520	19.704	23.011
0.500	123.886	203.354	19.701	23.004
1.000	122.194	202.659	19.630	22.976
1.500	120.430	201.916	19.421	22.955
2.000	118.598	201.125	19.138	22.923
2.500	116.704	200.285	18.805	22.871
3.000	114.752	199.397	18.442	22.796
3.500	112.748	198.461	18.068	22.697
4.000	110.696	197.476	17.696	22.571
4.500	108.603	196.443	17.340	22.419
5.000	106.472	195.362	17.008	22.240
5.500	104.310	194.232	16.707	22.036
6.000	102.120	193.054	16.441	21.807
6.500	99.909	191.828	16.215	21.556
7.000	97.680	190.553	16.029	21.285
7.500	95.440	189.230	15.884	20.996
8.000	93.194	187.858	15.776	20.692
8.500	90.945	186.439	15.704	20.377
9.000	88.701	184.971	15.664	20.055
9.500	86.465	183.454	15.653	19.729
10.000	84.242	181.889	15.665	19.402
10.500	82.038	180.276	15.695	19.079
11.000	79.858	178.614	15.739	18.763
11.500	77.707	176.904	15.791	18.458
12.000	75.590	175.146	15.848	18.167
12.500	73.512	173.340	15.906	17.894
13.000	71.478	171.485	15.962	17.641
13.500	69.493	169.581	16.013	17.412
14.000	67.563	167.630	16.059	17.207
14.500	65.691	165.630	16.101	17.030
15.000	63.884	163.581	16.141	16.882
15.500	62.147	161.485	16.183	16.762
16.000	60.484	159.340	16.233	16.671
16.500	58.901	157.146	16.300	16.608
17.000	57.402	154.904	16.395	16.572
17.500	55.994	152.614	16.532	16.560
17.750	55.325	151.541	16.621	16.562

TABLE XIII

Test Data

Test 70764   1.025 inches I.D. Tube
Counterflow coolant   Coolant rate = 3.03 lb_m/sec.
                    Condensing length = 16.8 ft.

L	T_c	T_o	P	P_o
DIST (FEET)	TCOOL (DEGF)	TOUTWALL (DEGF)	PSTAT (PSIA)	PSTAG (PSIA)
0.000	119.000	204.139	21.000	23.490
0.125	118.491	204.056	20.967	23.496
0.250	117.984	203.966	20.933	23.498
0.375	117.476	203.868	20.898	23.497
0.500	116.970	203.763	20.863	23.493
1.000	114.950	203.272	20.710	23.450
1.500	112.940	202.670	20.546	23.365
2.000	110.940	201.961	20.375	23.245
2.500	108.950	201.148	20.200	23.095
3.000	106.970	200.236	20.024	22.922
3.500	105.001	199.228	19.850	22.729
4.000	103.042	198.128	19.680	22.522
4.500	101.092	196.941	19.517	22.304
5.000	99.153	195.669	19.363	22.081
5.500	97.224	194.317	19.220	21.854
6.000	95.305	192.889	19.089	21.629
6.500	93.397	191.388	18.971	21.406
7.000	91.498	189.818	18.868	21.191
7.500	89.610	188.184	18.780	20.983
8.000	87.732	186.489	18.709	20.786
8.500	85.863	184.737	18.653	20.602
9.000	84.005	182.931	18.613	20.430
9.500	82.157	181.077	18.590	20.273
10.000	80.320	179.177	18.581	20.131
10.500	78.492	177.235	18.587	20.004
11.000	76.675	175.255	18.607	19.892
11.500	74.867	173.242	18.639	19.795
12.000	73.070	171.198	18.681	19.713
12.500	71.283	169.129	18.732	19.643
13.000	69.506	167.037	18.790	19.584
13.500	67.739	164.927	18.852	19.536
14.000	65.983	162.802	18.916	19.495
14.500	64.236	160.666	18.978	19.460
15.000	62.500	158.524	19.036	19.428
15.500	60.773	156.378	19.087	19.395
16.000	59.057	154.233	19.126	19.358
16.500	57.351	152.093	19.150	19.314
17.000	55.655	149.962	19.155	19.258

TABLE XIV

Test Data

Test 72064   1.025 inches I.D. Tube
Counterflow coolant   Coolant rate = 3.40 lb_m/sec.
                    Condensing length = 17.1 ft.

L	T_c	T_o	P	P_o
DIST (FEET)	TCOOL (DEGF)	TOUTWALL (DEGF)	PSTAT (PSIA)	PSTAG (PSIA)
0.000	172.000	252.000	60.400	64.380
0.125	170.968	251.837	60.379	64.385
0.250	169.939	251.677	60.349	64.378
0.375	168.914	251.519	60.311	64.360
0.500	167.892	251.363	60.265	64.332
1.000	163.836	250.755	60.016	64.125
1.500	159.832	250.166	59.686	63.799
2.000	155.881	249.588	59.304	63.385
2.500	151.981	249.010	58.894	62.913
3.000	148.135	248.421	58.476	62.407
3.500	144.340	247.814	58.067	61.888
4.000	140.598	247.177	57.680	61.372
4.500	136.908	246.501	57.326	60.873
5.000	133.270	245.776	57.010	60.403
5.500	129.685	244.993	56.738	59.968
6.000	126.152	244.141	56.511	59.573
6.500	122.671	243.210	56.331	59.222
7.000	119.242	242.192	56.195	58.915
7.500	115.866	241.076	56.100	58.652
8.000	112.542	239.852	56.043	58.430
8.500	109.271	238.511	56.017	58.246
9.000	106.051	237.043	56.018	58.095
9.500	102.884	235.437	56.040	57.972
10.000	99.769	233.685	56.076	57.871
10.500	96.707	231.777	56.121	57.787
11.000	93.697	229.701	56.170	57.714
11.500	90.739	227.450	56.217	57.647
12.000	87.833	225.013	56.261	57.581
12.500	84.980	222.380	56.298	57.514
13.000	82.179	219.542	56.329	57.442
13.500	79.430	216.488	56.355	57.365
14.000	76.734	213.209	56.381	57.284
14.500	74.090	209.695	56.413	57.202
15.000	71.498	205.937	56.459	57.123
15.500	68.958	201.924	56.533	57.056
16.000	66.471	197.647	56.651	57.012
16.500	64.036	193.096	56.831	57.003
17.000	61.653	188.261	57.097	57.047

TABLE   XV

Test Data

Test 72164   1.025 inches I.D. Tube
Counterflow coolant   Coolant rate = 5.51 lb_m/sec.
                    Condensing length = 15.9 ft.

L	T_c	T_o	P	P_o
DIST (FEET)	TCOOL (DEGF)	TOUTWALL (DEGF)	PSTAT (PSIA)	PSTAG (PSIA)
0.000	131.500	251.200	60.300	65.460
0.125	130.678	251.118	60.277	65.416
0.250	129.859	251.019	60.244	65.364
0.375	129.044	250.903	60.201	65.306
0.500	128.231	250.772	60.149	65.242
1.000	125.016	250.102	59.865	64.933
1.500	121.853	249.235	59.489	64.555
2.000	118.744	248.208	59.054	64.130
2.500	115.688	247.058	58.591	63.675
3.000	112.686	245.816	58.122	63.205
3.500	109.736	244.507	57.668	62.733
4.000	106.840	243.154	57.243	62.268
4.500	103.997	241.776	56.859	61.818
5.000	101.207	240.386	56.523	61.389
5.500	98.471	238.993	56.240	60.983
6.000	95.787	237.604	56.012	60.604
6.500	93.157	236.218	55.838	60.253
7.000	90.580	234.833	55.715	59.928
7.500	88.056	233.442	55.639	59.628
8.000	85.586	232.032	55.605	59.353
8.500	83.168	230.588	55.605	59.098
9.000	80.804	229.089	55.632	58.861
9.500	78.493	227.511	55.680	58.639
10.000	76.236	225.825	55.742	58.429
10.500	74.031	223.998	55.809	58.229
11.000	71.880	221.993	55.878	58.035
11.500	69.782	219.769	55.944	57.847
12.000	67.737	217.278	56.004	57.665
12.500	65.746	214.473	56.058	57.488
13.000	63.807	211.297	56.107	57.319
13.500	61.922	207.693	56.157	57.160
14.000	60.090	203.598	56.215	57.018
14.500	58.311	198.945	56.293	56.900
15.000	56.586	193.662	56.406	56.814
15.500	54.913	187.673	56.574	56.773
16.000	53.294	180.900	56.821	56.791

TABLE XVI

Test Data

Test 72764   1.025 inches I.D. Tube
Counterflow coolant   Coolant rate = 5.61 lb$_m$/sec.
                  Condensing length = 17.2 ft.

L	T$_c$	T$_o$	P	P$_o$
DIST (FEET)	TCOOL (DEGF)	TOUTWALL (DEGF)	PSTAT (PSIA)	PSTAG (PSIA)
0.000	120.000	234.000	40.290	45.120
0.125	119.276	233.435	40.289	45.087
0.250	118.561	232.885	40.276	45.051
0.375	117.855	232.349	40.251	45.010
0.500	117.157	231.827	40.214	44.966
1.000	114.446	229.871	39.972	44.752
1.500	111.862	228.111	39.607	44.488
2.000	109.396	226.527	39.155	44.180
2.500	107.044	225.097	38.649	43.837
3.000	104.798	223.801	38.115	43.464
3.500	102.651	222.618	37.577	43.068
4.000	100.598	221.527	37.054	42.656
4.500	98.632	220.507	36.560	42.233
5.000	96.745	219.538	36.107	41.803
5.500	94.932	218.597	35.703	41.373
6.000	93.187	217.665	35.353	40.945
6.500	91.502	216.721	35.059	40.525
7.000	89.871	215.743	34.823	40.115
7.500	88.287	214.711	34.643	39.719
8.000	86.745	213.604	34.515	39.339
8.500	85.237	212.401	34.435	38.977
9.000	83.756	211.081	34.397	38.636
9.500	82.298	209.623	34.396	38.317
10.000	80.854	208.007	34.423	38.020
10.500	79.418	206.211	34.472	37.747
11.000	77.984	204.215	34.537	37.497
11.500	76.545	201.997	34.611	37.270
12.000	75.095	199.537	34.689	37.066
12.500	73.627	196.814	34.767	36.883
13.000	72.135	193.807	34.841	36.720
13.500	70.612	190.495	34.912	36.575
14.000	69.051	186.858	34.979	36.445
14.500	67.446	182.874	35.046	36.329
15.000	65.791	178.522	35.119	36.222
15.500	64.079	173.782	35.207	36.121
16.000	62.303	168.633	35.323	36.022
16.500	60.457	163.053	35.482	35.920
17.000	58.534	157.023	35.704	35.812

TABLE XVII

Test Data

Test 82764   1.025 inches I.D. Tube
Counterflow coolant   Coolant rate = 6.94 lb_m/sec.
                Condensing length = 17.0 ft.

L	T_c	T_o	P	P_o
DIST	TCOOL	TOUTWALL	PSTAT	PSTAG
(FEET)	(DEGF)	(DEGF)	(PSIA)	(PSIA)
0.000	52.500	215.000	40.350	46.027
0.125	52.896	214.932	40.301	46.025
0.250	53.292	214.867	40.247	46.023
0.375	53.688	214.804	40.187	46.020
0.500	54.083	214.744	40.123	46.017
1.000	55.667	214.526	39.825	45.896
1.500	57.250	214.336	39.484	45.638
2.000	58.833	214.166	39.119	45.290
2.500	60.417	214.006	38.749	44.879
3.000	62.000	213.847	38.389	44.424
3.500	63.583	213.679	38.051	43.945
4.000	65.167	213.493	37.743	43.458
4.500	66.750	213.280	37.472	42.975
5.000	68.333	213.031	37.242	42.506
5.500	69.917	212.735	37.056	42.061
6.000	71.500	212.384	36.912	41.646
6.500	73.083	211.969	36.811	41.264
7.000	74.667	211.479	36.750	40.917
7.500	76.250	210.906	36.724	40.608
8.000	77.833	210.241	36.730	40.336
8.500	79.417	209.473	36.763	40.099
9.000	81.000	208.595	36.816	39.895
9.500	82.583	207.595	36.885	39.721
10.000	84.167	206.466	36.964	39.572
10.500	85.750	205.198	37.048	39.446
11.000	87.333	203.781	37.133	39.338
11.500	88.917	202.205	37.215	39.243
12.000	90.500	200.463	37.292	39.158
12.500	92.083	198.544	37.364	39.079
13.000	93.667	196.439	37.430	39.003
13.500	95.250	194.139	37.493	38.928
14.000	96.833	191.634	37.558	38.853
14.500	98.417	188.915	37.632	38.778
15.000	100.000	185.973	37.724	38.703
15.500	101.583	182.798	37.846	38.633
16.000	103.167	179.382	38.015	38.571
16.500	104.750	175.714	38.248	38.525
17.000	106.333	171.785	38.568	38.503

APPENDIX I

DETERMINATION OF THE LOCAL INTERFACIAL

AND WALL SHEAR STRESS

In order to obtain useful analytical solutions to the system of

differential equations of change developed in Appendixes B through E, and

summarized in Table II, page 20, it is necessary to introduce heat trans-

fer and flow friction data which correspond closely to the physical con-

ditions which would be encountered in the condenser tube. A discussion

and analysis of the input heat transfer data and correlation is given in

Appendix J of this paper. In this appendix, a discussion and analysis of

the correlation of flow friction data for a condenser tube is undertaken.

For the flow of fluids in tubes or channels, it has been customary

practice to correlate the wall shear stresses generated in the system by

means of the Fanning friction factor function. The friction factor is a

dimensionless quantity which usually relates the average wall shear

stress or overall pressure loss encountered in the tube to the velocity

pressure of the fluid flowing in the tube; thus $f \equiv 2\tau/\rho V^2$. In calcula-

ting the velocity pressure the cross sectional average velocity of the

fluid is used.

Work has been done by a number of investigators on the problem of

flow friction determination and the prediction of pressure loss in two-

phase flow. Most of the experimental data reported in the literature has

been for two-phase mixtures such as air and water and other gas-liquid

135

systems with no interphase mass transfer. Correlation parameters commonly used are friction factors with liquid and vapor Reynolds numbers using velocities calculated by use of the total tube cross section for both the liquid and the vapor calculated independently. Per unit area mass flow rates calculated in this fashion are obviously fictitious; consequently, Reynolds numbers calculated from such quantities are commonly referred to as fictitious or superficial. Dukler, et al. (14) derive a two-phase Reynolds number from similarity considerations. However, they then define a local friction factor which considers only the local pressure gradient in a system where the velocity and, therefore, the momentum of both vapor and liquid may be changing. In condensing annular flow, the transfer of mass from vapor to liquid involves a sharp local change of momentum. This momentum change has been considered in the derivation of both equations (2C) and (11C), which give explicit expressions for the interfacial vapor shear stress τ_v and the wall shear stress τ_w respectively.

In a high velocity condensing system, several factors enter into the picture which make it clear that those methods of correlation which have so far been reported in the literature cannot give satisfactory results for either the correlation or prediction of pressure losses in such a system. Some important differences between the adiabatic two-phase multi-component system and the high velocity single component condensing system are listed below:

    1. The momentum change of the condensing vapor plays a significant role in both equation (2C), the vapor momentum equation, and in equation (11C), the combined liquid-vapor momentum equation. Thus, this momentum force enters into the determination of both the interfacial shear stress τ_v and the wall shear stress τ_w. The momentum

force resulting from the change of phase is not ordinarily present in adiabatic, two-phase, two-component flow.

2. In high velocity condensing flow, the vapor velocity and the static pressure may both rise and fall along the condensing length (see Figs. 11 through 18). The local derivatives of these flow properties may therefore be both positive and negative at different axial locations. It is not surprising then that considerable variation of both the interfacial and wall shear stress may occur over the length of a single condenser tube. For this reason, the use of overall average axial flow properties and overall pressure drop in correlating the average shear stress or the average friction factor for a condensing system must lead to inconclusive results for correlations based on such quantities.

3. In condensing two-phase flow, it has been observed that under certain conditions it is possible to have boundary layer flow separation occur on the condensing surface with a resulting local upstream or reverse flow of the liquid at the tube wall. This condition will exist when rapid deceleration of the vapor results in a local momentum induced pressure rise in the axial flow direction (see Figs. 17 and 18). Since no significant pressure gradient exists in the radial direction, a corresponding pressure rise in the annular liquid layer must occur at the same axial location. The rate of liquid velocity deceleration necessary to support the same pressure rise that occurs in the vapor core sometimes results in a reverse flow in the liquid layer close to the tube wall. The net or average liquid velocity remains positive since the liquid carried forward by the interfacial liquid waves and any entrained liquid

fraction in the vapor core dominates the total liquid flow. A local
reverse liquid flow at the tube wall results in a reverse wall shear
stress τ_w and a corresponding negative wall friction factor f_w at
that axial location. Such a condition will not ordinarily be en-
countered in adiabatic two-phase, two-component flow except possibly
with vertical upflow at low gas velocities. It is obvious that the
correlation of negative, local wall friction factors would be diffi-
cult by any method of correlation. It should be noted that the
local interfacial shear stress quantity τ_v apparently does not en-
counter such a sign reversal during the condensation process.

In the mathematical development given in Appendix C, equation (2C)
gives the interfacial shear stress τ_v as an explicit function of the sev-
eral vapor flow variables and their derivatives. This result is possible
because of the several simplifications of the physical system which have
been made in constructing the mathematical model disscused earlier on
page 10. Rather than a smooth conical interface the actual physical in-
terface consists of an interfacial region that extends from the bottom of
the wave troughs to the wave crest. It is possible that the interfacial
shear stress at the wave trough is less than that at the wave crest; how-
ever, no attempt has been made in this investigation to compare the rela-
tive magnitude of these quantities - either experimentally or analytically.
The value of τ_v which has been calculated from experimental data by use of
equation (2C) must therefore be a time average quantity at each particu-
lar axial location.

Two-Phase Friction Factors

It is possible to define two-phase friction factors in several different forms; for example, the following friction factors:

$$f_{wL} \equiv 2\tau_w / \rho_L V_L^2 \qquad (1I)$$

$$f_w \equiv 2\tau_w / \rho_V V_V^2 \qquad (2I)$$

$$f_V \equiv 2\tau_V / \rho_V (V_V - V_L)^2 \qquad (3I)$$

Since usually $V_L << V_V$, it is convenient to simplify equation (3I) to the form

$$f_V = 2\tau_V / \rho_V V_V^2 \qquad (4I)$$

Other definitions for two-phase friction factors have been employed; for example, sometimes the liquid and vapor velocities used are purely fictitious quantities calculated without regard to the actual vapor or liquid cross section area of flow. Equations (2I) and (4I), have been used in this investigation for all work involving the use of friction factors.

Because of the physical nature of the condensing system, a small variation in the input of local flow friction data has a cumulative and magnified effect on the downstream values of stream pressure and vapor velocity. Figs. 11 through 14 have been included in order to demonstrate the marked effect which a small divergence in input value of either friction factor has on the analytical solution of the system of differential equations.

Figs. 17 through 19 compare the computer determined solutions of the four independent differential equations (1), (2), (4), and (6) of Table II, page 20, with data calculated from experimental measurements. For these analytical solutions the friction factor data for f_v was arbitrarily controlled (programmed) so that the vapor velocity determined from the solution of the four equations agreed closely with the vapor velocity calculated from experimental measurements. This procedure was necessary since empirical correlations of sufficient precision for the local inter-facial vapor friction factor f_v do not exist. Thus, in effect, the system of four independent equations was used to analytically determine the local values of the four dependent variables, P, V_L, W_v, and f_v. The method of stepwise, numerical solution of the four differential equations was straightforward except for the necessary arbitrary input of the values of f_v. The analytically determined values of the above variables show fairly good agreement with the experimental values (see Figs. 17, 18, and 19). The agreement between the analytical and experimental data is in fact quite gratifying, considering the rigor of the test conditions chosen for analytical examination. For example, for the experimental case analyzed, the test data (see Figs. 17 and 18) show that the vapor accelerates sharply to slightly supersonic velocity, then decelerates rapidly to the low liquid velocity at exit. This is accompanied at first by a sharp fall in static pressure, followed by a pressure rise to the exit pressure.

The analytical solutions described above demonstrate that an analytical solution of the system of the four equations used will agree well with the experimental data if the input friction factor data for f_v can be determined with sufficient accuracy from an empirical correlation. To

date no such correlation appears to be available. However, the favorable results obtained certainly demonstrate the general validity of the mathematical model which has been proposed and the equations which have been developed therefrom. This is not to imply that a more precise model and accompanying analysis cannot be found. Indeed, it is expected that eventually one must consider the presence of entrained liquid droplets in the vapor as well as the mechanics of the interfacial wave activity before a completely satisfactory analytical solution to the problem of high speed vapor condensation can be found.

Considerable effort was expended in attempts to find empirical correlations for the two local friction factors f_v and f_w in terms of the local flow properties of vapor and liquid. Such correlation methods as those used by Chien and Ibele (8), Kegel (14), Bergelin, et al. (2) were tried without much success.

An explicit expression for the interfacial friction factor has been given in Appendix H as follows:

$$f_v = \frac{-1}{V_v} \left[\frac{W_v}{\pi \rho_v V_v} \right]^{\frac{1}{2}} \left[\frac{V_v - V_i}{W_v} \frac{dW_v}{dL} + \frac{dV_v}{dL} + \frac{1}{\rho_v V_v} \frac{dP}{dL} \right] \qquad (11H)$$

and, similarly, for the wall friction factor:

$$f_w = \frac{-2}{\pi D \rho V_v^2} \left[W_L \frac{dV_L}{dL} + W_v \frac{dV_v}{dL} + (V_v - V_L) \frac{dW_v}{dL} + A \frac{dP}{dL} \right] \qquad (12H)$$

It is possible to split each of the two friction factor quantities as follows:

$$f_v \equiv f_{v\theta} + f_{v\beta} + f_{v\phi} = f_{v\theta\beta\phi} \qquad (5I)$$

and

$$f_w \equiv f_{w\theta} + f_{w\alpha} + f_{w\beta} + f_{w\phi} = f_{w\theta\alpha\beta\phi} \qquad (6I)$$

where the four subscripts θ, α, β, and ϕ relate to the term that includes one of the respective four derivatives dW_v/dL, dV_L/dL, dV_v/dL, and dP/dL. Using only the last two of the terms from equation (11H) results in the

partial friction factor

$$f_{v\beta\phi} = \frac{-1}{V_v} \left[\frac{W_v}{\pi\rho_v V_v} \right]^{\frac{1}{2}} \left[\frac{dV_v}{dL} + \frac{1}{\rho_v V_v} \frac{dP}{dL} \right] \tag{7I}$$

This fraction of the interfacial vapor friction factor has been plotted in Figs. 41 and 42. These figures also show the local variation of the component fractions of the friction factor over the condensing length.

A similar treatment of the wall friction factor f_w as expressed by equation (12H) leads to the partial friction factor

$$f_{w\alpha\beta\phi} = \frac{-2}{\pi D\rho_v V_v^2} \left[W_L \frac{dV_L}{dL} + W_v \frac{dV_v}{dL} + A \frac{dP}{dL} \right] \tag{8I}$$

Values of the partial wall friction factor are plotted in Figs. 43 and 44. Note that in equation (8I) the derivative dV_L/dL relates to the partial friction factor $f_{w\alpha}$ which usually plays a minor role in the composite quantity $f_w \equiv f_{w\alpha\beta\phi\theta}$. It is observed that the condensation rate derivative dW_v/dL appears in each of the explicit shear stress equations (2C) and (11C), as well as the resulting friction factor equations (11H) and (12H). Examination of the magnitude of the partial friction factor quantities plotted in Figs. 41 and 44 indicates that the partial friction factors $f_{v\theta}$ and $f_{w\theta}$, which are direct functions of the rate derivative dW_v/dL, make significant contributions to the respective total friction factors f_v and f_w. It should be noted here that the rate derivative dW_v/dL is mainly a function of the local radial heat transfer rate. The local heat transfer rate, in turn, is usually affected by external factors such as the temperature of the cooling fluid and the external heat transfer resistance as well as the internal heat transfer resistance of the condensing system. It seems apparent, therefore, that a successful empirical correlation of the local friction factors f_v and f_w must include
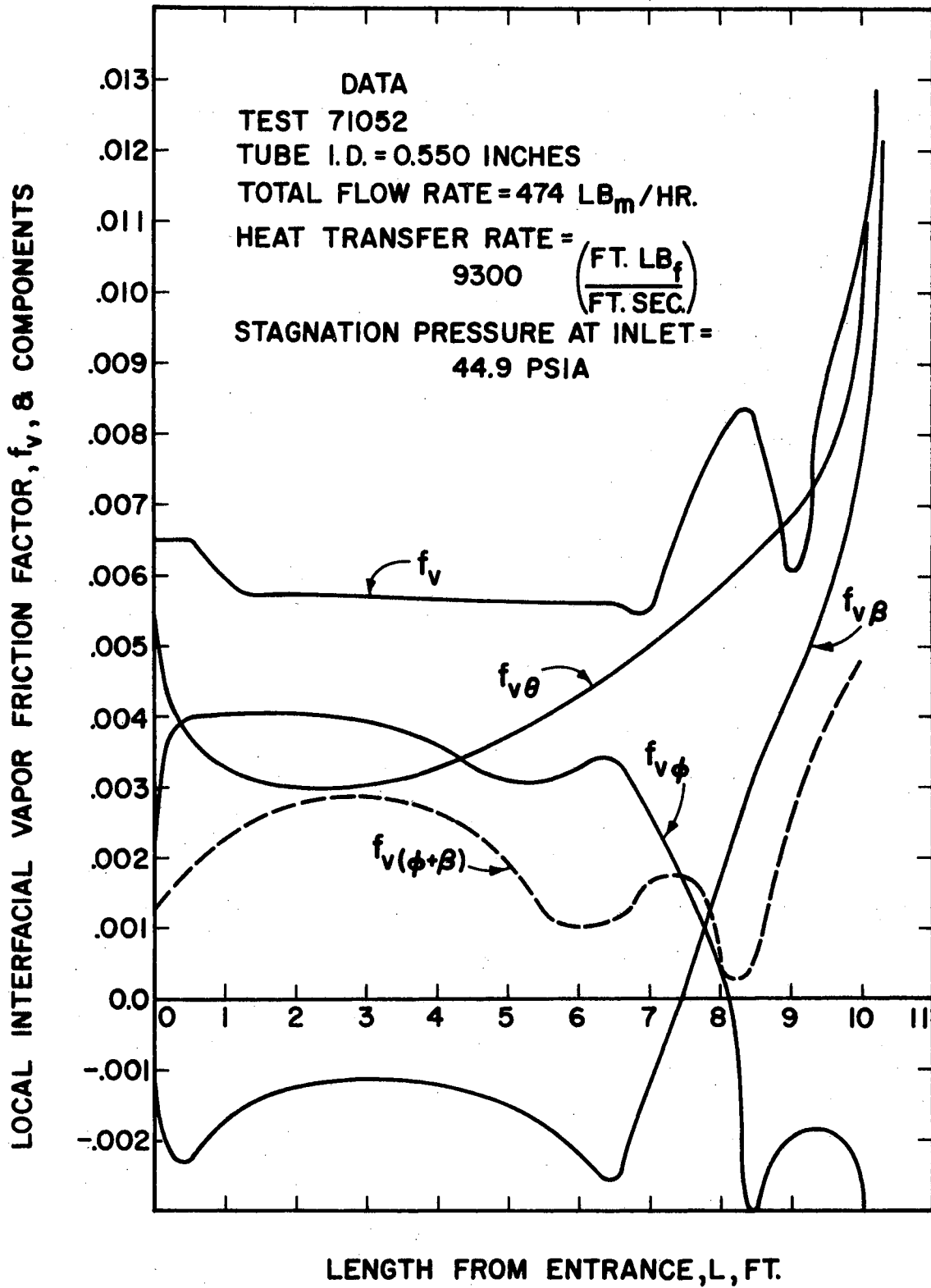
Figure 41. Experimental Interfacial Vapor Friction Factor With Components for 0.550 Inch I.D. Tube
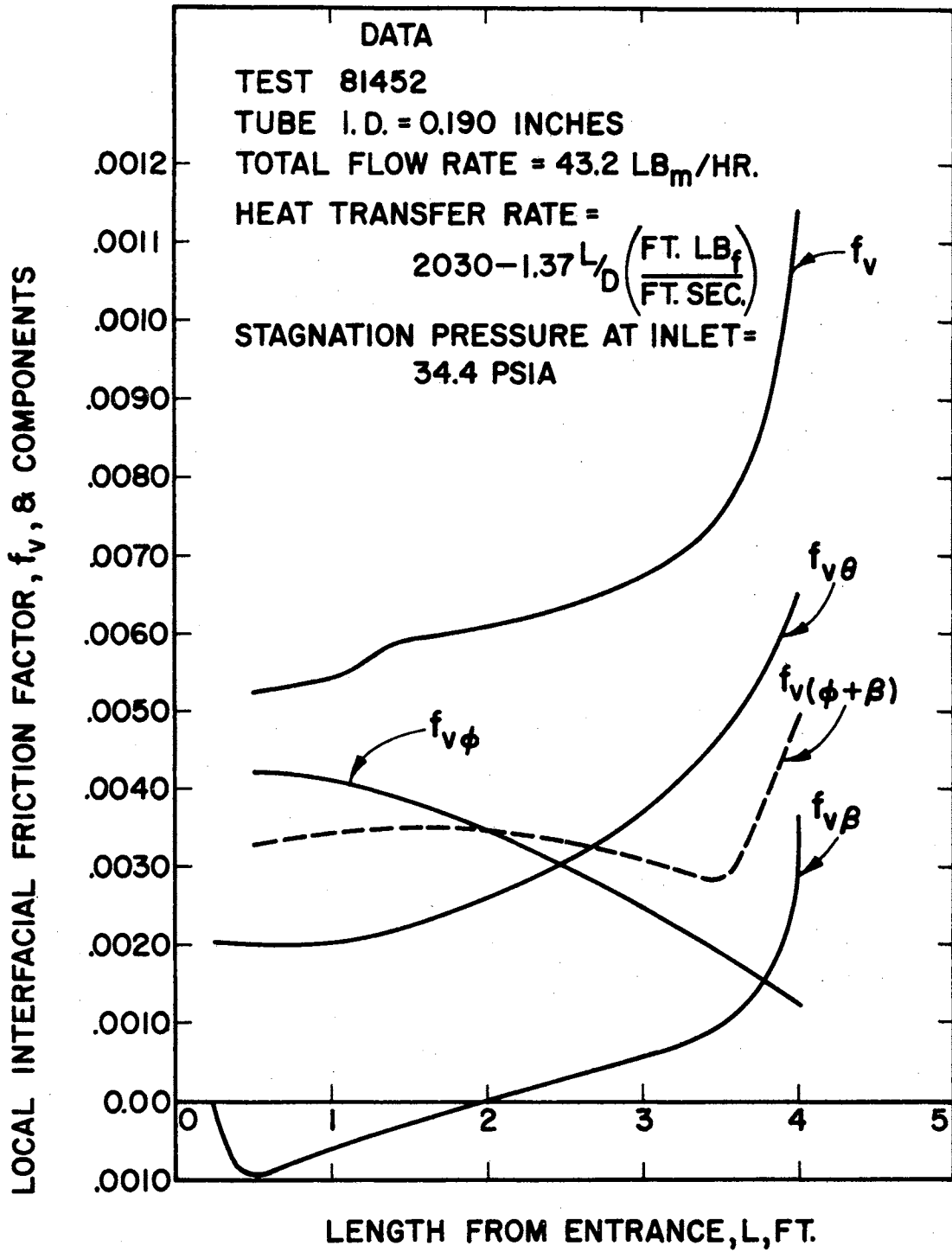
Figure 42.   Experimental Interfacial Vapor Friction Factor
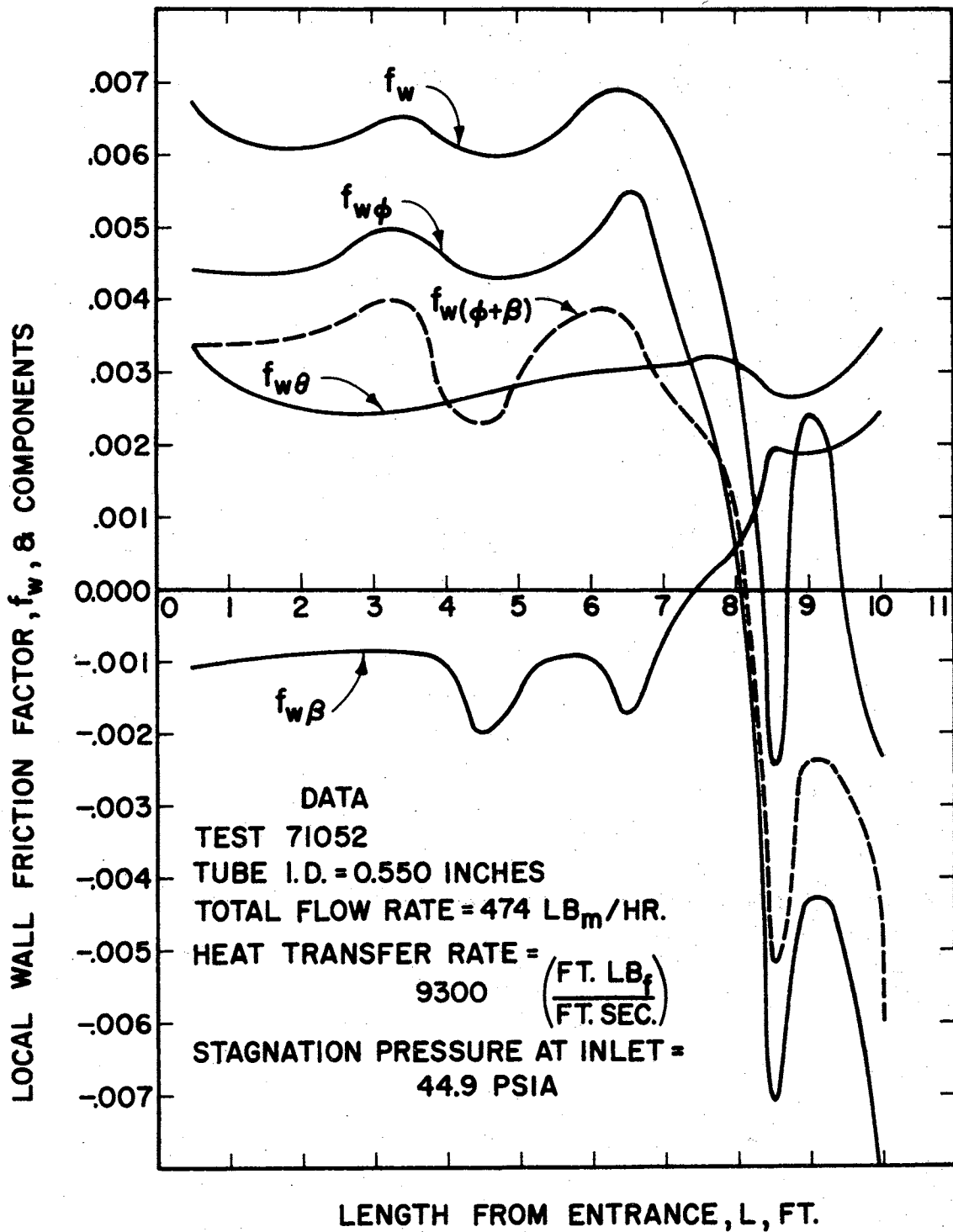With Components for 0.190 Inch I.D. Tube

Figure 43. Experimental Wall Friction Factor With Components
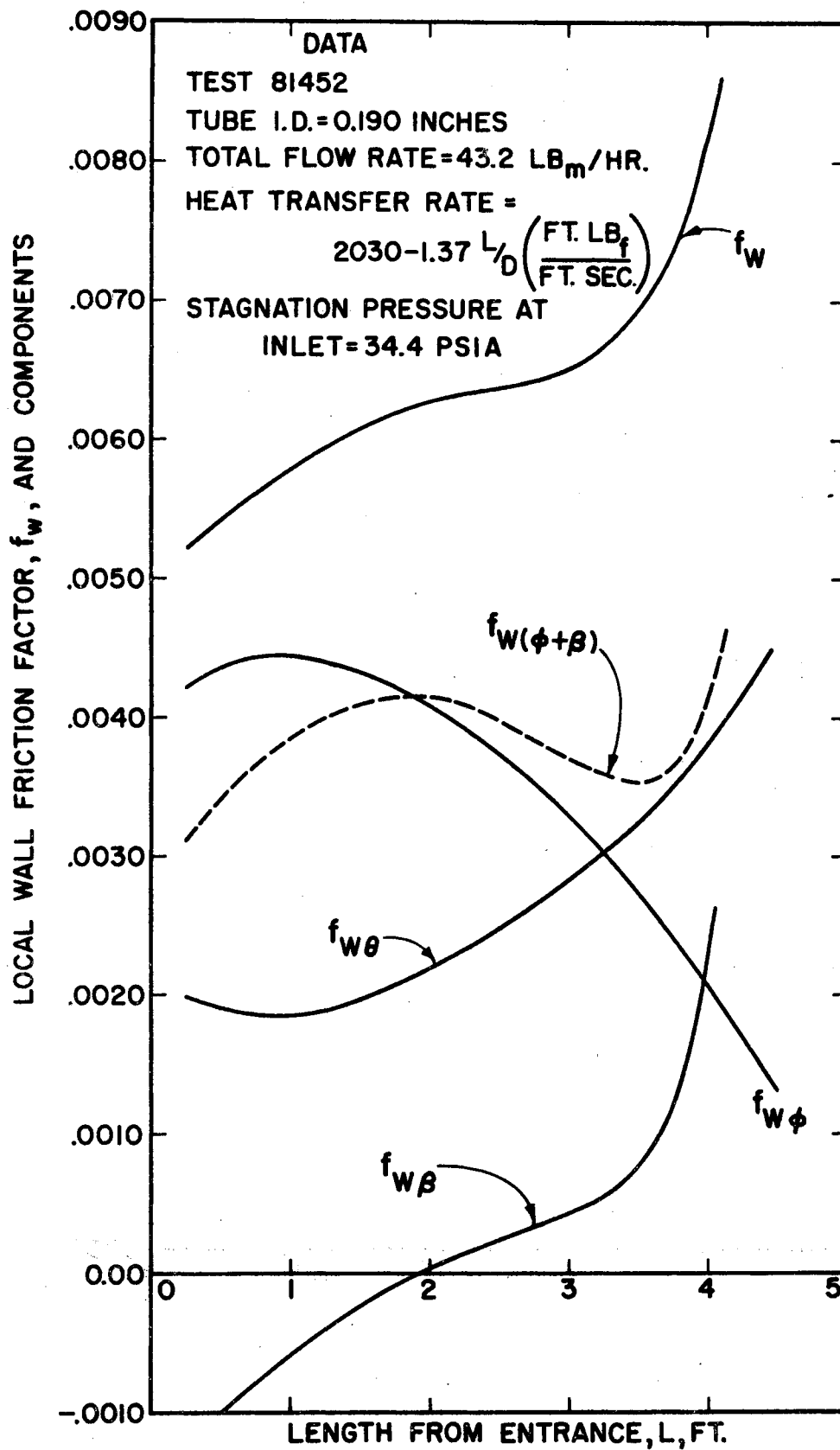for 0.550 Inch I.D. Tube

Figure 44. Experimental Wall Friction Factor With Components
for 0.190 Inch I.D. Tube

the local heat transfer rate or the local condensation rate as one
independent variable in such a correlation.

Figs. 41 through 44 have been presented in order to demonstrate the
relative magnitude of the several local momentum and pressure forces act-
ing on the two-phase condensing system. They show, for example, that a
rapid deceleration of the vapor can result in a boundary layer separation
in the annular liquid layer at the wall. Whatever radial distribution of
the axial velocity occurs in the two-phase system, will obviously be
a result of the interaction of these several forces. The velocity gradi-
ent in the liquid at the wall will, of course, determine the wall shear
stress, which evidently may act locally either in opposition to or in the
axial direction of flow. It should be understood that there was no inten-
tion to suggest the possibility of individual empirical correlation of
the partial friction factors presented herein.

The introduction of the idea of partial friction factors was intend-
ed to emphasize the complexity of the problem of determination of the
value of the local friction factor of local shear stress in high speed
condensing flow. The interaction of variable heat transfer rates with
increasing and/or decreasing velocities and pressures presents the pic-
ture of a problem whose complete solution will be difficult. The re-
marks of McManus in his discussion at the end of reference (8) are of
interest. McManus points out the inadequacy of the current correlations
of friction factors for two-component, two-phase flow over wide ranges
of fluid variables and tube diameters. The situation with regard to
the correlation of friction factors for high velocity condensing vapors
is in a worse state. Evidently there has been no empirical correlation
available that can be used with confidence to predict the local friction

factors in high velocity condensing flow.

<div align="center">

Local Wall Shear Stress Determination by

Velocity Distribution Analysis

</div>

The analysis of the velocity distribution in the annular liquid layer appears to be a more enlightening and rewarding approach to an adequate understanding of the mechanics of two-phase flow than the more empirical friction factor correlations attempted heretofore. It is possible, for example, to express the mass flow rate of liquid in the liquid annulus in terms of the radial distribution of the time average axial velocity of the liquid. If a satisfactory approximation of this velocity distribution can be established, including that in the laminar sublayer, then it is possible to calculate the local wall shear stress indirectly from the distribution function. In the following paragraphs a relationship between the mass flow rate of condensed liquid W_L, and the wall shear stress τ_w, is derived for two different universal velocity distribution functions.

The liquid flow rate in a layer of differential thickness may be expressed by the relation
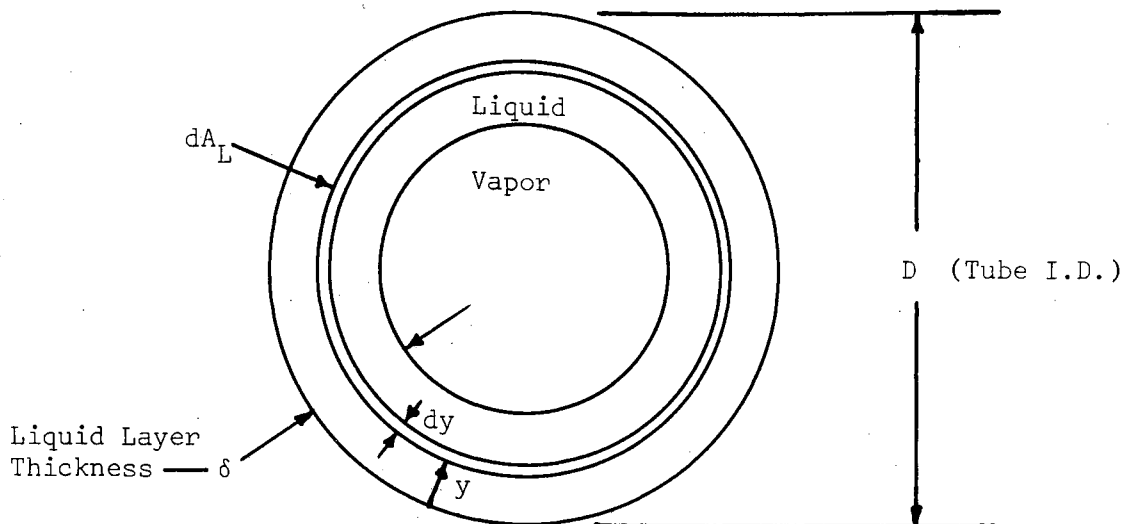
$$dW_L = \rho_L V_L dA_L \qquad (9I)$$

where $V_L = V_L(y)$. The differential cross section area dA_L is given by the equation

$$dA_L = \pi(D - 2y)dy \qquad (10I)$$

Substituting equation (10I) into (9I) and dividing by the circumference leads to

$$dW_L' = \rho_L V_L(1 - \frac{2y}{D})dy \qquad (11I)$$

Cross Section Sketch of Model

By integrating equation (11I) implicitly over the liquid layer thickness δ, the following function is obtained

$$W_L' = \rho_L \int_{y=0}^{y=\delta} V_L(y) \left(1 - \frac{2y}{D}\right)dy \qquad (12I)$$

where W_L' represents the total mass flow rate of liquid per unit periphery. At this point the dimensionless quantity y^+, sometimes called the friction Reynolds number, is introduced and defined by

$$y^+ \equiv \frac{y V_{Lw}^*}{\nu_L} \qquad (13I)$$

where V_{Lw}^* has the units of velocity, e.g., feet per second, and has been called the wall friction velocity, defined by

$$V_{Lw}^* \equiv \sqrt{\tau_w / \rho_L} \qquad (14I)$$

where the term τ_w is the local wall shear stress. The quantity y^+ is a linear function of the normal wall distance y and thus when $y = \delta$,

equation (13I) becomes

$$\delta^+ \equiv \frac{\delta V_{Lw}^*}{\nu_L} \tag{15I}$$

Now also introducing the dimensionless velocity function

$$V_L^+(y^+) \equiv \frac{V_L(y)}{V_{Lw}^*} \tag{16I}$$

and substituting from equations (13I), (15I), and (16I) into (12I) leads to the very useful dimensionless equation

$$W_L'/\mu_L = \int_{y^+=0}^{y^+=\delta^+} V_L^+(y^+) \left[1 - \frac{2\delta/D}{\delta^+} y^+\right] dy^+ \tag{17I}$$

If the universal velocity distribution function $V_L^+(y^+)$ is known or can be approximated over the liquid layer thickness then equation (17I) can be integrated over the range $0 \le y^+ \le \delta^+$, resulting in the relation

$$W_L'/\mu_L = f(\delta^+) \tag{18I}$$

Equation (18I) can sometimes be solved explicitly for δ^+, thus obtaining the functional form

$$\delta_u^+ = \delta_u^+(W_L'/\mu_L) \tag{19I}$$

where the subscript u has been used to signify that the friction Reynolds number δ_u^+ has been determined from a universal velocity distribution function $V_L^+(y^+)$. The wall shear stress τ_{wu} can then be calculated directly from the friction Reynolds number δ_u^+ if the thickness of the liquid layer is known. The thickness of the annular liquid layer for a wide range of two-phase flow conditions is included in the calculated experimental data of Tables IV through XVII. These data have been utilized in the analyses of this section in calculating the local wall

shear stress τ_{wu}.

For the highly turbulent flow of a homogeneous fluid over a flat surface or in a tube, von Karman, after the earlier work of Prandtl, Nikuradse, and others, established the following universal velocity distribution functions:

$$\left.\begin{array}{ll} V_L^+ = y^+ & \text{for } 0 \leq y^+ \leq 5 \\[2ex] V_L^+ = 5.0 \ln y^+ - 3.05 & \text{for } 5 \leq y^+ \leq 30 \\[2ex] V_L^+ = 2.5 \ln y^+ + 5.5 & \text{for } 30 \leq y^+ \leq \delta^+ \end{array}\right] \qquad (20\mathrm{I})$$

By introducing equation (20I) into equation (17I) and integrating, the following three functions are obtained:

1. For the range $0 \leq \delta^+ \leq 5$

$$\delta_u^+ = \left[\frac{6W_L'/\mu_L}{3 - 4\delta/D}\right] \qquad (21\mathrm{I})$$

2. For $5 \leq \delta^+ \leq 30$

$$W_L'/\mu_L - 12.5 = \delta_u^+\left[5 \ln \delta_u^+ - 8.05 + 2\delta/D \ (2.775 - 2.5 \ln \delta_u^+ - 10.2/\delta_u^{+2})\right] \qquad (22\mathrm{I})$$

3. For $30 \leq \delta^+$

$$W_L'/\mu_L + 64 = \delta_u^+\left[2.5 \ln \delta_u^+ + 3.0 - 2\delta/D \ (2.125 \ln \delta_u^+ - 574.6/\delta_u^{+2})\right] \qquad (23\mathrm{I})$$

Note that an explicit equation for δ_u^+ can not be obtained from equations (22I) and (23I); however, a numerical value for δ_u^+ is easily obtained from these equations by a simple iterative process.

Analytical values of δ_u^+ have been calculated by use of either equations (21I), or (22I), or (23I) — whichever equation applies to the liquid flow rate in question — for the three condenser tube sizes (0.190,

0.550, and 1.025 inches I.D.) for which data were available. The experimental data include the local liquid flow rate W_L, as well as calculated values of the liquid layer thickness δ, at each axial position over the condensing length. This information is necessary for each solution of equations (21I), (22I), and (23I), and for the evaluation of the local wall shear stress τ_{wu} from the value of δ_u^+ found from each solution. Note that $\tau_{wu} = \rho_L(\delta_u^+ \nu_L/\delta)^2$. Values of δ_u^+ and τ_{wu} so calculated have been compared with values of δ_m^+ and τ_{wm}, as calculated from the combined momentum equation, equation (11C), for the same experimental test conditions, for all three tube sizes, and by the equation

$$\delta_m^+ \equiv (\delta/\nu_L)\sqrt{\tau_{wm}/\rho_L} \tag{24I}$$

Fig. 46 is a plot of the ratio τ_{wm}/τ_{wu} versus the total liquid fraction $(1 - \theta)$ present. For the very thin laminar liquid layer near the start of condensation ($\theta \gtrsim 1$) it is seen that the upper curve of Fig. 46, which is derived from equations (20I), approaches unity, i.e., $\tau_{wm} \to \tau_{wu}$. When the condenser tube begins to fill with liquid at the other end ($\theta = 0$), again $\tau_{wm} \to \tau_{wu}$.

The condition $\tau_{wm}/\tau_{wu} \to 1$ might be expected to exist at the beginning and the end of condensation since the von Karman equations (20I) have been shown to hold for the full pipe flow of a single homogeneous fluid, as well as for a thin laminar sublayer such as the thin liquid film which occurs at the start of condensation. The trend of $\tau_{wm} \to \tau_{wu}$ at the two end states is considered to be a partial confirmation of the validity of both the experimental data and the analytical methods which have been used to calculate the wall shear stress τ_w by the two entirely independent means.
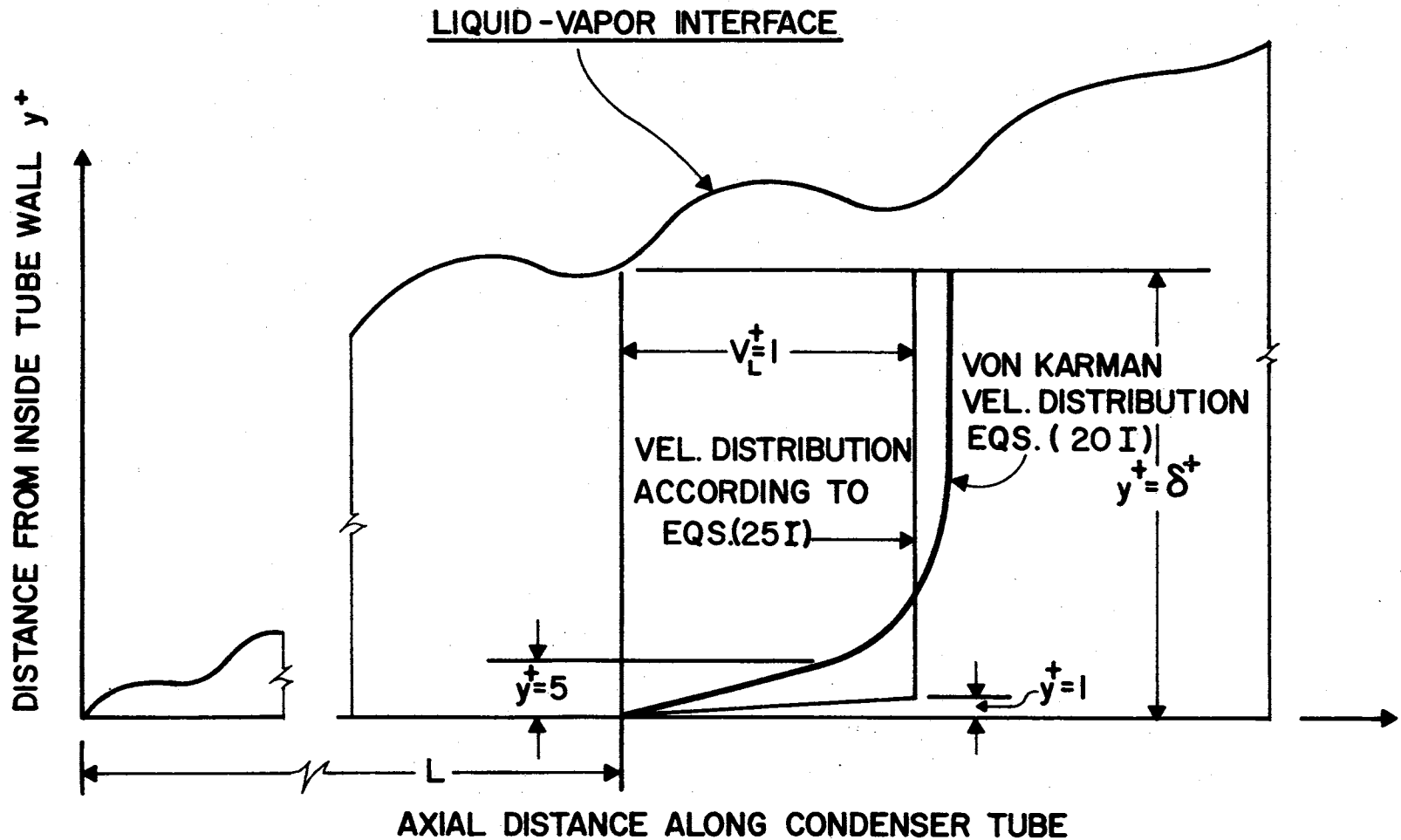
Figure 45. A Schematic Representation of the Two Velocity Distribution Functions Used for the Analytical Determination of the Friction Reynolds Number δ_u^+, for the Liquid Layer
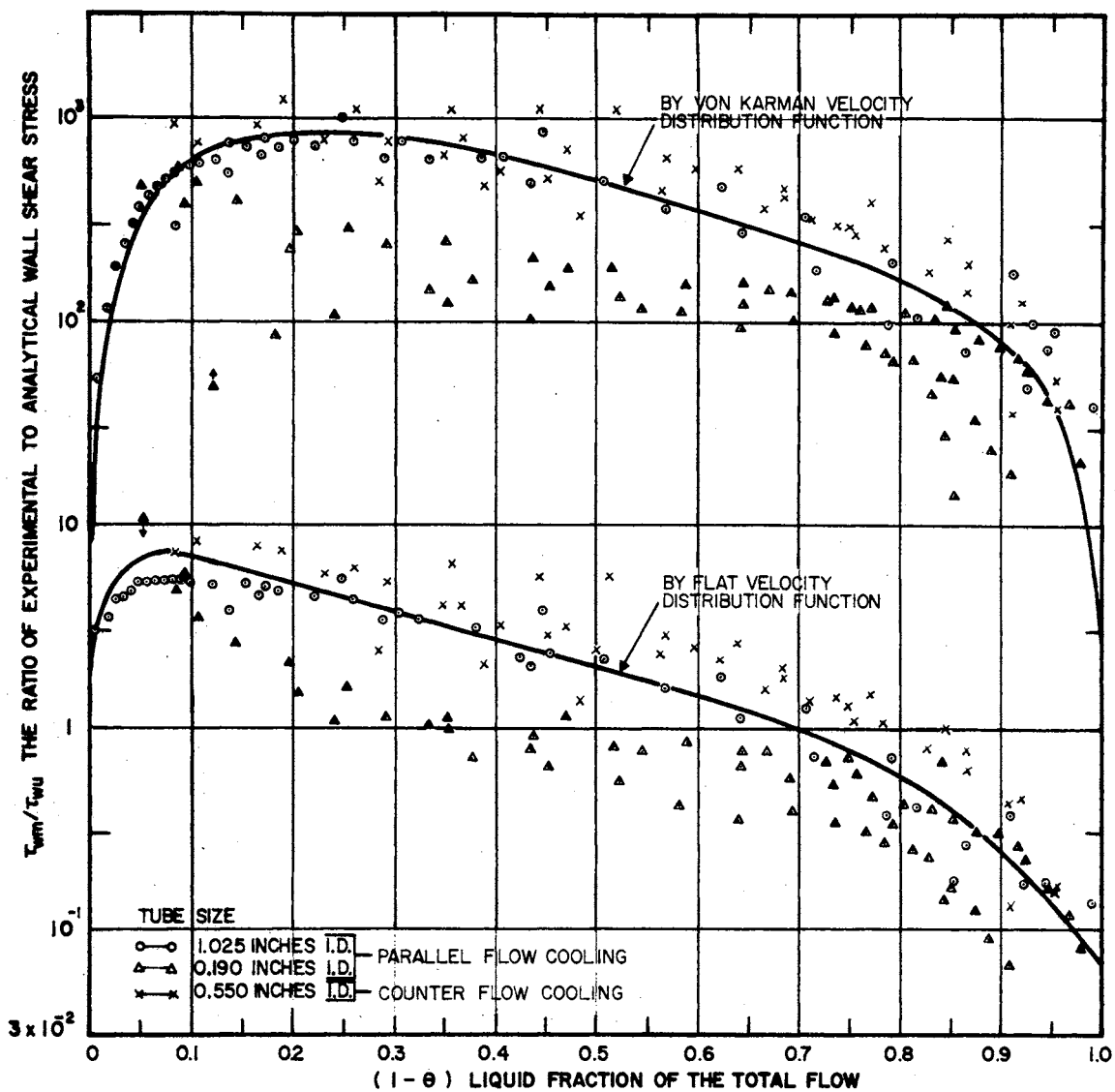
Figure 46. The Variation of the Ratio of Experimental to Analytical
Wall Shear Stresses Versus Liquid Fraction of the
Total Flow for Two Universal Velocity Distribution
Functions

Further examination of the upper curve of Fig. 46 shows that the ratio τ_{wm}/τ_{wu} has a value of from 100 to 1000 over the major portion of the condensing length. It was discovered during this investigation that the wide divergence between the two values of τ_{wm} and τ_{wu} over the middle range of the condenser tube could be reduced by approximately a factor of 100, by adopting in place of the von Karman functions a much flatter universal velocity distribution function with a smaller range of the laminar sublayer. Fig. 45 is a comparative sketch of the two different universal velocity distribution functions which have been used for calculating τ_{wu} and δ_u^+. The flat velocity distribution is represented by the following functions:

$$V_L^+ = y^+ \quad \text{for} \quad 0 \leq y^+ \leq 1$$
$$V_L^+ = 1 \quad \text{for} \quad 1 \leq y^+ \leq \delta^+$$
(25I)

Introducing equations (25I) into equation (17I) and integrating yields the following two functions:

1. For the range $0 \leq \delta^+ \leq 1$

$$\delta_u^+ = \left[\frac{6W_L'/\mu_L}{3 - 4(\delta/D)} \right]$$
(26I)

which is the same as equation (21I).

2. For $1 \leq \delta^+$

$$W_L'/\mu_L = \delta_u^+(1 - \delta/D) + \frac{1}{3}\left[\frac{\delta/D}{\delta_u^+}\right] - \frac{1}{2}$$
(27I)

Equation (27I) can be solved explicitly for δ_u^+, but it is more convenient to leave it in the above form and to obtain analytical data by a simple iterative program.

Analytical values of δ_u^+ and τ_{wu} were calculated by use of equations

(26I) and (27I) for the same test conditions used with the von Karman based functions (21I), (22I), and (23I). Examination of these data, plotted as before on Fig. 46, shows plainly that the flat velocity distribution function represented by equations (25I) gives analytical values of the wall shear stress τ_{wu} very much closer to the experimental data represented by τ_{wm} than do the von Karman functions.

Fig. 47 has been plotted to show the relationship between the analytically derived friction Reynolds number δ_u^+ and the experimentally based quantity δ_m^+. The objective, of course, is to find a universal velocity distribution function which will give perfect agreement between the analytical and experimental quantities. By examination of Fig. 47 it is seen that the flat velocity distribution functions (equations (25I)) come much closer to giving this agreement than the von Karman distribution functions (equations (20I)). It should be observed again, for Fig. 47 as it was for Fig. 46, that the von Karman based curve tends toward perfect agreement at the curve ends, which correspond virtually to the beginning and end of condensation respectively.

One further important observation which may be found by examination of Fig. 46, is that the flat distribution functions (equations (25I)) predict local wall shear stresses much too high near the end of condensation. This condition must be expected since the laminar sublayer thickness of $y^+ \simeq 1$ used in this velocity distribution is much too small for the full pipe flow of the liquid which occurs at this point. On the other hand, it is seen that at the start of condensation the trend is toward perfect agreement for the same curve at this point. Since the von Karman distribution and the flat distribution both incorporate the same function for the region $0 \leq \delta^+ \leq 1$, both must predict the same shear
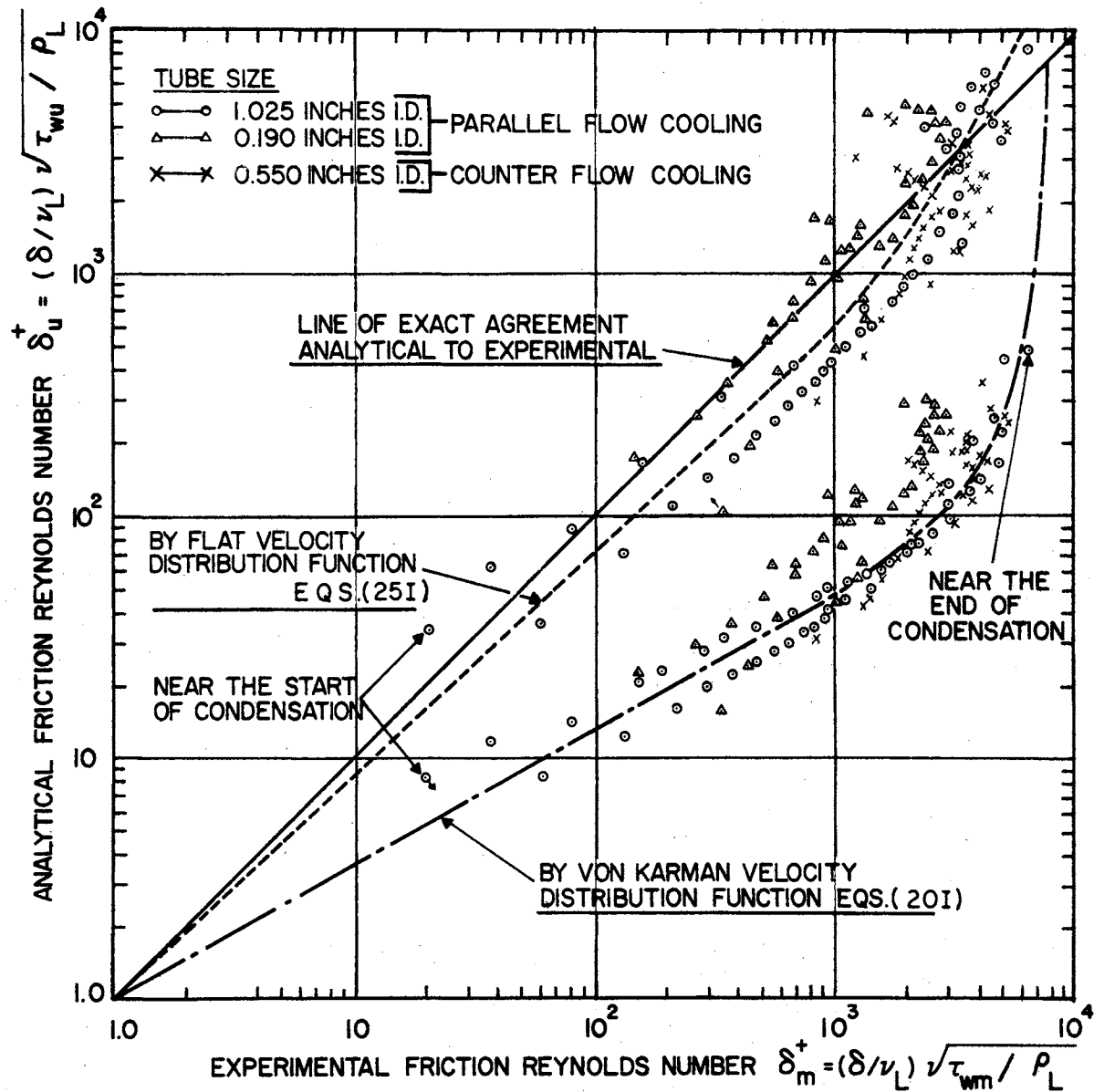
Figure 47. A Comparison of the Analytically Calculated Friction
Reynolds Number, δ_u^+, With the Experimentally
Determined Value of the Same Variable, δ_m^+. Two
Different Velocity Distribution Functions Used for
the Analytical Calculation are Represented.

stress in this region. It should be noted that it is very difficult to obtain experimental data in this region, so that it is necessary to rely on the extrapolation of the two curves toward the point of zero liquid fraction to demonstrate the convergence of the curves at this point.

A Universal Correlation for Local Wall Shear Stress

By using the ratio between the mass average velocity $\overline{V}_L$ in the annular liquid layer and the wall friction velocity V_{Lw}^* it is possible to define a non-dimensional velocity parameter for the liquid layer, thus

$$\overline{V}_L^+ \equiv \overline{V}_L/V_{Lw}^* = \overline{V}_L/\sqrt{\tau_{wm}/\rho_L} \qquad (28I)$$

Equation (28I) can also be written in the form

$$1/\overline{V}_L^{+2} = \tau_{wm}/\rho_L \overline{V}_L^2 \qquad (29I)$$

thus it is seen that $\overline{V}_L^{+2}$ is essentially an inverse friction factor function based on the mean liquid velocity. Note that the experimentally derived quantity τ_{wm} has been used in the definition of $\overline{V}_L^+$. For the purpose of empirical correlation of the wall shear stress τ_{wm} the friction Reynolds number δ_u^+ at $y = \delta$ (liquid-vapor interface) was chosen as the second parameter. For this comparison the quantity δ_u^+, as derived from the flat functions of equations (26I) and (27I), is plotted in Fig. 48 against $\overline{V}_L^+$. Data for three different tube sizes and a density variation range of about five to one are included. The vapor core Reynolds numbers include values from about 10^4 to 6×10^5.

Because of the considerable scatter of points found in Fig. 48 a third correlation parameter was needed to make the correlation useful. Such variables as vapor Reynolds number and the liquid layer thickness
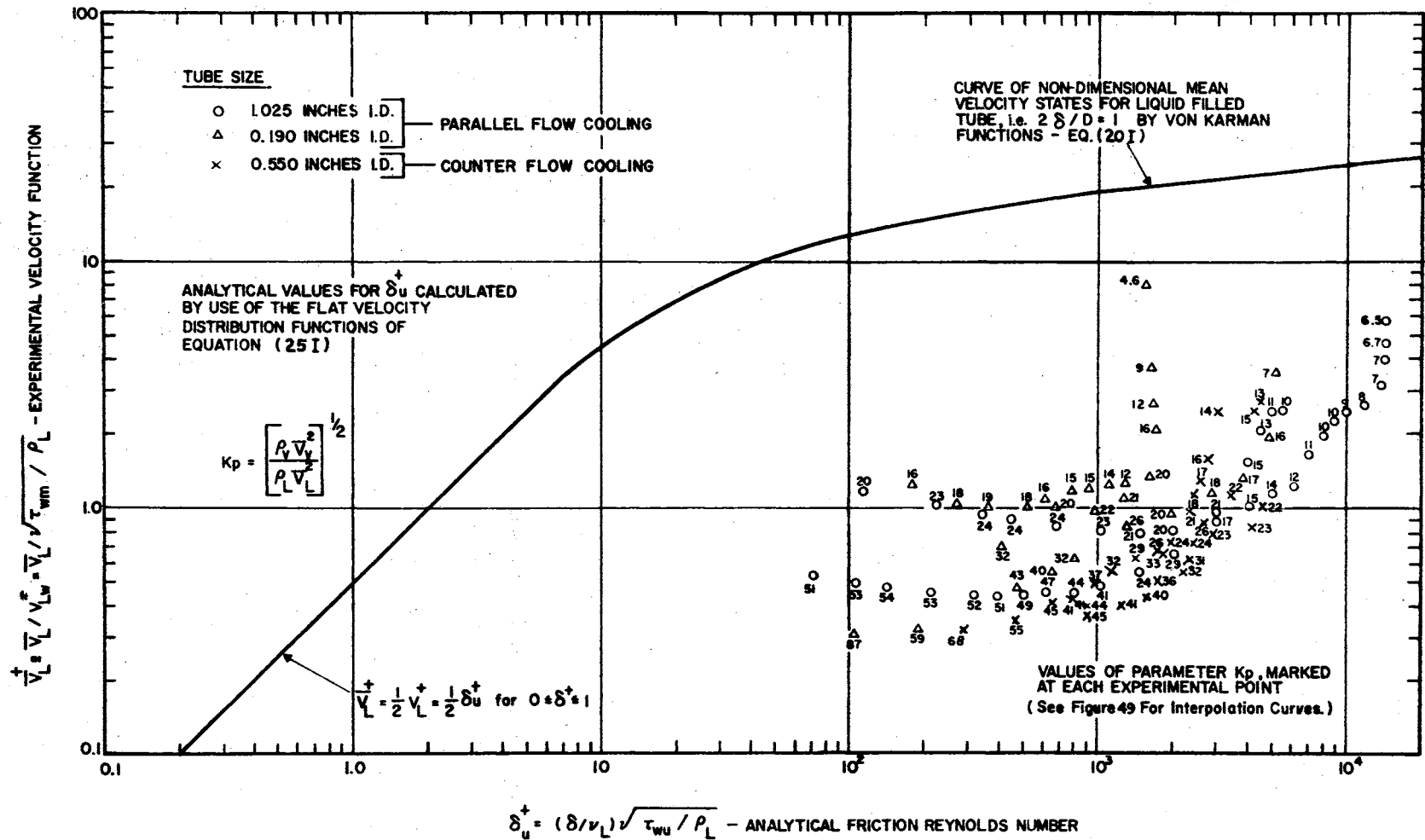
Figure 48. Experimental Values of $\overline{V}_L^+$ Versus Analytical Values of δ_u^+ With Experimental Values of Ratio K_p as a Parameter

to diameter ratio δ/D were tried with no success. In addition the interfacial friction Reynolds number was also tried as a possible correlation parameter. The interfacial friction Reynolds number, of course, incorporates the interfacial shear stress τ_v and is defined by

$$\delta_i^+ \equiv \frac{\delta\sqrt{\tau_v/\rho_L}}{\nu_L} \tag{30I}$$

The interfacial shear stress τ_v is a fundamental term in the third correlation parameter used by Dukler (12) in his analysis of this problem. Neither the interfacial friction Reynolds number nor the Dukler parameter gave a fully satisfactory correlation of the wall shear stress. The parameter which is apparently necessary to bring order to the correlation is the ratio K_p. This quantity approximates the square root of the ratio of vapor to liquid dynamic pressures, thus

$$K_p \equiv \left[\frac{\rho_v \bar{V}_v^2}{\rho_L \bar{V}_L^2}\right]^{\frac{1}{2}} \tag{31I}$$

Values of the parameter K_p are given alongside each data point on Fig. 48. By the technique of alternating the parameters K_p and δ_u^+ and cross plotting back and forth it was possible to establish a whole family of curves for the parameter K_p from the data of Fig. 48 . Fig. 49, which is the result of this work, shows lines of constant K_p. The data points for the path of a typical condensing test are also shown on Fig. 49. The test points given cover about 93 percent of the condensing length for the particular test.

In order to make use of Fig. 49 to predict the local wall shear stress it is necessary to know the local liquid flow rate as well as both the local liquid and vapor average velocities and densities. δ_u^+ can then be evaluated from equation (26I) or (27I). K_p is then
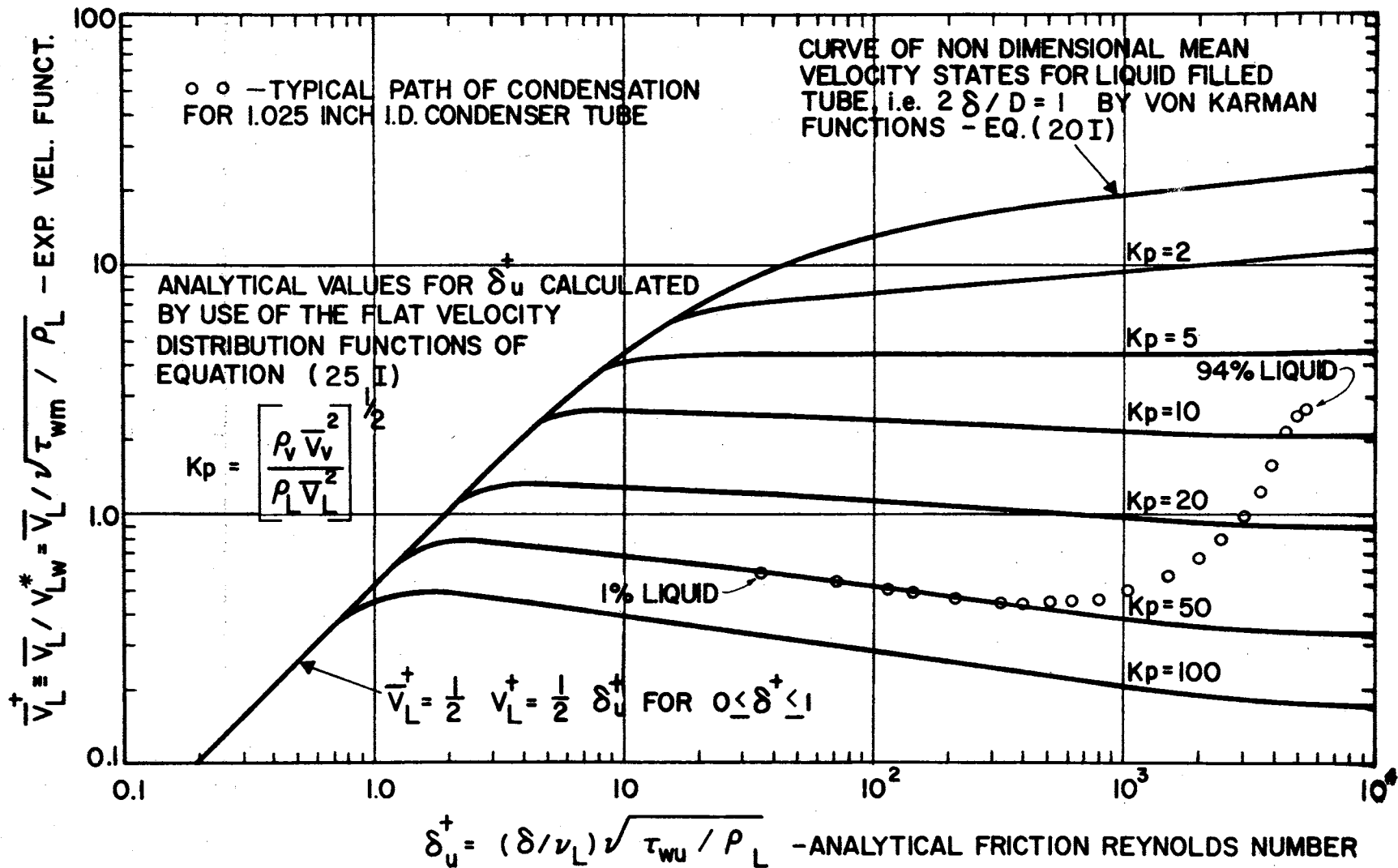
Figure 49. An Empirical Correlation of $\overline{V}_L^+$ as a Function of δ_u^+ and K_p for Condensing Flow (Interpolated From the Data of Figure 48)

calculated from equation (31I). The value of $\bar{V}_L^+$ can then be found from Fig. 49, and the shear stress τ_{wm} finally calculated by the following equation,

$$\tau_{wm} = \rho_L \bar{V}_L^2 / \bar{V}_L^{+2} \tag{32I}$$

which is a form of equation (28I), rewritten to be explicit in τ_{wm}.

The method of determing τ_{wm} described above can be used only with the type of stepwise solution where the condensation process is followed analytically or empirically from the start to the end of condensation. In such a process the necessary local flow properties are determined at each axial location. This permits the evaluation of τ_{wm} at each point from Fig. 49 or its equivalent mathematical representation.

The third parameter K_p, which was found necessary to give a successful correlation of the experimentally determined wall shear stress, includes the quantity $\rho_v \bar{V}_v^2$ which, at moderate velocities, is approximately twice the dynamic pressure of the vapor. Examination of the curves of Fig. 49 indicates that the dynamic pressure of the vapor plays a major role in determining the wall shear stress in condensing flow. The functional relationship between the wall shear stress τ_{wm} and the dynamic vapor pressure is approximately linear, except at very low vapor velocities where other forces may contribute more significantly to the determination of τ_{wm}.

The strong role of the dynamic vapor pressure in the correlation of Fig. 49 suggests the possibility of using the vapor friction factor $f_w = 2\tau_w / \rho_v \bar{V}_v^2$ in conjunction with one of the several non-dimensional liquid layer variables as a basis for correlation. For example, a form of correlation similar to that of Bergelin, et al. (2), but using the actual rather than the apparent vapor velocity in the vapor Reynolds

number, with the friction Reynolds number for the liquid layer as a third parameter, might be successful.

No empirical friction correlation presented to date has included a parameter which takes into account the effect of the momentum forces resulting from local accelerations or decelerations of the vapor or liquid or from the condensation process itself. The several terms of equation (11C) demonstrate that the above mentioned forces enter significantly into the determination of the wall shear stress τ_w and should not be neglected. In addition such factors as wave heights, lengths, and velocities, as well as liquid entrainment in the vapor core, all add complexities to the actual physical model of annular two-phase flow. Considerable experimental information about interfacial wave activity is already available, and experimental studies of the liquid entrainment in the vapor core have been made. Eventually this information must be incorporated into a coherent analytical treatment of the model of wavy annular-mist flow with condensation.

Turbulence Intensity in the Liquid Layer

It may be observed from Fig. 48 that the majority of the experimental values of $\overline{V}_L^+$ fall in the range of $0.4 \leq \overline{V}_L^+ < 2$. If, according to equations (25I), $V_L^+ \backsim 1$ for $1 \leq y^+ \leq \delta^+$ then from equation (16I)

$$V_L(y) \backsim \overline{V}_L \backsim V_{Lw}^* \tag{33I}$$

over the major portion of the condensing length.

In the region outside the laminar sub-layer the fluid shear stress τ_{yx} may be represented by the equation

$$\tau_{yw} = \mu_L \frac{\partial \overline{u}}{\partial y} + \frac{\partial \overline{v}}{\partial x} - \rho_L \overline{u'v'} \tag{34I}$$

Note that for convenience the notation used by Schlichting (32) has been adopted temporarily, where u' and v' represent the turbulent or fluctuating components of the velocities u and v in the x and y directions respectively. In the turbulent region the Reynolds or turbulent stresses usually far outweigh the viscous components and therefore equation (34I) may be simplified to

$$\tau_{yx} = - \rho_L \overline{u'v'} \tag{35I}$$

If the flat distribution functions of equation (25I) are approximately correct for annular condensing flow, then

$$\tau_w \simeq \tau_{yx} = - \rho_L \overline{u'v'} \tag{36I}$$

Equation (36I) may now be substituted into the expression for the wall friction velocity, equation (14I), which leads to

$$V_{Lw}^{*} = \sqrt{|\overline{u'v'}|} \tag{37I}$$

Now combining equations (16I), (33I) and (37I) results in the interesting relation

$$V_L^+ \simeq \frac{\overline{V}_L}{V_{Lw}^{*}} \simeq \frac{\overline{V}_L}{\sqrt{|\overline{u'v'}|}} \simeq 1 \tag{38I}$$

The level of intensity of turbulence I_T in a homogeneous isotropic fluid is sometimes defined by the quantity

$$I_T = \frac{\sqrt{\frac{1}{3}(\overline{u'^2} + \overline{v'^2} + \overline{w'^2})}}{U_\infty} \tag{39I}$$

where U_∞ is the main stream or free velocity of the fluid. If in the annular liquid condensate layer the fluctuating velocity components u', v', and w' are of the same order of magnitude, then the equivalent equation

for turbulence intensity in the liquid layer is

$$I_T \backsim \frac{\sqrt{\overline{u'^2}}}{\overline{V}_L} \tag{40I}$$

Now comparing equations (38I) and (40I), it may be concluded that the intensity of turbulence across the annular liquid layer is often of the order unity and greater; except, of course, in the very thin laminar sublayer. Thus in most cases $I_T \backsim 1$ over the major portion of the condensing length. This means that the fluctuating velocity components are of the same order of magnitude as the mass average axial liquid velocity.

For the flow of isotropic fluids in wind tunnels, the background turbulence intensity is often of the order of 1 to 3 percent. For the flow of a homogeneous fluid in the vicinity of a smooth, flat surface, a magnitude of $I_T = \sqrt{\overline{u'^2}}/u \backsim 10$ percent is usually observed. By comparison with such systems it is obvious that a wavy condensing liquid layer develops an unusually intense level of turbulence from near the tube wall to the liquid-vapor interface. It is interesting to note that turbulence intensities of the order of unity have also been measured at the edge of a free jet involving a single homogeneous fluid. It should be understood that the analysis given in this section is strictly an order of magnitude study of the turbulence intensity in a wavy, somewhat inhomogeneous, non-isotropic liquid layer.

No evidence has been presented in this paper which would indicate the level of intensity of turbulence in the vapor core. The experimental data presented by Kegel (24) and Chien and Ibele (8) exhibit very high wall friction factors when plotted against the gas Reynolds number. The values given are equivalent to the flow of a homogeneous fluid in a

very rough pipe. In this connection, Schlichting (32) has cited an example of the extremely high roughness equivalence of relatively small annular rib-like corrugations in pipe flow.

The radial traverse measurements of the axial dynamic pressure of high velocity vapor surrounded by an annular liquid layer, given in Fig. 37, show very little variation of the dynamic vapor pressure across the vapor core. This result indicates a nearly constant vapor velocity across the core diameter — virtually up to the wavy liquid vapor inter- face. The above information indirectly indicates that the level of turbulence in the vapor core is very high, but no numerical figure can be given. Data on the turbulence intensity in the vapor core would be a useful addition to the available information on the mechanics of two- phase flow.

APPENDIX J

CORRELATION OF LOCAL HEAT TRANSFER SURFACE COEFFICIENTS

IN HIGH VELOCITY CONDENSING TWO-PHASE FLOW

Depending on the external resistance to heat transfer from the condenser tube, the internal or condensing layer resistance plays a lesser or greater role in determining the flow characteristics in the tube during condensation. For the case of low external resistance to heat transfer, it is necessary to determine the internal local surface coefficient accurately.

Very little experimental data on local heat transfer coefficients for high velocity condensing flow have been found in the literature. Several investigators have proposed methods for correlating surface heat transfer coefficients in two-phase condensing flow.

Powell (30) proposed a method to predict average coefficients of heat transfer in two-phase flow with condensation on the basis of a weighting or equivalent flow procedure. .

Carpenter (6) suggested a method whereby the local liquid Nusselt number is given as a function of the liquid Prandtl number and the liquid "friction Reynolds number" where the inside tube diameter is the length dimension required. Carpenter's correlation, when applied to the conditions of high velocity vapor developed in this investigation, predicted surface coefficients about 70 percent lower than the experimentally determined values.

In a lengthy analysis of the turbulent condensate film, Kutateladse (25) developed an expression for the local surface coefficient for the condensation of a high velocity vapor in a pipe. This expression is approximated by the following equation:

$$N_x \overset{\sim}{\sim} 0.125 \, Pr^{0.4} \, (Re_L)^{-0.1} \tag{1J}$$

where, in terms of the current nomenclature,

$$N_x \equiv \frac{\overset{*}{h}_i}{\rho_L C_L \overset{*}{V}_{Li}} \tag{2J}$$

$$Pr_L \equiv \frac{\mu_L C_L}{k_L} \tag{3J}$$

and

$$Re_L \overset{\sim}{=} \vec{V}_L \delta / \nu_L \tag{4J}$$

Kutateladse did not use this expression to compare analytical and experimental values of the local heat transfer coefficient. He did, however, use equation (1J) to obtain an expression for the average coefficient over the condensing length. Experimental values of the average surface coefficient for condensing steam were found to average about 25 percent higher that those determined from the resulting semi-analytical expression.

In an earlier investigation (18) the author used the well-known technique of dimensional analysis to arrive at the following empirical equation for the local coefficient of heat transfer for the condensation of high velocity steam:

$$\frac{\overset{*}{h}_i \Delta t}{\rho_v V_v \delta g} = f \left[Re_v^{\prime\, -8/9} \, (Re_L)^{3/8} \, (V_v / V_L)^{1/6} \, (D/\delta)^{13/9} \right] \tag{5J}$$

where

$$Re_v' \equiv \frac{D\rho_v V_v}{\mu_v} \qquad (6J)$$

and

$$Re_L \equiv \frac{\delta \rho_L V_L}{\mu_L} \qquad (7J)$$

Fig. 50 shows experimental data for high velocity steam condensing in 0.190 and 0.550 inch I.D. tubes. In Fig. 50 the left side of equation (5J) is the ordinate and the right side is the abscissa. It is seen that the functional relationship between the two terms is not a simple power function. Obviously this correlation applies specifically to condensing H_2O vapor and may be unsatisfactory for other vapors. The necessary data on the local heat transfer and local flow characteristics of other vapors is apparently not available at the present time.

It is interesting to compare the role of each variable as found in the equation (1J) of Kutateladse (25) and the authors equation (5J). The Kutateladse equation may be written in the form

$$\overset{*}{h}_i \sim (\delta^{-1/10} \; \rho_v^{1/2} \; \rho_L^{3/10} \; V_v^{1.0} \; V_L^{-1/10} \; \mu_L^{1/2} \; k_L^{-2/5} \; c_L^{7/5}) \qquad (8J)$$

For equation (5J) the expanded form is

$$\overset{*}{h}_i \Delta t \sim f(D^{5/9} \; \delta^{-1/14} \; \rho_v^{1/9} \; \rho_L^{3/8} \; V_v^{5/18} \; V_L^{5/24} \; \mu_v^{8/9} \; \mu_L^{-3/8}) \qquad (9J)$$

It is observed that the two expressions tend to agree on the role of some terms, but disagree sharply on others. The positive role of the vapor velocity in determing the heat transfer coefficient is confirmed by both expressions. Both expressions indicate that the liquid layer thickness δ has a negligible effect on the surface coefficient. Evidently the deep wave penetration into the liquid layer with resulting
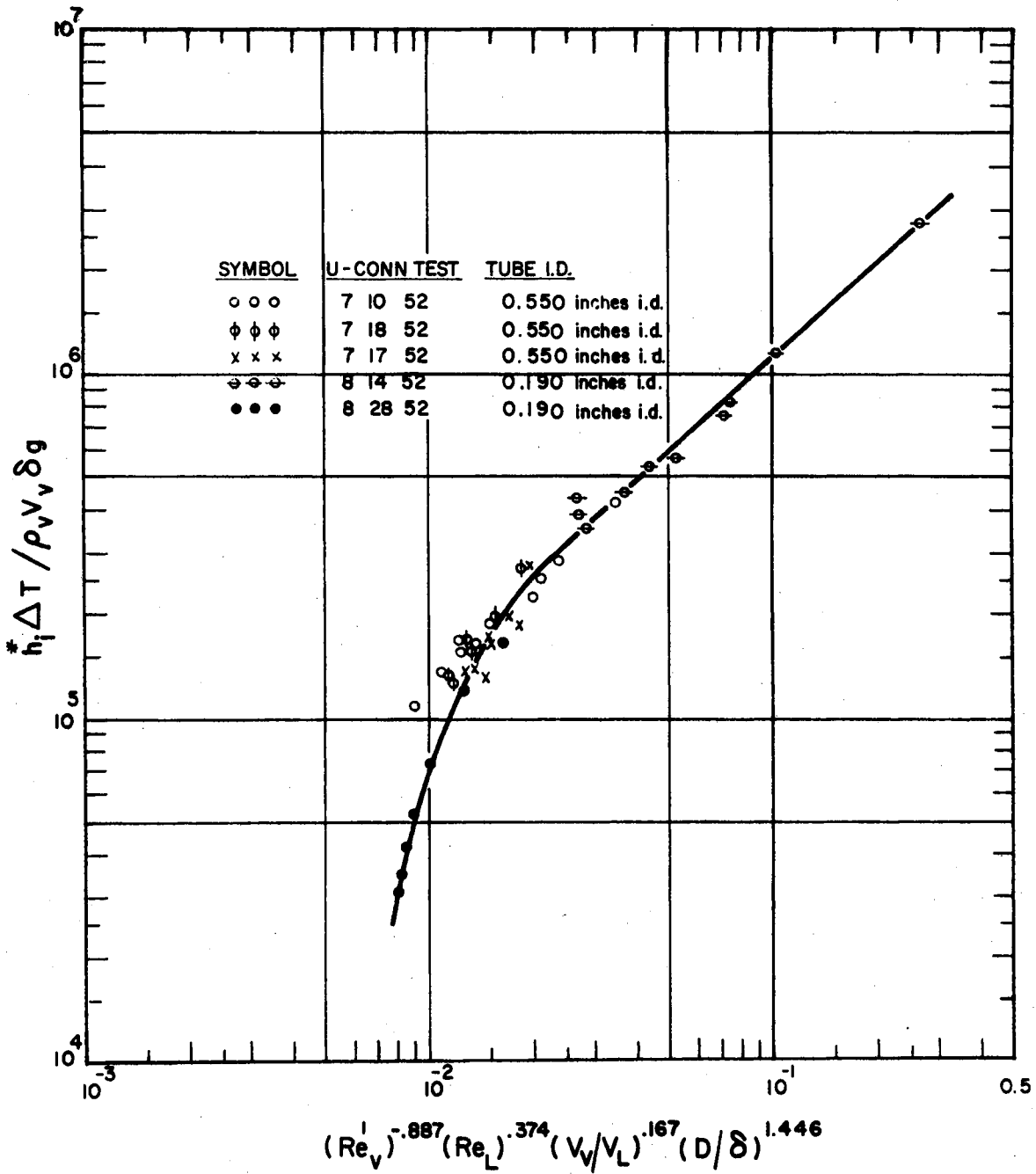
Figure 50. Dimensionless Correlation for Local Heat Transfer
Coefficient (Two Tube Sizes)

high liquid layer turbulence overcomes any increase in resistance to

heat transfer due to increasing liquid layer thickness.

The details of the method of determining the exponents of the

correlation, expressed by equation (5J), will be described briefly. In

order to derive the desired exponent values from the available volume of

experimental data, the following equation set was established:

$$
\left.
\begin{aligned}
X_{10} &= C\,(X_{11})^a\,(X_{12})^b\,(X_{13})^c\,\ldots\,(X_{1n})^z \\
X_{20} &= C\,(X_{21})^a\,(X_{22})^b\,(X_{23})^c\,\ldots\,(X_{2n})^z \\
X_{m0} &= C\,(X_{m1})^a\,(X_{m2})^b\,(X_{m3})^c\,\ldots\,(X_{mn})^z
\end{aligned}
\right] \qquad (10J)
$$

where m = n + 1 since there are n unknown exponents and also one unknown

constant. Eliminating the constant C from the m equations by dividing

the first equation by the second, the first by the third, and so on

leads to the following set of n equations:

$$
\left.
\begin{aligned}
\frac{X_{10}}{X_{20}} &= \frac{X_{11}}{X_{21}}^a\,\frac{X_{12}}{X_{22}}^b\,\frac{X_{13}}{X_{23}}^c\,\ldots\,\frac{X_{1n}}{X_{2n}}^z \\[2em]
\frac{X_{10}}{X_{m0}} &= \frac{X_{11}}{X_{m1}}^a\,\frac{X_{12}}{X_{m2}}^b\,\frac{X_{13}}{X_{m3}}^c\,\ldots\,\frac{X_{1n}}{X_{mn}}^z
\end{aligned}
\right] \qquad (11J)
$$

Taking the natural logarithm of both sides of all equations results in

the following equation set:

$$
\left.
\begin{aligned}
\ln\frac{X_{10}}{X_{20}} &= a\,\ln\frac{X_{11}}{X_{21}} + b\,\ln\frac{X_{12}}{X_{22}} + c\,\ln\frac{X_{13}}{X_{23}} \cdots + z\,\ln\frac{X_{1n}}{X_{2n}} \\[1.5em]
\ln\frac{X_{10}}{X_{m0}} &= a\,\ln\frac{X_{11}}{X_{m1}} + b\,\ln\frac{X_{12}}{X_{m2}} + c\,\ln\frac{X_{13}}{X_{m3}} \cdots + z\,\ln\frac{X_{1n}}{X_{mn}}
\end{aligned}
\right] \qquad (12J)
$$

In this system of equations, X quantities represent the experi-

mental data. The equation set (12J) consists of a set of simple linear

algebraic equations with unknowns a, b, c, d, ..., z and with coefficients determined from experimental data. Using a digital computer program available at the University of Connecticut Computer Center, in conjunction with a sub-program written to evaluate the natural logarithms, it was possible to solve for the desired exponents on an I.B.M. 1620 computer.

As indicated previously, the results of this work are shown in Fig. 50. In addition, Figs. 51 and 52 have been plotted to show the wide variation in local surface coefficients which are encountered in high velocity condensation of steam vapor. Since the data plotted in Figs. 51 and 52 were the source information used in obtaining the correlation presented in this Appendix, it is not surprising that values of the local surface coefficient calculated by use of the empirical equation (5J) give close agreement with the experimental data.

It should be noted that the necessary data to obtain a satisfactory correlation for the local surface coefficient for condensing steam include: 1) The local mean thickness of the liquid layer (δ); 2) The local mean liquid layer velocity (V_L); 3) The local vapor velocity (V_v); and 4) The local surface to vapor temperature difference (Δt), plus the local physical properties of the liquid and vapor. Experimental data on the value of these local flow properties are difficult to obtain. No other investigators known to the author have made the necessary experimental measurements to permit determination of these local flow properties. However, such data will probably be necessary in order to obtain a general correlation for local heat transfer surface coefficients for condensing vapors in high velocity two-phase flow.
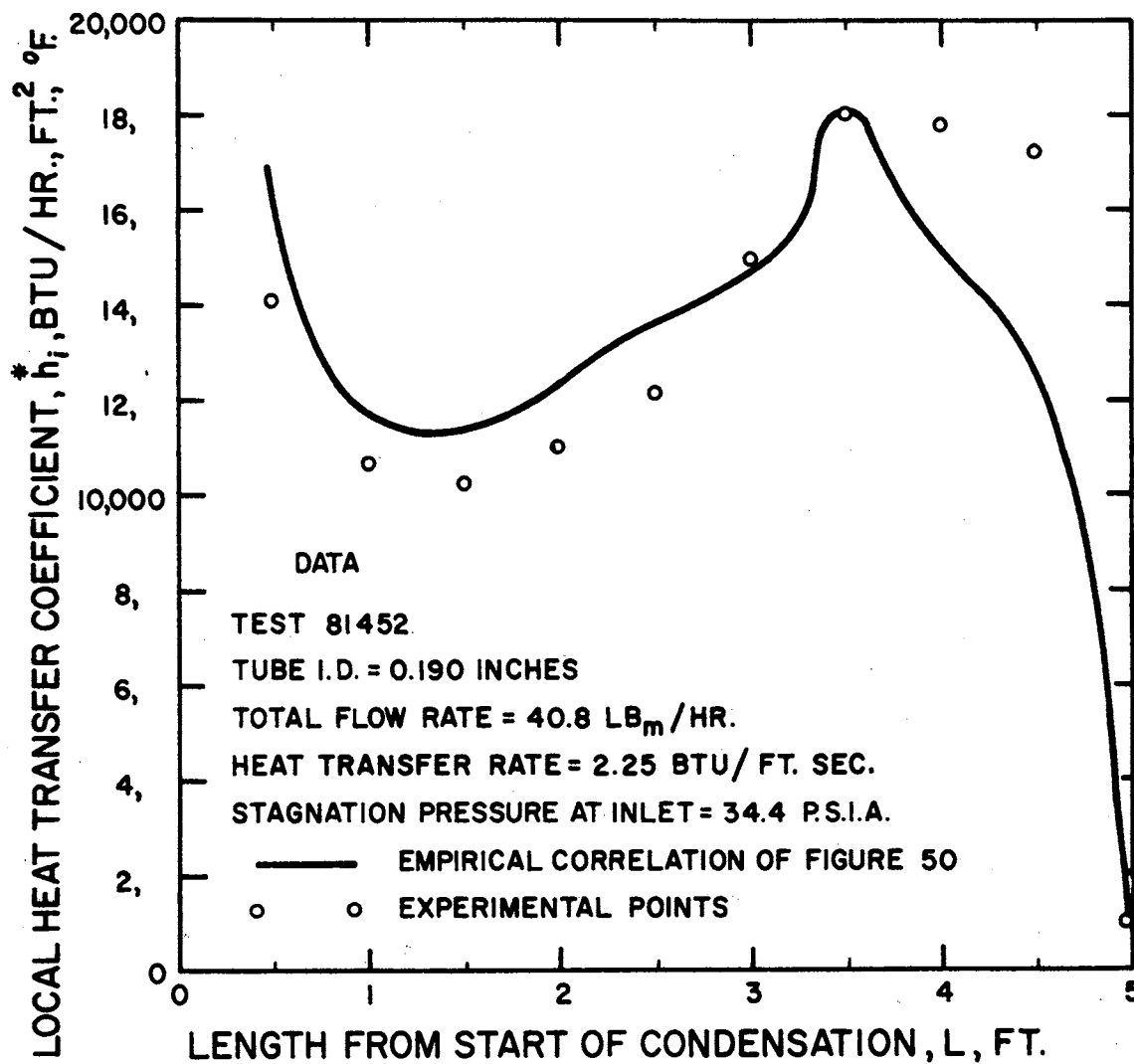
Figure 51. Variation of Local Heat Transfer Coefficient Over
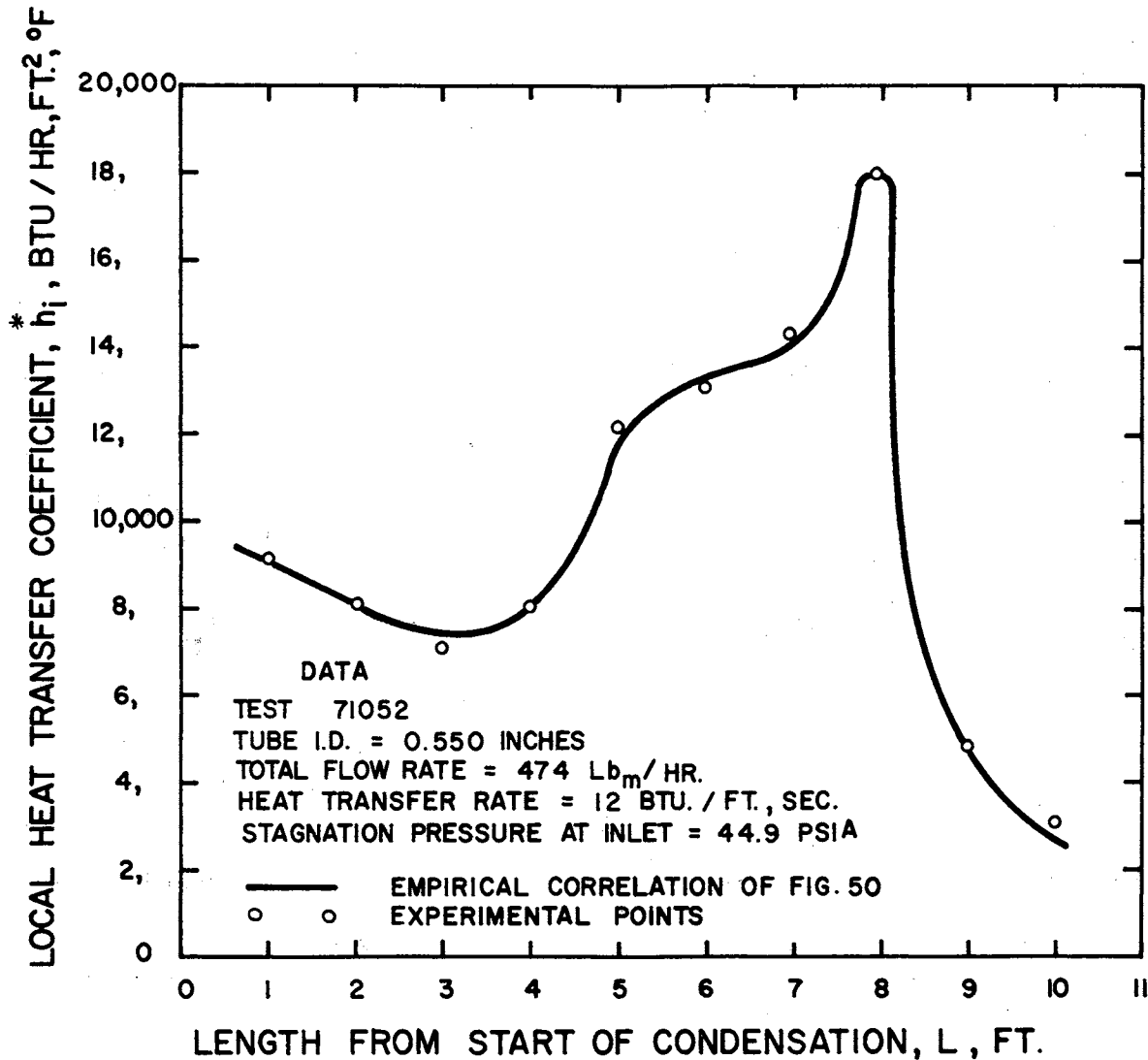Condensing Length-0.190 Inch I.D. Tube

Figure 52. Variation of Local Heat Transfer Coefficient Over
Condensing Length-0.550 Inch I.D. Tube

APPENDIX K

NUMERICAL TECHNIQUE FOR THE COMPUTER SOLUTION OF THE SIMULTANEOUS NON-
LINEAR FIRST ORDER DIFFERENTIAL EQUATIONS OF CHANGE FOR HIGH SPEED,
TWO-PHASE FLOW WITH CONDENSATION IN SMALL STRAIGHT TUBES

Summary of Method of Solution

The one independent variable occurring in the system of equations
given in Table II is the dimensionless distance X from the start of con-
densation in diameters ($X = L/D$). At the initial value of X all values
of the dependent variables (α, β, θ, ϕ) must be known or calculated by
the methods given in Appendix G. The four unknowns which must be eval-
uated by the simultaneous solution of four algebraic equations are the
four derivatives $d\alpha/dX$, $d\beta/dX$, $d\theta/dX$, and $d\phi/dX$. The required algebraic
equations are obtained by evaluating the five coefficients of each of
four applicable equations selected from Table II. Both the combined con-
tinuity equation (equation (1)) and the combined energy equation (equa-
tion (4)) are used in every solution at all times. Either the vapor mo-
mentum equation (equation (2)) or the combined momentum equation (equa-
tion (3)) may be used, depending on the accuracy of the available infor-
mation about the wall shear stress or interfacial shear stress functions.
The shear stress function may be represented in these equations in the
form of a friction factor or in terms of a boundary layer distribution
function if the latter representation turns out to be more dependable.
In addition either the velocity pressure equation for compressible flow

175

(equation (6)) or the initial liquid boundary layer equation (equation (7)) must be used in this system of equations.

Following is an outline of the steps normally followed in obtaining an analytical solution to these equations:

1. The flow conditions at the start of condensation must be known or calculated. These include: (1) vapor velocity V_v; (2) liquid velocity V_L; (3) total steam rate W; (4) static pressure P; (5) vapor density ρ_v; (6) total quality θ (usually $\theta \simeq 1$ near start); (7) enthalpies h_v, h_L, h_{fg}; and (8) inside tube diameter D. In addition the local heat transfer rate Q' must be known as a function of the distance X. A complete discussion of the method used to calculate entrance conditions is given in Appendix G.

2. The numerical values of all constants (e.g., λ, ϵ, η, σ, etc.)[1] must be calculated for the particular case under consideration.

3. Decide which four equations will be used and under what conditions over the condensing length. These conditions have been discussed above and also in Appendix F.

4. Calculate the first values of the coefficients of the four equations chosen for the start of the solution — see Appendix G. These coefficients are put in a 4 x 5 matrix which is operated on by a conventional technique to solve for the four unknowns, i.e., the four derivatives $d\alpha/dX$, $d\beta/dX$, $d\theta/dX$, and $d\phi/dX$. The numerical values of the four dependent variables α, β, θ, and ϕ and their derivatives are now known at a very small but finite value of X in the condenser. New values of the variables, α, β, θ,

---

[1] See nomenclature for definition of these constants.

and ϕ are now calculated at the position $(X + \Delta X)$ by applying
the derivatives over the small increment ΔX of the condenser
length and adding the resulting change of variable, e.g., ΔX to
the original value of X. All other properties have been ex-
pressed in terms of the four fundamental variables, e.g., vapor
density ρ_v is represented as a function of the pressure P, and
may now be evaluated at $X + \Delta X$ also.

5. With these new values of α, β, θ, and ϕ at the new position
of $X + \Delta X$, it is possible to repeat the cycle of calculations
again for another increment of ΔX. This cycle of calculations
must be repeated as the solution advances incrementally over
the condensing length until all vapor has been condensed. At
this point the overall pressure drop for the condensation pro-
cess may be determined as well as the required condensing
length.

Higher order integration techniques may be used if desired, but for
this simple first order equation system it appears to be just as econom-
ical in the use of computer time to use the system described above with
rather short incremental distances for each step — e.g., a fraction of one
tube diameter $(\Delta X \leq 1)$.

An Explanation of the Computer Program Used

On the IBM-7040 Computer

A copy of one of the computer programs that have been developed to
solve the two-phase flow equations is given at the end of this Appendix.
The program follows the method of solution outlined in the five steps
above. This program is set up to run on an IBM-7040 digital computer.

An outline of the function of the major sections of the program is given below:

The section of the program up to statement 20 reads and prints out the initial data.

Statements 20 up to 80 calculate the constants of the system.

Statements 80 up to 90 calculate the coefficients of the combined continuity equation.

Statements 90 up to 100 calculate the coefficients of the combined energy equation.

Statements 100 up to 200 calculate the coefficients of the vapor momentum equation.

Statements 200 up to 400 allow the use of both the vapor and combined momentum equations.

Statments 400 up to 500 calculate the coefficients of the combined momentum equation.

Statements 500 up to 700 calculate the coefficients of the velocity pressure equation for compressible flow.

Statements 700 up to 800 calculate the coefficients of the initial liquid layer equation.

Statements from 800 through 910 rearrange to 4 x 5 matrix of the coefficients A(1,1) through A(4,5) that have been calculated, and operate according to a diagonal elimination technique to solve for the four unknown derivatives $d\alpha/dX$, $d\beta/dX$, $d\theta/dX$, and $d\phi/dX$ which are given the symbols DX(1), DX(2), DX(3), and DX(4) respectively.

Statements 1000 up to 1050 apply the derivatives over an increment in order to calculate the new variables at $X + \Delta X$.

Statements 1050 up to 1100 calculate the output data at position

$X + \Delta X$.

Statements from 1100 through 1250 print out the data corresponding to the new variables that have been calculated, and then refer the computer to statment 70 in order to repeat the cycle of calculations at the new value of X.

(Program on Following Page)

PROGRAM FOR SOLUTION OF TWO-PHASE FLOW EQUATIONS

```
      INTEGER  TEST,BLEQ
      REAL   NDDIST,NDLQVL,NDVPVL,NDVPFL,NDPRES,LQFL,LQSVOL,LQREYN,LQVISC
     1,LQVL,LQAREA,LQTHIK,LQDEN,NDDEN,NPRINT,NPRNT
      DIMENSION  A(4,5),DX(4),X(4),FRVPE(30),FRWLE(30)
      READ(5,5)  TEST,VPVLE,PRESE,TOTFL,HFGE,HVPE,HLQE,AJ,AK,BB,DIAM,
     1VMUXP,XP,LQSVOL,NDVPVL,NDVPFL,NDPRES,SHF,AAA,BK,BS,TT,NDDIST,
     2VPSVOL,NDLQVL,VPVISC,LQVISC,MOMVAP,MOMCMB,BLEQ,MOMBTH,N,DELTAX,COU
     3NTR,NPRINT
    5 FORMAT(I5,6F7.2,F8.2,2F7.2/F7.4,2F5.3,6F8.5/3F8.5,4E12.5/E12.5,5I3
     1,E12.5,2F9.1)
      READ(5,6)((FRVPE(L),FRWLE(L)),L=1,N)
    6 FORMAT (6E10.3)
      WRITE(6,10) TEST,VPVLE,PRESE,TOTFL,DIAM,HFGE,HVPE,HLQE,VPSVOL,
     1LQSVOL,VPVISC,LQVISC,MOMVAP,MOMCMB,BLEQ,MOMBTH,NDVPVL,NDVPFL,NDPRE
     2S,NDDIST,BB,VMUXP,XP,SHF,AAA,BK,BS,TT,N,DELTAX,COUNTR
   10 FORMAT(14HOINPUT DATA...  //132H  TEST   VPVLE   PRESE     TOTFL    DIAM
     1      HFGE     HVPE     HLQE      VPSVOL   LQSVOL     VPVISC       LQVIS
     2C    MOMVAP MOMCMB   BLEQ MOMBTH /I6,F8.2,F8.3,F8.2,F7.4,3F8.2,E12.
     35,F8.5,2E12.5,I4,I7,I6,I7//126H   NDVPVL    NDVPFL     NDPRES       NDDIS
     4T        BB     VMUXP    XP       SHF      AAA        BK         BS         TT
     5  N    DELTAX        COUNTR /3F9.5,E13.5,F8.2,F7.3,F6.3,F9.5,4F8.5,I3
     6,E12.5,F9.1)
   20 CHEQ=(778.28*32.174*LQVISC*3.14159*HFGE*25.0)/(2.*AJ)
      DIST=CHEQ*DIAM
      WRITE(6,30) CHEQ,DIAM,DIST
   30 FORMAT(40HO  CHEQ           DIAM           DIST           //E12.5,2E14.5)
   60 VPDEN=1./VPSVOL
      LQDEN=1./LQSVOL
      VES=1./(VPVLE**2)
      B=(32.174*DIAM*VES*3600.)/(TOTFL*12.)
      PRESF=PRESE*144.
      NDDEN=VPDEN/LQDEN
      D=32.174*PRESF*VES/VPDEN
      AM=25031.02*HFGE*VES
      EPL=25031.02*HVPE*VES
      ETA=25031.02*HLQE*VES
      CONTR=0.0
      NPRNT=0.0
      DELU=5.
      TTAREA=(3.14159*(DIAM**2))/576.
   70 HO=AJ+AK*NDDIST
      H=HO*B
C     COMBINED CONTINUITY EQUATION (ALWAYS USED)
   80 A(1,1)=NDDEN*NDVPVL*(NDPRES**AAA)*(1.-NDVPFL)/(NDVPFL*(NDLQVL**2))
      A(1,2)=1./NDVPVL
      A(1,3)=((NDDEN*NDVPVL*(NDPRES**AAA))/NDLQVL-1.)/NDVPFL
      A(1,4)=AAA/NDPRES
      A(1,5)=0.
C     COMBINED ENERGY EQUATION (ALWAYS USED)
   90 A(3,1)=(1.-NDVPFL)*NDLQVL
      A(3,2)=NDVPVL*NDVPFL
      A(3,3)=AM/(NDPRES**SHF)+((NDVPVL)**2-(NDLQVL)**2)*0.5
      A(3,4)=((1.-BK)*EPL*NDVPFL)/(NDPRES**BK)+((1.-BS)*ETA*(1.-NDVPFL))
     1/(NDPRES**BS)
      A(3,5)=-H
      IF (MOMVAP) 400,400,100
```

```
C        VAPOR MOMENTUM EQUATION
  100 A(2,1)=0.
      A(2,2)=NDVPFL
      A(2,3)=NDVPVL-2.*NDLQVL
      A(2,4)=(NDVPFL*D)/(NDVPVL*(NDPRES**AAA))
      L=1
      FRVP=FRVPE(L)
      A(2,5)=-2.*(NDVPVL**1.5)*((NDVPFL*(NDPRES**AAA))**0.5)*FRVP
      IF (NDDIST-CHEQ) 200,210,210
  200 IF (BLEQ) 210,210,700
  210 IF (MOMCMB) 500,500,300
C        USING BOTH MOMENTUM EQUATIONS
  300 A(4,1)=A(2,1)
      A(4,2)=A(2,2)
      A(4,3)=A(2,3)
      A(4,4)=A(2,4)
      A(4,5)=A(2,5)
C        COMBINED MOMENTUM EQUATION
  400 A(2,1)=1.-NDVPFL
      A(2,2)=NDVPFL
      A(2,3)=NDVPVL-NDLQVL
      A(2,4)=D
      IF (NDDIST-CHEQ)420,420,410
  410 IF (FRVPE(1))430,430,420
  420 L=1
      FRWL=FRWLE(L)
      GO TO 440
  430 CALL SHEAR (LQFL,DIAM,LQVISC,LQSVOL,LQTHIK,LQVL,VPVL,VPSVOL,DELU,T
     1AUWLU,TAUWL,FRWL)
      IF (DELU-15.)431,431,432
  431 FRWL=0.006
      GO TO 440
  432 IF (DELU-30.)433,433,440
  433 FRWL=0.008
  440 A(2,5)=-2.*FRWL*NDVPVL*NDVPVL*(NDPRES**AAA)
      IF (MOMBTH) 500,500,800
  500 IF(NDDIST-CHEQ) 700,600,600
C        EQUALITY OF INTERFACIAL VELOCITY PRESSURE EQUATION
  600 A(4,1)=2./NDLQVL
      SON=BB*(NDPRES*PRESE)**TT
      CAM=NDVPVL*VPVLE/SON
      DUM=1.+(XP-1.)*CAM*CAM/2.
      XPO=1./(XP-1.)
      XPK=XPO*XP
      SS=(XP*DUM**XPO)/(DUM**XPK-1.)
      A(4,2)=-SS*CAM*CAM/NDVPVL
      A(4,3)=0.
      A(4,4)=(SS*CAM*CAM*TT-2.*TT-AAA)/NDPRES
      A(4,5)=0.
      GO TO 800
C        INITIAL LIQUID BOUNDARY LAYER EQUATION
  700 A(4,1)=2./NDLQVL
      A(4,2)=0.
      A(4,3)=1./(1.-NDVPFL)
      A(4,4)=-0.5*AAA/NDPRES
      A(4,5)=-1./(2.*NDDIST)
C        METHOD OF DIAGONAL ELIMINATION
  800 K=1
```

```
  810 DO 850 I=1,4
      IF (I-K) 820,850,820
  820 P=A(I,K)/A(K,K)
      DO 830 J=1,5
  830 A(I,J)=A(I,J)-P*A(K,J)
  850 CONTINUE
      K=K+1
      IF(K-5) 810,900,900
  900 DO 910 I=1,4
      DX(I)=A(I,5)/A(I,I)
  910 CONTINUE
C     NUMERICAL INTERGRATION SCHEME
 1000 NDDIST=NDDIST+DELTAX
      NDLQVL=NDLQVL+DELTAX*DX(1)
      NDVPVL=NDVPVL+DELTAX*DX(2)
      NDVPFL=NDVPFL+DELTAX*DX(3)
      NDPRES=NDPRES+DELTAX*DX(4)
      DIST=NDDIST*DIAM/12.
 1050 LQVL=NDLQVL*VPVLE
      VPVL=NDVPVL*VPVLE
      VPFL=NDVPFL*TOTFL
      LQFL=TOTFL-VPFL
      PRES=NDPRES*PRESE
      CALL STEAMT(TEMP,PRES,7,3,S,VPSVOL,H)
      LQTHIK=(DIAM-SQRT(DIAM**2-(LQFL*LQSVOL*0.04)/(3.14159*LQVL)))/2.
      VPAREA=(VPVL*VPSVOL)/(VPVL*3600.)
      DIAMVP=DIAM-LQTHIK*2.
      VPREYN=(VPVL*DIAMVP)/(VPVISC*VPSVOL*12.*32.174)
      PERMTR=3.14159*(DIAMVP+DIAM)
      LQAREA=TTAREA-VPAREA
      HYDIAM=(48.*LQAREA)/PERMTR
      LQREYN=(LQVL*HYDIAM)/(LQVISC*LQSVOL*32.174)
      IF (NDDIST-(DELTAX+CHEQ))1100,1100,1070
 1070 CONSQ=LQSVOL*(VPVL**2)*2.*((DUM**XPK)-1.)/(XP*CAM*CAM*VPSVOL*(LQVL
     1**2))
      CONST=SQRT(CONSQ)
 1100 IF(CONTR-(NPRINT+30.))1215,1150,1150
 1150 IF(NPRNT-NPRINT)1200,1210,1210
 1200 NPRNT=NPRNT+1.0
      GO TO 1240
 1210 NPRNT=1.0
 1215 WRITE(6,1220)DX(1),DX(2),DX(3),DX(4)
 1220 FORMAT(15H-OUTPUT DATA...//52H  DELNDLQVL     DELNDVPVL     DELNDVPF
     1L    DELNDPRES  /4E13.5)
      WRITE (6,1230) DIST,NDDIST,VPVL,NDVPVL,LQVL,NDLQVL,VPFL,NDVPFL,LQF
     1L,PRES,NDPRES,TEMP,VPSVOL,LQSVOL,VPAREA,LQAREA,LQTHIK,FRVP,VPREYN,
     2FRWL,LQREYN,CONTR,DELU,TAUWLU,TAUWL,CONST
 1230 FORMAT(121H0    DIST        NDDIST      VPVL      NDVPVL     LQVL      ND
     1LQVL       VPFL       NDVPFL    LQFL    PRES   NDPRES  TEMP     VPSVOL
     2//2E13.5,F7.2,F9.5,F7.2,E12.5,F9.3,F9.5,F8.2,F7.2,F8.5,F7.2,E12.5/
     3/105H   LQSVOL       VPAREA        LQAREA       LQTHIK         FRVP
     4 VPREYN       FRWL        LQREYN        CONTR /E13.5,7E12.5,F8.2//44
     5H   DELU   TAUWLU      TAUWL     CONST      /F7.1,E13.5,2E12.4)
 1240 CONTR=CONTR+1.0
      IF(COUNTR-CONTR)1300,1300,1250
 1250 IF (VPFL) 1300,1300,70
 1300 CALL EXIT
      END
```

VITA

Winthrop Edward Hilding

Candidate for the Degree of

Doctor of Philosophy

Thesis: AN ANALYTICAL AND EXPERIMENTAL STUDY OF THE TWO-PHASE FLOW OF A HIGH VELOCITY VAPOR CONDENSING IN A TUBE

Major Field: Engineering

Biographical:

Personal Data: Born in Hartford, Connecticut, June 4, 1918, the son of Albert Wallace and Ethel Porter Hilding. Married to Dolores Agnes Tondat March 5, 1949. Children: Sherry Cavallon, born 1950, Nancy Doreen, born 1951, Alison Ann, born 1954.

Education: Attended elementary school in Hebron, Connecticut; graduated from Windham High School, Willimantic, Connecticut in 1934; received the Bachelor of Science degree from the University of Connecticut in June, 1938; received the Master of Science degree from the Pennsylvania State University in October, 1944; completed requirements for the Doctor of Philosophy degree at Oklahoma State University in May 1968.

Professional Experience: Served as assistant instructor in Mechanical Engineering at Brown University, Providence, Rhode Island, 1939-1940; was a test engineer and then assistant project engineer at the Pratt and Whitney Division of United Aircraft Co. from 1940 through 1947; has taught in the Mechanical Engineering Department at the University of Connecticut since 1947; is now professor of Mechanical Engineering.

Professional Organizations: Member of the American Society for Engineering Education; member of the American Society of Mechanical Engineers; is a registered professional engineer in the state of Connecticut.

Honorary Organizations: Member of Sigma Xi; honorary member of Tau Beta Pi; honorary member of Pi Tau Sigma.